1949

The effects of spin-orbit coupling on many-body quantum systems

Thesis for the Degree of Doctor of Philosophy (PhD)

Nóra Kucska

Supervisor

Dr. Zsolt Gulácsi

UNIVERSITY OF DEBRECEN
Doctoral Council of Natural Sciences and Information Technology
Doctoral School of Physics

Debrecen, 2022

Hereby I declare that I prepared this thesis within the Doctoral Council of Natural Sciences and Information Technology, Doctoral School of Physics, University of Debrecen in order to obtain a PhD Degree in Natural Sciences at Debrecen University.
The results published in the thesis are not reported in any other PhD theses.

Debrecen, 2022. August

Kucska Nóra
candidate

Hereby I confirm that Nóra Kucska candidate conducted her studies with my supervision within the Solid State Physics and Material Science Program of the Doctoral School of Physics between 2018. and 2022. The independent studies and research work of the candidate significantly contributed to the results published in the thesis.
I also declare that the results published in the thesis are not reported in any other theses.
I support the acceptance of the thesis.

Debrecen, 2022. August

Dr. Zsolt Gulácsi
supervisor

The effects of spin-orbit coupling on many-body quantum systems

Dissertation submitted in partial fulfilment of the requirements for the doctoral (PhD) degree in physics

Written by Nóra Kucska certified physicist

Prepared in the framework of the Doctoral School of Physics of the University of Debrecen
Solid State Physics and Material Science Program

Dissertation advisor: Dr. Zsolt Gulácsi

The official opponents of the dissertation:

Dr. ....
Dr. ....

The evaluation committee:

chairperson:	Dr.	.....
members:	Dr.	.....
	Dr.	.....
	Dr.	.....
	Dr.	.....

The date of the dissertation defence: .....

Acknowledgements

I would like to express my gratitude to my supervisor Dr. Zsolt Gulácsi. His support, work morale and meaningful insights to the science of strongly correlated systems carried me through this presented research.

I am deaply grateful for the financial and scientific support from the Department of Physics and from the Doctoral School of Physics, at the University of Debrecen. From the many great scientists I had the privilege to get to know, I want to thank for the three professors who endeared physics to me the most: prof. Dezső Beke, prof. Csaba Cserháti and prof. Zsolt Gulácsi.

I want to convey my heartfelt appreciation towards all my peers and great friends from the Doctoral School of Physics. Laura Juhász, Gabriella Jáger, Gergő Vecsei and not least of all Réka Vig, thank you for all that you have done.

I would also like to thank my family for the love and support they provided. To my fiance, mother and dear sister. Last, but not least my father, who would certainly be very proud. Thank you, dad.

Contents

Chapter 1

Introduction

1.1 An overview

This chapter is meant to provide the motivation behind my work presented in this thesis and also to introduce the studied systems and their importance. In my thesis I focused on how the spin-orbit interaction (SOI) is able to affect the physical behaviour of different many-body, itinerant electron systems.

In the first section of this chapter (**Section 1.2**), I discuss the many-body spin-orbit coupling, first by deriving it from the Dirac equation (Subsection 1.2.1) and then introducing the Rashba- (Subsection 1.2.2), and Dresselhaus type spin-orbit interactions (Subsection 1.2.3) and their influence of modern physics.

In **Section 1.3**, I present the various effects SOI has on band structures. I also introduce the Rashba- and Dresselhaus splitting, which refer to splitting of energy bands due to SOI (Subsection 1.3.1). In this section I introduce flat bands and the latest developments about systems with flat bands in the presence of SOI.

In this chapter, my aim is also to give context to-, and present the systems studied in my thesis. In my thesis I first investigate flat bands of polythiophene type conductive polymers (with pentagonal monomer) influenced by SOI and external magnetic field. I introduce conductive polymers and their broad field of application in **Section 1.4**.

In my thesis I also study a 2D strongly-correlated, not integrable itinerant electron system in the presence of SOI and Hubbard interaction. I investigate the influence of SOI on surfaces and interfaces, especially in the light of magnetic properties and charge carrier mobility. I give an overview of the effects SOI has formerly found to have on surfaces and interfaces in **Section 1.5**.

In **Section 1.6**, I introduce the method of positive semidefinite operators, which I use to deduct exact ground state wave functions for the studied 2D system. I also aim to provide motivation to why is it necessary to use the method of positive semidefinite operators to study a 2D, not integrable, strongly correlated system with SOI and inter-electron correlation.

1.2 The many-body spin orbit coupling

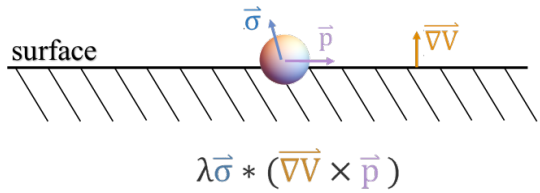

Figure 1.1: A schematic depiction of spin-orbit interaction H_{SO} of an electron on the surface. An electron with spin $\vec{\sigma}$ is moving with momentum $\vec{p}$. On the surface, a potential gradient $\vec{\nabla}V$ is automatically present, generating the interaction $H_{SO} = \lambda\vec{\sigma} \cdot \left(\vec{\nabla}V \times \vec{p}\right)$, where λ is the coupling strength.

In essence, the many-body spin-orbit interaction (SOI) is a relativistic effect (i.e. can be derived from the Dirac equation, as presented in Section 1.2.1). It is a relativistic correction to the Schrödinger equation, which is linked to an electron holding spin $\vec{\sigma}$ and moving with momentum $\vec{p}$. If this electron feels a potential gradient $\vec{\nabla}V$ during this movement, which is not collinear to $\vec{p}$, an interaction of the form $H_{SO} = \lambda\vec{\sigma} \cdot \left(\vec{\nabla}V \times \vec{p}\right)$ occurs (see Fig.1.1), which is called the spin orbit interaction, and λ is its coupling-constant (i.e. strength). Note, that in central field $\vec{\nabla}V \propto \vec{r}$, and the orbital moment is $\vec{r} \times \vec{p}$, thus H_{SO} correctly describes spin-orbit coupling.

1.2.1 The derivation of SOI from the Dirac equation

In this subsection, I derive the first quantized form of spin-orbit interaction from the Dirac equation of an electron moving in a V external potential, given by:

$$(E - V - c\alpha\vec{p} - \beta mc^2)\psi = 0, \tag{1.1}$$

where β and α are 4×4-es matrices, which have a following properties: $\beta^2 = \alpha_i^2 = 1$, $i = x, y, z$; $\sum_i \alpha_i\beta + \beta\alpha_i = \sum_i \sum_{j,j\neq i} \alpha_i\alpha_j + \alpha_j\alpha_i = 0$. In this case the ψ wave function is a 4×4 matrix. α and β are the following

$$\beta = \begin{pmatrix} \mathbb{I} & 0 \\ 0 & -\mathbb{I} \end{pmatrix}, \quad \alpha = \begin{pmatrix} 0 & \sigma_i \\ \sigma_i & 0 \end{pmatrix},$$

where σ_i, $i = x, y, z$ are the Pauli matrices, $\mathbb{I}$ is the 2×2 identity matrix. Let us write ψ in the following way:

$$\psi = \begin{pmatrix} \psi_1 \\ \psi_2 \end{pmatrix}, \qquad \psi_1 = \begin{pmatrix} v_1 \\ v_2 \end{pmatrix}, \qquad \psi_2 = \begin{pmatrix} v_3 \\ v_4 \end{pmatrix},$$

in order to write Eq.(1.1) in the following form:

$$(E-V)\begin{pmatrix}\mathbb{I} & 0\\ 0 & \mathbb{I}\end{pmatrix}\begin{pmatrix}\psi_1\\ \psi_2\end{pmatrix} - c\begin{pmatrix}0 & \vec{\sigma}\\ \vec{\sigma} & 0\end{pmatrix}\vec{p}\begin{pmatrix}\psi_1\\ \psi_2\end{pmatrix} - \begin{pmatrix}\mathbb{I} & 0\\ 0 & -\mathbb{I}\end{pmatrix}mc^2\begin{pmatrix}\psi_1\\ \psi_2\end{pmatrix} = 0.$$

The resulting Dirac equation can be simplified to

$$\begin{pmatrix}E-V-mc^2 & -c\vec{\sigma}\vec{p}\\ -c\vec{\sigma}\vec{p} & E-V+mc^2\end{pmatrix}\begin{pmatrix}\psi_1\\ \psi_2\end{pmatrix} = 0,$$

which leads us to two equations

$$(E-V-mc^2)\psi_1 - c\vec{\sigma}\vec{p}\psi_2 = 0, \qquad (E-V+mc^2)\psi_2 - c\vec{\sigma}\vec{p}\psi_1 = 0. \tag{1.2}$$

At this point let us introduce the non-relativistic energy $E^{'} = E - mc^2$.

$$(E^{'}-V)\psi_1 - c\vec{\sigma}\vec{p}\psi_2 = 0, \qquad (E^{'}-V+2mc^2)\psi_2 - c\vec{\sigma}\vec{p}\psi_1 = 0. \tag{1.3}$$

One calculates ψ_2 from the second equation of Eq.(1.3) , $\psi_2 = \frac{c\vec{\sigma}\vec{p}}{E^{'}-V+2mc^2}\psi_1$, then substitutes this expression into the first equation of Eq.(1.3). Therefore

$$\begin{aligned}&\Big[\frac{(\vec{\sigma}\vec{p})c^2(\vec{\sigma}\vec{p})}{E^{'}-V+2mc^2}+V\Big]\psi_1 = E^{'}\psi_1,\\ &\Big[\frac{1}{2m}(\vec{\sigma}\vec{p})\frac{1}{1+\frac{E^{'}-V}{2mc^2}}(\vec{\sigma}\vec{p})+V\Big]\psi_1 = E^{'}\psi_1.\end{aligned} \tag{1.4}$$

One then applies series expansion on the function $\frac{1}{1+\frac{E^{'}-V}{2mc^2}}$. This results $\frac{1}{1+\frac{E^{'}-V}{2mc^2}} = 1 - \frac{E^{'}-V}{2mc^2} + \mathcal{O}(\frac{1}{m^2c^4})$, since it was expanded only to the first order, meaning terms of order $\frac{1}{m^2c^4}$ (the order of the relativistic energy) were omitted. This leads us to

$$\Big[\frac{1}{2m}(\vec{\sigma}\hat{p})\Big(1-\frac{E^{'}-V}{2mc^2}\Big)(\vec{\sigma}\hat{p})+V\Big]\psi_1 = E^{'}\psi_1. \tag{1.5}$$

Using [1] $(\vec{\sigma}\vec{p})(\vec{\sigma}\vec{p}) = \vec{p}^{\,2}$ and [2] $\vec{p}V = V\vec{p} - i\hbar\vec{\nabla}V$ the above equation simply becomes

$$\Big[\underbrace{(\frac{\vec{p}^{\,2}}{2m})}_{I.} - \underbrace{\frac{V-E^{'}\vec{p}^{\,2}-i\hbar\vec{\nabla}V\vec{p}}{4m^2c^2}}_{II.} + \underbrace{\frac{\hbar}{4m^2c^2}\vec{\sigma}(\vec{\nabla}V\times\vec{p})}_{III.}\Big]\psi_1 = E^{'}\psi_1. \tag{1.6}$$

Here Term I. corresponds to the kinetic terms in the standard Schrödinger equation, Term II. has the first order relativistic corrections. Term III. describes the interaction between

[1] $(\vec{\sigma}\vec{p})(\vec{\sigma}\vec{p}) = (\sigma_x p_x + \sigma_y p_y + \sigma_z p_z)(\sigma_x p_x + \sigma_y p_y + \sigma_z p_z)$, utilizing the properties of the Pauli matrices, i.e. $\sigma_i^2 = 1, \{\sigma_i, \sigma_j\} = 2\delta_{i,j}I$, where I is the 2×2 unity matrix, the above relation becomes $(\vec{\sigma}\vec{p})(\vec{\sigma}\vec{p}) = (p_x^2 + p_y^2 + p_z^2)I = \vec{p}^{\,2}$

[2] Take an arbitrary wave functions ϕ. The $\vec{p}V\phi = -i\hbar\vec{\nabla}(V\phi) = -i\hbar(\vec{\nabla}\phi V + \vec{\nabla}V\phi) = -i\hbar(V\vec{\nabla} + \vec{\nabla}V)\phi$. Then omitting the wave function, one gets $\vec{p}V = -i\hbar(V\vec{\nabla} + \vec{\nabla}V)$, which is the property of the operators, since the wave functions ϕ is arbitrary.

the spin and the orbital angular momentum, which I denoted with H_{SO}.

$$H_{SO} = \frac{\hbar}{4m^2c^2}\vec{\sigma}(\vec{\nabla}V \times \vec{p}) = \lambda\vec{\sigma} \cdot \left(\vec{\nabla}V \times \vec{p}\right). \tag{1.7}$$

Note that starting with the Dirac equation, first order terms were deducted. In the deduced terms $\vec{p}$ is present in a linear form, thus the calculated spin-orbit interactions also contain $\vec{p}$ linearly, the higher order terms are omitted.

The derivation of the SOI coupling from the Dirac equation was done by many before, for example in Ref.[1].

1.2.2 Rashba spin-orbit coupling

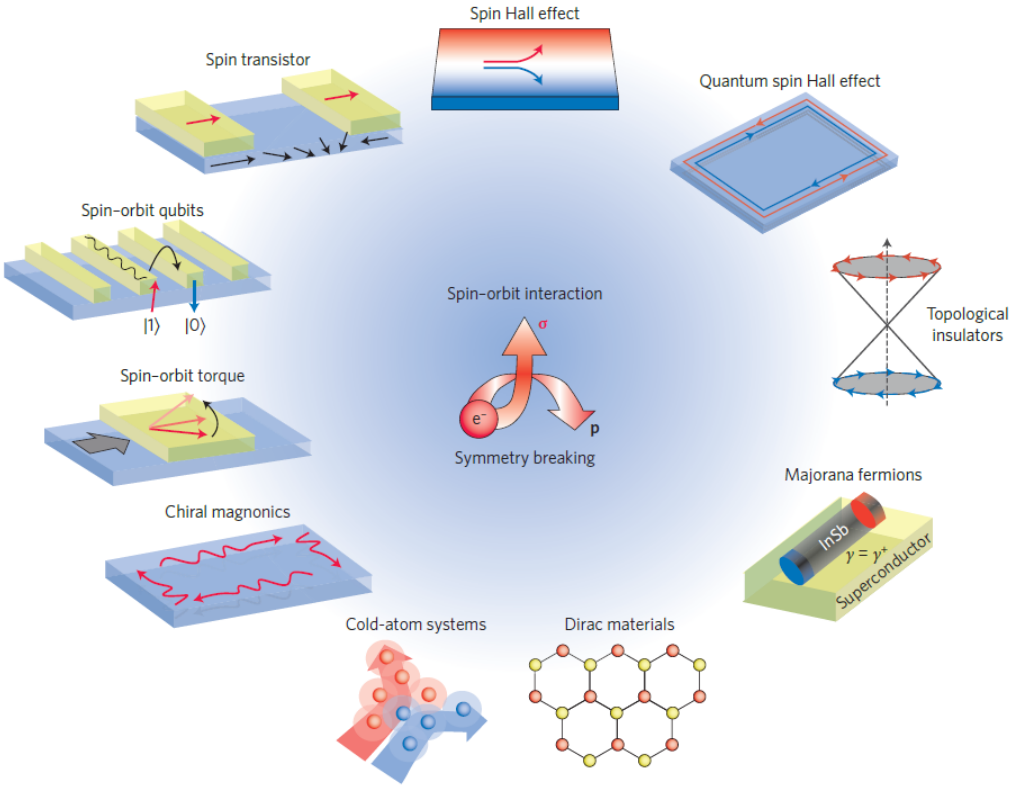

Figure 1.2: The rich field of Rashba physics, i.e. the possible applications of spin-orbitronics, where the spin-directions can be influenced electrically. The source of this figure is Ref.[2].

If the origin of V is an electric field ($\vec{\nabla}V = -\vec{\varepsilon}$), which points to the direction of the normal vector $\vec{n}$ of the surface (to the z direction), H_{SO} becomes H_R; the Rashba type spin-orbit coupling. To deduce the form of H_R starting with Eq.(1.7) let us express

the cross product, in the standard, orthonormal basis of $\vec{l}, \vec{m}, \vec{n}$ vectors:

$$-\lambda|\vec{\varepsilon}|\vec{n}(\vec{p}\times\vec{\sigma}) = -\frac{\hbar|\vec{\varepsilon}|}{4m^2c^2}\vec{n}\left(\vec{l}(\sigma_z p_y - \sigma_y p_z) + \vec{m}(\sigma_x p_z - \sigma_z p_x) + \vec{n}(\sigma_y p_x - \sigma_x p_y)\right), \quad (1.8)$$

where $\vec{l}, \vec{m}, \vec{n}$ are the unit vectors pointing to the x, y, z directions respectively. Expanding the scalar product in Eq.(1.8), the final form of the Rashba spin-orbit interaction becomes

$$H_R = -\frac{\hbar|\vec{\varepsilon}|}{4m^2c^2}(\sigma_y p_x - \sigma_x p_y) = \beta_R(\sigma_x p_y - \sigma_y p_x). \quad (1.9)$$

The result for H_{SO} derived this way is the so called Rashba-Bychkov spin-orbit interaction (H_R), which is a result of the electric field perpendicular to the surface of the crystal [3]. In Eq.(1.9) β_R is the coupling of the Rashba-Bychkov spin-orbit interaction. In the literature, the Rashba interaction is sometimes referred to as the Rashba-Bychkov interaction. The Rashba effect was first reported by Emmanuel Rashba with Valentin I. Sheka in 1959. In this publication, the effect was investigated for a three-dimensional system, which Rashba and Yurii A. Bychkov later extended to 2D systems in 1984 to describe electron spin-resonance in 2D semiconductors [4]. In the light of these result, the interaction is sometimes referred to as the Bychkov-Rashba interaction.

After this type of SOI was realized we can rightly say that it has opened the way to a whole new field of physics, often called Rashba physics. Fig.1.2 aims to present the wide field of the most recent developments of Rashba physics across various fields of physics, engineering and materials science. Devices capable of generating, detecting and modulating spin-current have been designed utilising Rashba effects [5].

The exploration of this field is now at the heart of a growing research area of spin–orbitronics. Spin-orbitronics is a subfield of spintronics aiming to investigate how SOI can influence the properties of different types of materials [6]. In spin-orbitronics the effects of spin-orbit coupling are used to form the desired spin configuration, thereby manipulating the spin degrees of freedom. Spintronics is a word formed by combining the words spin and electronics. It differs from conventional electronics in that it utilizes not only the charge but also the spin of the electron for data storage and transmission. Thus, it encodes the information to be stored in the different spin configurations. The discovery of GMR (giant magnetoresistance) is considered the beginning of spintronics. Albert Fert and Peter Grünberg received the Nobel Prize in 2007 for their pioneering research work on GMR [7, 8]. This technique can be used to create and manipulate spin-polarized current. The high magnetoresistance is due to the multi-layer structure, which is created by layering ferromagnetic and non-magnetic conductive materials. Depending on the direction of the magnetization of the ferromagnetic layers, an enormous maximum can be achieved in the electrical resistance. The technique is mainly used for magnetic field sensors.

1.2.3 Dresselhaus spin-orbit coupling

Dresselhaus was first to realize that zinc-blende semiconductor compounds lack centre of inversion and it leads to effects related to the SOI [10]. For crystals which lack inversion

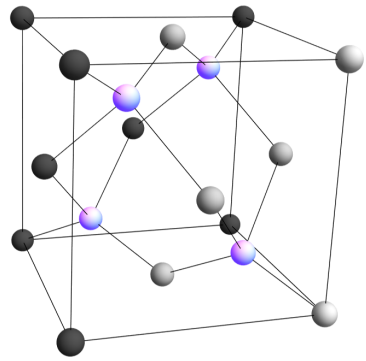

Figure 1.3: The zincblende structure, with the nearest neighbour bonds linked. It can be understood as two interpenetrating cubic lattices, where the gray sites represent one of the two sublattices, while the purple the other one. Moreover in zincblende the two sublattices are occupied by two different kind of ions [9].

symmetry Dresselhaus spin orbit coupling is present.

Inversion symmetry in a crystal means that, if we pick any lattice site as the origin and take any lattice site in the unit cell, e.g. at $\vec{r}$, the lattice site at $-\vec{r}$ must be the same. In the case of zincblende this is not the case (see Fig.1.3), since one can find, that a different ion occupies the lattice site at $-\vec{r}$ than at $\vec{r}$. On Fig.1.3 I show a diamond type lattice. If we imagine C atoms on each lattice site, i.e. diamond, in which case the purple and gray atoms are identical, the crystal does not lack inversion symmetry anymore.

The form of the Desselhaus spin-orbit coupling was calculated by Dresselhaus using first-order perturbation theory [10]. The first quantized form of the Dresselhaus spin-orbit coupling is

$$H_D = \alpha_D(\sigma_y p_y - \sigma_x p_x), \tag{1.10}$$

where α_D is the strength of the interaction. H_D from Eq.(1.10) is know in the literature as linear Dresselhaus SO coupling [11].

1.3 The effects of many body spin-orbit coupling on the band structure

In solid state physics the motion of electrons in a crystalline solid is often characterized by the band structure, which contains the energy bands $E_n(\vec{k})$, where n is the band index, $\vec{k}$ is the wave vector. SOI leads to the fascinating phenomenon of spin-splitting of electron states in systems without inversion symmetry even without external magnetic field present.

In this thesis I studied the SOI effects on band structure, thus experienced SOI splitting for both the studied system in Chapter 2 (See Section 3.2) and Chapter 3 (See Section 2.4 and Section 2.5).

1.3.1 Dresselhaus and Rashba splitting

The influence SOI has on the band structure $E_n(\vec{k})$ has been widely studied in several different systems. It was first reported in the case of semiconductors (e.g. GaAs, InSb), where it was found to split the topmost valence band [10]. Generally in a system with broken inversion symmetry, spin-orbit coupling is present, which is able to lift the double spin degeneracy of energy bands.

Inversion symmetry may be broken by an electric field $\vec{E}$, giving rise to the Bychkov-Rashba SOI (See Subsection 1.2.2). The source of this electric field can be from the spatial inhomogeneity of an interface or surface. It may also arise from the bulk asymmetry of uniaxial crystals, such as hexagonal crystals of CdS and CdSe. Both ways the Rashba spin–orbit coupling leads to energy band splitting.

The Dresselhaus spin-splitting arises from the lack of inversion symmetry in the crystal itself (See Subsection 1.2.3). This happen if the crystal lattice lacks this symmetry, meaning the reciprocal lattice does too. In this case, in the band structure of this type of material (e.g. GaAs and InAs) the energy of a wave function with wave vector $\vec{k}$ ($E(\vec{k})$) is very often not the same as that of with $-\vec{k}$ ($E(-\vec{k})$).

1.3.2 Flat bands

A flat band (FB) is a specially structured band with constant energy, independent of the crystal momentum $\vec{k}$. The name comes from the fact that in the band structure i.e the dispersion relation for electrons $E_n(k)$ we find the flat band to be a constant function.

Electronic systems with flat bands can be extremely beneficial from the point of view of application, since due to their huge degeneracy, they can be easily pushed to an ordered phase of interest by introducing a small perturbation. Even the smallest perturbation is able to change the energy of the flat band states and simultaneously their transport properties [12]. For this reason FBs seem to be a promising starting point for emerging exciting phenomena such as unconventional magnetism and superconductivity [12].

Flat bands have been identified in several occasions e.g. in electronic systems, various metamaterials, ultracold atomic gases and photonic waveguide arrays [13, 14]. Many flat-band systems were observed and investigated in the presence of SOI in the past [15, 16]. Formerly SOI was found to transform existing flat bands to quasiflat and gap them from the dispersive bands [17].

1.4 Conducting polymers

Usually organic polymers are insulators, whereas conducting polymers (CPs) represent a group of organic polymers which are semiconductors or conductors. These properties considered to be a result of their structure, since they possess conjugated chain structures,

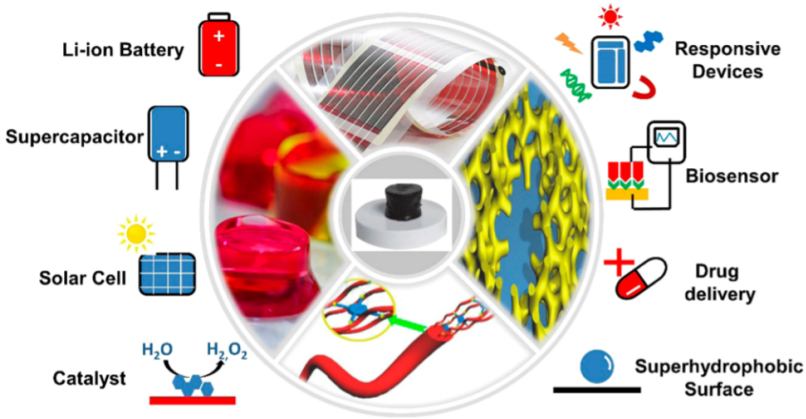

Figure 1.4: The broad application possibilities of conductive polymers, in form of conductive polymer gels. The source of this figure is Ref.[18].

with conjugated π-electrons [19]. Conjugated bonds are alternated single and double bonds. By alternating single and double bonds, a conjugated pi bond system is created.

CPs have the best of both; they have the appealing attributes of organic polymers, while possessing the electronic properties of metals or semiconductors [20]. The importance of the topic is well indicated by the fact that the Nobel Prize in Chemistry in 2000 was awarded jointly to Alan J. Heeger, Alan G. MacDiarmid and Hideki Shirakawa for the discovery and development of conductive polymers. The field of conductive polymers is especially interesting for researchers, given their outstanding attributes such as the tunable electrical conductivity [21]. As a promising factor that adds to this property, it is also predicted that the properties of conductive polymer in bulk forms translates to the conductive polymer nanostructures [20]. At the same time, nanostructured CPs provide even more interesting chemical/physical properties thanks to their large surface areas and shortened pathways for charge transport [20, 22]. CP nanostructures take many shapes [22, 23], such as nanowires and nanotubes [24, 25], nanoshperes [26] or nanosheets [27]. Given their diversity conductive polymers represent great opportunities in several fields of technology for application in many different forms (See Fig.1.4).

1.5 Many-body quantum behaviour on surfaces and interfaces

In this dissertation I studied how SOI influences a 2D itinerant, strongly correlated system. In this section I provide the motivation behind this work.

Many-body quantum behaviour on surfaces plays a prominent role in modern technology. For instance, essential components of computer hardware are formed on semiconductor surfaces, graphene surfaces are used to create various special effects. In

several cases spin-orbit interaction is strong at the inferfaces (for instance between heavy elements, such as Bi, Pb, SI). Application of multilayered structures is widespread, while interfaces between such layers often result in special behaviour [28], such as surface density waves [29] or charge- to spin-current conversion [30].

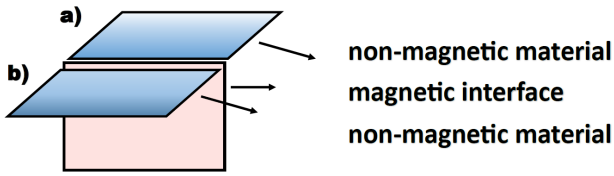

Figure 1.5: Magnetic interface was found between various non-magnetic materials. For the specific experiments see text.

For example a peculiar magnetic behaviour was reported on the interface of two insulating dielectric perovskite oxides at low temperature ($LaAlO_3$ and $SrTiO_3$) [31], see Fig.1.5. It was also shown that highly mobile electron system can be induced at the interface between these perovskite oxides [32]. Similar results were achieved for interface polarization on chromia (Cr_2O_3) with overlayers of both Pd and Pt [33]. Interface magnetization was also shown between dissimilar magnetic materials, i.e Fe/Cu multilayers [34] and organic semiconductor C_6O with a non-magnetic metallic thin film (Cu or Pt) [35].

A study from Caviglia et al. aimed to describe the $LaAlO_3$ and $SrTiO_3$ interface [36]. In this study a highly mobile two-dimensional electron system was found at the interface of the two perovskite.

SOI is proved to be extremely important in explaining the magnetic properties of the aforementioned interfaces [36, 37]. In Ref.[36] the interfacial breaking of inversion symmetry is stressed, which results in large Rashba spin-orbit interaction on the perovskite interfaces [36]. In fact as stated before in this thesis, SOI is present when the charge carrier in its frame of motion experiences a potential gradient (see Section 1.2), which always happens at interfaces.

SOI is used to influence spin control in electron transport processes in many 2D systems [38], for example graphene [39], Aharonov-Bohm rings [40], and even at interfaces, such as between graphene and metallic substrates and complex oxide interfaces (e.g. LaAlO3/SrTiO3) [32]. These properties seem to suggest a great applicability in spin-orbitronics.

In this dissertation I used repulsive Hubbard type interaction to describe the interaction between the electrons. This interaction has the form $H_U = U \sum_i n_{i,\uparrow} n_{i,\downarrow}$, where $U > 0$. The original Hubbard model replaces the long- range Coulomb interaction by an on-site repulsion. This choice can be justified, since in matter, where there are many electrons present the Coulomb repulsion is screened, usually with an exponential damping factor [9]. The difficulty of solving the Hubbard model is caused by the highly correlated electrons, which means that first-order approximations (perturbative methods) cannot be used to make physically correct conclusions about the state of the system. An

exact solution to the Hubbard model is known in 1 dimension, the solutions in higher dimensions mostly belong to low concentration systems.

In general, inter-electron interactions are neglected in the description of processes on surfaces, and the same applies to cases where the properties of the system is explained by possible special features of the band structure, e.g. for graphene. Despite the importance of these phenomena, exact or very good approximations are very rare in this field.

However, there are cases when the studied systems behave as multi-band, highly correlated systems. In the study and description of these we get a very poor quality characterization of the physical properties of the system without taking the interactions between the charge carriers into account. In many cases, these are related to the magnetic properties that appear on the surface, for instance magnetic behaviour on the surface of non-magnetic materials, which in the case of nanostructures makes materials acting as macroscopically dia- or paramagnetic, while at the nano level ferromagnetic [41, 42], or cases where the contact surface of non-ferromagnetic materials becomes ferromagnetic [34, 43, 44]. In several cases, such an effect is thought to occur due to the presence of a spin-orbit interaction [28].

1.6 The method of positive semidefinite operators

In the previous chapter I showed how the spin-orbit coupling can influence the physical behaviour of different many-body systems. Since these effects are usually not negligible, when it comes for either the application or the theoretical understanding of said materials, it is important to further investigate the spin-orbit interaction. This presents a difficulty in the case of strongly correlated systems.

In strongly correlated systems, by definition the strength of the interaction between the electrons is much larger, than the magnitude of the kinetic terms, thus many-body interaction energies dominate the kinetic energies. In order to study many-body strongly correlated systems, the perturbative methods cannot provide solutions, since the SOI coupling is usually many orders of magnitude smaller (often in order of 10^{-2} eV), than the coupling of the electron-electron interaction. Thus several exact methods exist for strongly correlated systems. However, these methods are usually developed for integrable systems [45].

In integrable systems the number of conserved quantities equals to the number of degrees of freedom. This sets a huge constraint, since in real physical systems this is barely never the case, only in very special structures. For example let us consider the following. In a quantum system due to the Heisenberg's uncertainty principle the position $\vec{r}$ and the momentum $\vec{p}$ of a particle can not be simultaneously known with absolute precision. This means that the $\vec{r}$ and $\vec{k}$ field is separated, meaning that in coordinate representation the degrees of freedom is determined by the coordinates in the $\vec{r}$ field. In a realistic many-body system this is of the order of the Avogadro number. This would consequently require $\sim 10^{23}$ constants of motion in the case of integrable systems. This is obviously far from the reality, as in real systems only a couple of constants of motion is preserved.

Thus integrability can only be achieved at the cost of generality and under special circumstances, such as in 1D systems, where the conservation of momentum simplifies to a scalar form and the particles upon colliding exchange their momentum completely. As a result every momentum is preserved, thus for every degree of freedom there is a constant of motion which is conserved ensures the integrability of the system. Not surprisingly most of the integrable systems is one dimensional [46].

For the reasons elaborated above, I use an exact solution method in my research, which can be applied to two-band non-integrable systems, operates on a 2D many-body quantum interacting system, and provides an exact ground state in the presence of spin-orbit interaction. This method is called the method of positive semidefinite operators (PSOs).

The method of PSOs have been successfully applied to study non-integrable systems from the 90's by Brandt and Giesekus [47]. In their work they transformed the Hamiltonian to positive semidefinite form to give exact lower limit to ground state energy. Then they used variation principle to calculate the upper limit, to which compared to the upper limit result gave the ground state energy of the studied system. This was done in the case Hubbard-, and periodic Anderson model. This work from Brand and Giesekus opened the way for many to apply this method on other interesting many-body systems, to derive superconducting [48], ferromagnetic [49], resonating-valence-bond [50] ground states. The method was also applied to study several many-body models, such as the extended Emery-model in 1D and 2D [51], the extended Anderson model [52], the periodic Anderson model in D= $1, 2, 3$ [51, 53, 54, 55] the Falicov-Kimbal model [56], Hubbard model with nearest-neighbour and bond-charge interaction [57]. These studies mostly concentrate on deducing a ground state with already known properties in the frame of the investigated model.

In contrast, a new approach for the PSO method unfolded in the 2000s. In this approach the studied model itself is the starting point, without any knowledge or expectation on the properties of the ground state. In my studies I applied this approach to study the formerly mentioned 2D system in the presence of SOI for two different system fillings: at low-, and high concentration. This technique was also implemented successfully many times before, first in 2007 for diamond square Hubbard chains [58] and after that for pentagon [59], zig- zag hexagon [60], polyphenylene [61] type of chains, thin armchair nanoribbons [62]. In the application of this method the group I work in has a lot of experience [63, 64, 65, 66, 67, 68].

The method has the following steps i) Transforming the Hamiltonian of the studied model in positive semidefinite form, ii) Determining the conditions of the transformation, iii) Deducing the ground state wave function, iv) Investigating the physical properties of the ground state through calculating the ground state expectation values.

The steps of the method were conducted in Chapter 3. Step i) in Section 3.3, Step ii) in Appendix B.3,B.4, Step iii) in Section 3.4, Step iv) in Sections 3.5 and 3.6.

The contents of this dissertation

In Chapter 2 I derive and study flat band conditions for organic conducting polymer chains, in the presence of SOI.

In Chapter 3 using the method based on the properties of positive semidefinite operators I deduced ground state wave functions for a 2D strongly correlated, non-integrable system, in the presence of SOI and Hubbard type interaction.

Based on the ferromagnetic ground state acquired for the 2D model, I presented a possible explanation for the size-dependent ferromagnetism in the case of golden nanograins, in Chapter 4.

The summary follows this chapter, in two languages; english and hungarian.

After the summary, Appendix A and B contains the appendices for Chapter 2 and 3 respectively.

Finally, at the end of this dissertation stands two separate bibliographies; one titled Own publications, where the list of own publications, which form the basis of this dissertation is present. The other one, titled Bibliography contains all the cited publications from the literature.

Chapter 2

Flat bands influenced by SOI in the case of conducting polymers

The contents of this chapter are based on the publications Refs.[O1, O2]. The band structure of a system can be calculated from the secular equation of the one particle part of the Hamiltonian. As such it is determined by the Hamiltonian parameters and have the form:

$$F(E, \{h_i\}, trig_j(\vec{k}\vec{b}_D)) = 0, \tag{2.1}$$

where E is the energy spectrum, $\{h_i\}$ is the set of Hamiltonian parameters, and $\vec{b}_D$ are the Bravais lattice vectors. The $\vec{k}$ momentum is present in the band structure via $trig(\vec{k}\vec{b}_D)$, i.e. as trigonometric functions. Note that the one particle part of the Hamiltonian does not contain inter-electron interaction terms, i.e. in this chapter the Hubbard term introduced in Section 1.5 was not taken into account in the analysed system.

In the case of flat bands, one must eliminate the k dependence from the band structure. $trig(\vec{k}\vec{b}_D)$ from Eq.(2.1) is present additively with the coefficients $X_j(\{h_i\})$.

$$F = X_0(E, \{h_i\}) + \sum_{j=1}^{n} X_j(E, \{h_i\}) trig_j(\vec{k}\vec{b}_D). \tag{2.2}$$

Eliminating k dependence gives us the flat band conditions, in the form of:

$$X_j(\{h_i\}) = 0, \qquad\qquad j = 1, 2..l. \tag{2.3}$$

With Eq.(2.3), a condition remains from Eq.(2.1), $X_{j=0} = 0$, which contains the terms without k dependency. This term is generally used to determine the position of the flat band.

What we can learn from Eq.2.3 is that flat band conditions cause interdependency between the Hamiltonian. If the number of trigonometric terms, with different $X_j(\{h_i\})$ ($j = 1, 2..l$) coefficients in the band structure is l, it means that l of the Hamiltonian parameters are rigidly fixed through the flat band conditions.

In this chapter I describe how the otherwise rigidly fixed flat band conditions can be relaxed by taking SOI into account. Results are presented for both in the presence-, and without applied external magnetic field. Since SOI can be continuously changed with applied external electric field, these results provide broader spectrum of possibilities in engineering flat bands in conducting polymers. The analysed system is a conducting pentagon polymer chain, where nearest neighbour hopping terms, nearest neighbour spin-flip hopping terms (which are the result of the SOI in the system), one-particle potentials are taken into account.

Contents of Chapter 2

In **Section 2.1** I present the studied system, by introducing the Hamiltonian (Subsection 2.1.2), then show how the many-body SOI is present in it (Subsection 2.1.1).

In **Section 2.2** I obtain the band structure from the Hamiltonian transformed to k-space.

Results relating the system without SOI and external magnetic field are presented in **Section 2.3**. Here, from the band structure I calculate the rigid flat band conditions in the system without SOI and external magnetic (B). Then in Subsection 2.3.1 I show the effects of introducing a small perturbation. First by taking small SOI into account, which results in spin-splitted dispersive bands, then by slightly changing a quantity rigidly fixed by the flat band condition, which results in a single double generate dispersive band.

The flat band conditions for the system with SOI are deduced in **Section 2.4** with maintaining the position of the flat band on the energy scale at the same place as the flat band for the system without SOI. In Subsection I present the solutions at 2.4.1 $B = 0$, while in Subsection 2.4.2 at $B \neq 0$.

In **Section 2.5** I derive flat bands for the system with SOI, without maintaining the position of the flat band on the energy scale. The solutions are shown both at $B = 0$ and at $B \neq 0$. In **Section 2.6** I discuss the physical interpretation of the acquired results and show the applied results on the whole band structure of an example, i.e. on a real polyaminotriazole type of polymer. I summarize the result of Chapter 2 in **Section 2.7**.

The appendices for Chapter 2 are in **Appendix A**. Here I first calculate the Peierls phase factors in Appendix A.1. In Appendix A.2 I define quantities seen in the secular equation of the diaganolized matrix of the one-particle part of the Hamiltonian. In Appendix A.3 I show details related to deducting the band structure. At last in Appendix A.4 I present the set of Hamiltonian parameters used to depict the figures in Chapter 2.

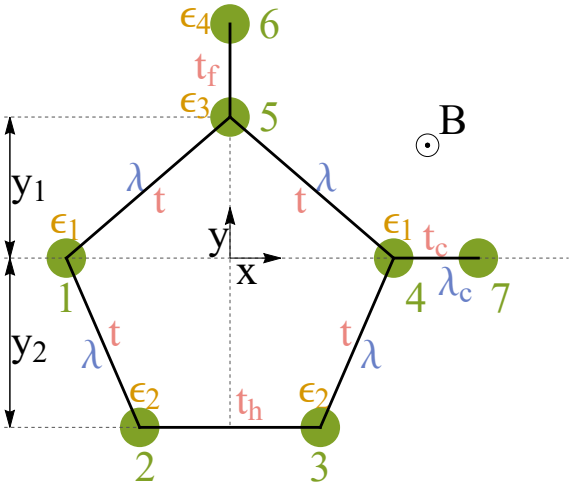

Figure 2.1: The pentagonal unit cell. The nearest neighbour hopping terms (t, t_h, t_c, t_f), nearest neighbour spin-flip hopping terms (λ, λ_c), one-particle potentials $(\epsilon_1, \epsilon_2, \epsilon_3, \epsilon_4)$ and the external magnetic field (B) are pictured. The notation of the in-cell sites are $n = 1, 2, 3, 4, 5, 6$.

2.1 The system analysed

2.1.1 The spin orbit coupling in the studied system

The spin-orbit coupling (H_{SO}) in general has the form $H_{SO} = \lambda\vec{\sigma}\cdot(\vec{\nabla}V \times \vec{p})$ (see Eq.(1.7)). I took Rashba type spin-orbit interaction into account, which in general has the form $H_R = \beta_R(\sigma_x p_y - \sigma_y p_x)$ (see Eq.(1.9)). The presented system is a conjugated polymer, with pentagonal unit cell and itinerant electrons, which move in the x direction (see Fig.2.1), i.e. $p_y = 0, p_x \neq 0$. Consequently in the case of the studied system the first quantized form of the Rashba Hamiltonian is $H_R = \beta_R\sigma_y p_x$ [69], where p_x is the momentum along the x axis, i.e. along the polymer chain. Hence the spin is oriented along the y axis. Since I took Rashba spin-orbit interactions into account, $t_{i,j}^{\uparrow,\downarrow} = -t_{j,i}^{\uparrow,\downarrow}$ [69] and $t_{i,j}^{\uparrow,\downarrow} = -t_{i,j}^{\downarrow,\uparrow}$ holds.

I considered two different spin-orbit couplings in the system (λ, λ_c), to be able to give better description for the systems similar to polyaminotriazole. Since spin-orbit coupling is able to affect the physical processes in carbon atoms to a high degree [70][71], I took into account spin-orbit coupling λ where carbon atoms are usually present (see Fig.2.2), i.e. between the sites of the pentagon except for bond (2,3). These bonds are also distinguished since they provide the conducting nature of the polymer. The second coupling strength λ_c was considered on the bonds between the pentagons (i.e. interbase bonds(4,7)).

In this chapter I discuss how by changing the value of spin-orbit coupling in the system we can achieve flat band in the band structure. It is a natural question then how one is able to change the value of the spin-orbit coupling.

The spin-orbit coupling strength (λ_c) on the interbase bonds can be changed by atomic intercalation on the intercell bonds [72].

In general the strengths of H_{SO} can be continuously tuned by an applied external

electric field [73, 74]. If we apply the external $\vec{\varepsilon} = \varepsilon\vec{n}$ field perpendicular to the plane of the chain, i.e. in the z direction, where $\vec{n}$ is the unit vector in z direction and the source of SOI is exclusively the external electric field, then $\lambda = \lambda_c$, and λ is connected to E via [75]

$$\lambda = \bar{c}\varepsilon, \quad \bar{c} = \frac{|q|\hbar^2}{4m^2c^2}\frac{2\pi}{\lambda_B}. \tag{2.4}$$

Here q and m are the charge and the rest mass of the charge carriers, λ_B is their de Broglie wavelength, and c is the speed of light.

2.1.2 The Hamiltonian of the studied system

To be able to to study the band structure of the system, I start by constructing the Hamiltonian. The system is a pentagon chain, similar to a polyaminotriazole type chain (see on Fig.2.2). The schematic representation of the unit cell is on Fig.2.1. The unit cell contains six sites, with an upper bond ending in one site representing the antenna of the pentagon chain. This consists of the bond (5,6), which is a good enough approach to describe the physical effects of the antenna in the band structure.

The Hamiltonian containing the following parameters (see Fig.2.1): 7 first neighbour hopping terms without spin-flip for each $\uparrow,\uparrow$ and $\downarrow,\downarrow$ (t), 5 first neighbour spin-flip hopping terms, 6 on-site one particle potentials (ϵ) has the form:

$$\begin{aligned} H = \textstyle\sum_i \sum_{\sigma,\sigma'} (\bar{t}_{1,5}^{\sigma,\sigma'} c_{i,1,\sigma}^\dagger c_{i,5,\sigma'} + \bar{t}_{2,1}^{\sigma,\sigma'} c_{i,2,\sigma}^\dagger c_{i,1,\sigma'} + \bar{t}_{4,3}^{\sigma,\sigma'} c_{i,4,\sigma}^\dagger c_{i,3,\sigma'} + \bar{t}_{5,4}^{\sigma,\sigma'} c_{i,5,\sigma}^\dagger c_{i,4,\sigma'} + \\ + \bar{t}_{32}^{\sigma,\sigma} c_{i,3,\sigma}^\dagger c_{i,2,\sigma} + t_c^{\sigma,\sigma'} c_{i+a,7,\sigma}^\dagger c_{i,4,\sigma'} + t_f c_{i,6,\sigma}^\dagger c_{i,5,\sigma} + \text{H.c.}) + \textstyle\sum_{i,n,\sigma} \epsilon_n c_{i,n,\sigma}^\dagger c_{i,n,\sigma}, \end{aligned} \tag{2.5}$$

where $c_{i,n,\sigma}^\dagger$ creates an electron on site $i + r_n$ with the spin σ, where $n = 1, 2, 3, 4, 5, 6$ is the in-cell notation of the sites as seen on Fig.2.1. The hopping terms with bars, are defined in Eq.(2.6) and for further explanation see the text below this paragraph.

The external magnetic field is perpendicular to the plane of the cell, coupled along the z axis. The magnetic induction and the spin vector are perpendicular, thus the Zeeman term provides zero contribution, and the external magnetic field acts only via the Peierls phase factor. The Peierls phase factors describe the effects of the external magnetic field on the orbital motion of the charge carriers.

The calculation detailing the specific Peierls phase factors are in Appendix A.1. As the result of these calculation we differentiate three different phase factors $(\varphi_1, \varphi_2, \varphi_3)$ as follows: $\varphi_{3,2} = \varphi_1, \varphi_{4,3} = \varphi_{2,1} = \varphi_2, \varphi_{5,4} = \varphi_{1,5} = \varphi_3, \varphi_{5,6} = \varphi_{7,4} = 0$. Here $\varphi_{i,j}$ represents the Peierls phase factor, which appears before the corresponding hopping term, i.e. the $t_{i,j}$ hopping, which describes a charge carrier moving from site j to a nearest neighbour site i. In the Hamiltonian the Peierls phase factors are connected to the hopping matrix elements in the following way

$$\begin{aligned} &\bar{t}_{32}^{\sigma,\sigma} = t_h e^{i\varphi_1}, \quad \bar{t}_{21}^{\sigma,\sigma} = te^{i\varphi_2}, \quad \bar{t}_{43}^{\sigma,\sigma} = te^{i\varphi_2}, \quad \bar{t}_{54}^{\sigma,\sigma} = te^{i\varphi_3}, \quad t_{15}^{\sigma,\sigma} = te^{i\varphi_3} \\ &\bar{t}_{21}^{\uparrow,\downarrow} = \lambda e^{i\varphi_2}, \quad \bar{t}_{43}^{\uparrow,\downarrow} = \lambda e^{i\varphi_2}, \quad \bar{t}_{54}^{\uparrow,\downarrow} = -\lambda e^{i\varphi_3}, \quad \bar{t}_{15}^{\uparrow,\downarrow} = -\lambda e^{i\varphi_3}. \end{aligned} \tag{2.6}$$

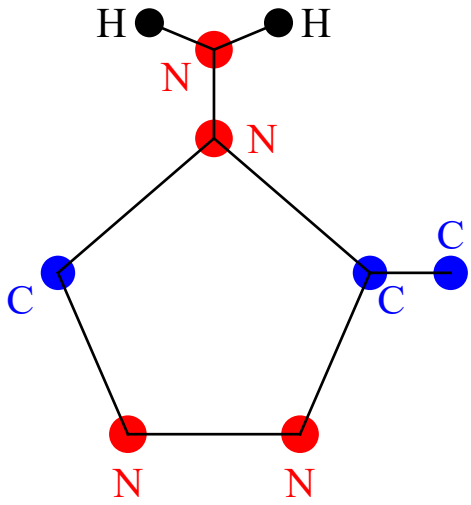

Figure 2.2: The polyaminotriazole cell

The $t^{\sigma,\sigma}_{n,n'}$ are the nearest neighbour hopping terms connecting the sites $i+r_n$ and $i+r_{n'}$ $(n=1,2,..,6)$, while $t^{\sigma,\sigma'\neq\sigma}_{n,n'}$ are the nearest neighbour spin-flip hopping terms, which are the result of spin-orbit interaction(SOI) in the system.

I use the notation $t^{\sigma,\sigma}_{4,7}=t_c, t_h=t^{\sigma,\sigma}_{3,2}, t_f=t^{\sigma,\sigma}_{5,6}, t=t^{\sigma,\sigma}_{1,5}=t^{\sigma,\sigma}_{1,2}=t^{\sigma,\sigma}_{3,4}=t^{\sigma,\sigma}_{4,5}, t^{\sigma,\sigma}_{i,j}=t^{\sigma,\sigma}_{j,i}$, and for the spin-orbit coupling strengths $\lambda=t^{\uparrow,\downarrow}_{5,1}=t^{\downarrow,\uparrow}_{1,5}=t^{\downarrow,\uparrow}_{1,2}=t^{\uparrow,\downarrow}_{2,1}=t^{\downarrow,\uparrow}_{3,4}=t^{\uparrow,\downarrow}_{4,3}=t^{\uparrow,\downarrow}_{4,5}=t^{\downarrow,\uparrow}_{5,4}, t^{\uparrow,\downarrow}_{c}=\lambda_c$.

Considering the symmetry of the unit cell I use the notations for the local one-particle potentials $\epsilon_1=\epsilon_{n=1}=\epsilon_{n=4}, \epsilon_2=\epsilon_{n=2}=\epsilon_{n=3}, \epsilon_3=\epsilon_{n=5}, \epsilon_4=\epsilon_{n=6}$ (see Fig.2.1).

2.2 The band structure

To transform the Hamiltonian (Eq.2.5) to $\vec{k}$-space, the fermionic operators are Fourier transformed as $c_{i,r_n,\sigma}=\frac{1}{\sqrt{N_c}}\sum_k e^{-ik(i+r_n)}c_{n,k,\sigma}$. Here N_c represents, the number of cells and $\vec{k}$ is directed along the x axis (see Fig.2.1). The transformed Hamiltonian becomes:

$$\begin{aligned} H=\sum_k\sum_{\sigma,\sigma'}[& \quad t^{\sigma,\sigma'}_{1,5}\, c^\dagger_{\vec{k},1,\sigma}c_{\vec{k},5,\sigma'}e^{i\vec{k}(\vec{r}_1-\vec{r}_5)} + t^{\sigma,\sigma'}_{2,1}\, c^\dagger_{\vec{k},2,\sigma}c_{i,1,\sigma'}e^{i\vec{k}(\vec{r}_2-\vec{r}_1)} + \\ + & \quad t^{\sigma,\sigma'}_{4,3}\, c^\dagger_{\vec{k},4,\sigma}c_{\vec{k},3,\sigma'}e^{i\vec{k}(\vec{r}_4-\vec{r}_3)} + t^{\sigma,\sigma'}_{5,4}\, c^\dagger_{\vec{k},5,\sigma}c_{\vec{k},4,\sigma'}e^{i\vec{k}(\vec{r}_5-\vec{r}_4)} + \\ + & \quad t^{\sigma,\sigma'}_{c}\, c^\dagger_{\vec{k},1,\sigma}c_{\vec{k},4,\sigma'}e^{i\vec{k}(\vec{a}-\vec{r}_4)} + t_h c^\dagger_{\vec{k},3,\sigma}c_{\vec{k},2,\sigma}e^{i\vec{k}(\vec{r}_3-\vec{r}_2)} + \\ + & \quad t_f c^\dagger_{\vec{k},6,\sigma}c_{\vec{k},5,\sigma}e^{i\vec{k}(\vec{r}_6-\vec{r}_5)} + \text{H.c.}] + \sum_n \epsilon_n c^\dagger_{\vec{k},n}c_{\vec{k},n}. \end{aligned} \tag{2.7}$$

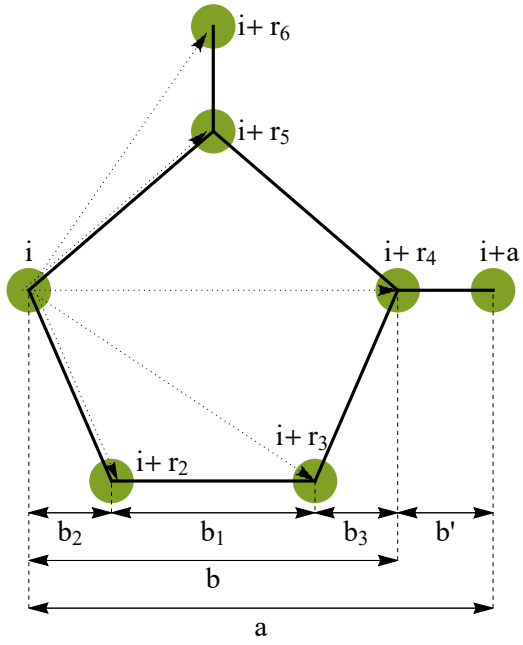

Figure 2.3: Pentagonal unit cell

Here $\vec{a}$ is the lattice vector, $\vec{r}_n$ is the position vector of the nth atom in the cell, while $\vec{r}_1 = 0$ (see Fig.2.3). The dot products in the exponents from Eq.(2.7) can be calculated and are the following

$$\vec{k}(\vec{r}_4 - \vec{r}_3) = \vec{k}(\vec{r}_2 - \vec{r}_1) = kb_2, \quad \vec{k}(\vec{r}_6 - \vec{r}_5) = 0, \quad \vec{k}(\vec{0} - \vec{r}_4) = kb', \quad \vec{k}(\vec{r}_3 - \vec{r}_2) = kb_1,$$
$$\vec{k}(\vec{r}_5 - \vec{r}_4) = \vec{k}(\vec{r}_1 - \vec{r}_5) = \frac{kb}{2}. \tag{2.8}$$

Substituting the exponents from Eq.(2.8) into Eq.(2.7) one gets

$$H = \sum_k \sum_{\sigma,\sigma'} [t_{1,5}^{\sigma,\sigma'} c^\dagger_{\vec{k},1,\sigma} c_{\vec{k},5,\sigma'} e^{i\frac{kb}{2}} + t_{2,1}^{\sigma,\sigma'} c^\dagger_{\vec{k},2,\sigma} c_{i,1,\sigma'} e^{ikb_2} + t_{4,3}^{\sigma,\sigma'} c^\dagger_{\vec{k},4,\sigma} c_{\vec{k},3,\sigma'} e^{ikb_2}$$
$$+ t_{5,4}^{\sigma,\sigma'} c^\dagger_{\mathbf{k},\mathbf{5},\sigma} c_{\vec{k},4,\sigma'} e^{i\frac{kb}{2}} + t_h c^\dagger_{\vec{k},3,\sigma} c_{\vec{k},2,\sigma} e^{ikb_1} + t_f c^\dagger_{\vec{k},6,\sigma} c_{\vec{k},5,\sigma}$$
$$+ t_c^{\sigma,\sigma'} c^\dagger_{\vec{k},1,\sigma} c_{\vec{k},4,\sigma'} e^{ikb'} + h.c.] + \sum_n \epsilon_n c^\dagger_{\vec{k},n} c_{\vec{k},n}. \tag{2.9}$$

We can extract the band structure by diagonalizing the transformed H from Eq.(2.9):

$$H = \sum_k v_k^\dagger \mathbf{M} v_k, \tag{2.10}$$

where $v_k^\dagger = (c_{k,1,\uparrow}^\dagger, \ldots, c_{k,6,\uparrow}^\dagger, c_{k,1,\downarrow}^\dagger, \ldots, c_{k,6,\downarrow}^\dagger)$ and $\mathbf{M}$ can be written in the following form:

$$\begin{pmatrix}
\epsilon_1 & te^{-i\bar{\varphi}_2} & 0 & t_c e^{ikb'} & te^{-i\bar{\varphi}_3} & 0 & 0 & -\lambda e^{-i\bar{\varphi}_2} & 0 & \lambda_c e^{ikb'} & -\lambda e^{-i\bar{\varphi}_3} & 0 \\
te^{i\bar{\varphi}_2} & \epsilon_2 & t_h e^{-i\bar{\varphi}_1} & 0 & 0 & 0 & \lambda e^{i\bar{\varphi}_2} & 0 & 0 & 0 & 0 & 0 \\
0 & t_h e^{i\bar{\varphi}_1} & \epsilon_2 & te^{-i\bar{\varphi}_2} & 0 & 0 & 0 & 0 & 0 & -\lambda e^{-i\bar{\varphi}_2} & 0 & 0 \\
t_c e^{-ikb'} & 0 & te^{i\bar{\varphi}_2} & \epsilon_1 & te^{i\bar{\varphi}_3} & 0 & -\lambda_c e^{-ikb'} & 0 & \lambda e^{i\bar{\varphi}_2} & 0 & \lambda e^{i\bar{\varphi}_3} & 0 \\
te^{i\bar{\varphi}_3} & 0 & 0 & te^{-i\bar{\varphi}_3} & \epsilon_3 & t_f & \lambda e^{i\bar{\varphi}_3} & 0 & 0 & -\lambda e^{-i\bar{\varphi}_3} & 0 & 0 \\
0 & 0 & 0 & 0 & t_f & \epsilon_4 & 0 & 0 & 0 & 0 & 0 & 0 \\
0 & \lambda e^{-i\bar{\varphi}_2} & 0 & -\lambda_c e^{ikb'} & \lambda e^{-i\bar{\varphi}_3} & 0 & \epsilon_1 & te^{-i\bar{\varphi}_2} & 0 & t_c e^{ikb'} & te^{-i\bar{\varphi}_3} & 0 \\
-\lambda e^{i\bar{\varphi}_2} & 0 & 0 & 0 & 0 & 0 & te^{i\bar{\varphi}_2} & \epsilon_2 & t_h e^{-i\bar{\varphi}_1} & 0 & 0 & 0 \\
0 & 0 & 0 & \lambda e^{-i\bar{\varphi}_2} & 0 & 0 & 0 & t_h e^{i\bar{\varphi}_1} & \epsilon_2 & te^{-i\bar{\varphi}_2} & 0 & 0 \\
\lambda_c e^{-ikb'} & 0 & -\lambda e^{i\bar{\varphi}_2} & 0 & -\lambda e^{i\bar{\varphi}_3} & 0 & t_c e^{-ikb'} & 0 & te^{i\bar{\varphi}_2} & \epsilon_1 & te^{i\bar{\varphi}_3} & 0 \\
-\lambda e^{i\bar{\varphi}_3} & 0 & 0 & \lambda e^{-i\bar{\varphi}_3} & 0 & 0 & te^{i\bar{\varphi}_3} & 0 & 0 & te^{-i\bar{\varphi}_3} & \epsilon_3 & t_f \\
0 & 0 & 0 & 0 & 0 & 0 & 0 & 0 & 0 & 0 & t_f & \epsilon_4
\end{pmatrix} \tag{2.11}$$

The new notations used are $\bar{\varphi}_3 = \frac{kb}{2} - \varphi_3, \bar{\varphi}_1 = kb_1 + \phi_1, \bar{\varphi}_2 = kb_2 + \phi_2$.

One derives the diagonalized energies (i.e. the bare band structure) from the secular equation of $\mathbf{M}$. I solved the secular equation, by reducing $\det(\mathbf{M} - E\mathbf{I})$, where E are the energy eigenvalues, $\mathbf{I}$ is the identity matrix. This leads to the following term:

$$\det(\mathbf{M} - E\mathbf{I}) = C(A + iV)(A - iV) = 0, \tag{2.12}$$

where $C = A_f^2 \bar{\epsilon}_2^2 \bar{\bar{\epsilon}}_2^2 \bar{\epsilon}_4^2 \bar{\bar{\epsilon}}_3^2$, $\bar{\bar{\epsilon}}_3 = \bar{\epsilon}_3 - \frac{|t_f|^2}{\bar{\epsilon}_4}$, $\bar{\bar{\epsilon}}_2 = \bar{\epsilon}_2 - \frac{|t_h|^2}{\bar{\epsilon}_2}$, $A_f = \bar{\epsilon}_1 - (t^2 + \lambda^2)\Big(\frac{\bar{\epsilon}_4}{\bar{\epsilon}_3 \bar{\epsilon}_4 - t_f^2} + \frac{\bar{\epsilon}_2}{\bar{\epsilon}_2^2 - t_h^2}\Big)$. Here $\bar{\epsilon}_i = \epsilon_i - E$, $(i = 1, 2, 3, 4)$. The expressions of A and V are detailed in Appendix A.2, while the simplified forms of the two brackets from Eq.(2.12) (i.e. $(A+iV), (A-iV)$) are

$$\begin{aligned}
A + iV = A_f - \frac{1}{A_f}\Bigg(& (\bar{t}_c^* e^{i\varphi_k} - \frac{-\lambda^2 + t^2}{\bar{\bar{\epsilon}}_3} e^{i\varphi} + \frac{-\lambda^2 + t^2}{\bar{\epsilon}_2 \bar{\bar{\epsilon}}_2} t_h) i(\bar{\lambda}_c e^{i\varphi_k} + \frac{2\lambda t}{\bar{\bar{\epsilon}}_3} e^{i\varphi} - \frac{2\lambda t}{\bar{\epsilon}_2 \bar{\bar{\epsilon}}_2} t_h) \Bigg) \\
& \Bigg((\bar{t}_c e^{-i\varphi_k} - \frac{-\lambda^2 + t^2}{\bar{\bar{\epsilon}}_3} e^{-i\varphi} + \frac{-\lambda^2 + t^2}{\bar{\epsilon}_2 \bar{\bar{\epsilon}}_2} t_h) - i(\bar{\lambda}_c^* e^{-i\varphi_k} + \frac{2\lambda t}{\bar{\bar{\epsilon}}_3} e^{-i\varphi} - \frac{2\lambda t}{\bar{\epsilon}_2 \bar{\bar{\epsilon}}_2} t_h) \Bigg), \\
A - iV = A_f - \frac{1}{A_f}\Bigg(& (\bar{t}_c^* e^{i\varphi_k} - \frac{-\lambda^2 + t^2}{\bar{\bar{\epsilon}}_3} e^{i\varphi} + \frac{-\lambda^2 + t^2}{\bar{\epsilon}_2 \bar{\bar{\epsilon}}_2} t_h) - i(\bar{\lambda}_c e^{i\varphi_k} + \frac{2\lambda t}{\bar{\bar{\epsilon}}_3} e^{i\varphi} - \frac{2\lambda t}{\bar{\epsilon}_2 \bar{\bar{\epsilon}}_2} t_h) \Bigg) \\
& \Bigg((\bar{t}_c e^{-i\varphi_k} - \frac{-\lambda^2 + t^2}{\bar{\bar{\epsilon}}_3} e^{-i\varphi} + \frac{-\lambda^2 + t^2}{\bar{\epsilon}_2 \bar{\bar{\epsilon}}_2} t_h) + i(\bar{\lambda}_c^* e^{-i\varphi_k} + \frac{2\lambda t}{\bar{\bar{\epsilon}}_3} e^{-i\varphi} - \frac{2\lambda t}{\bar{\epsilon}_2 \bar{\bar{\epsilon}}_2} t_h) \Bigg),
\end{aligned} \tag{2.13}$$

where $\bar{t}_c = t_c e^{2i\varphi_3}$,$\bar{\lambda}_c = \lambda_c e^{-2i\varphi_3}$, $\varphi_k = ka + \varphi$.

I derived the flat band conditions, from the expression of $(A + iV) = 0$. Note that one can arrive to the same conclusions from the expression of $(A - iV) = 0$. I show this in Appendix A.3.

The $(A + iV)$ from Eq.(2.13) can be written as:

$$(A + iV) = X_0 + X_1 \cos(\varphi_k) + X_2 \sin(\varphi_k) = 0. \tag{2.14}$$

The above equation is an example for the band structure written in the form of F from Eq.(2.2). In order to achieve flat bands in the band structure, we have to eliminate the k-dependence from Eq.(2.14) Thus the conditions for the flat bands considering a general

simple pentagon base are $X_0 = 0, X_1 = 0, X_2 = 0$:

$$
\begin{aligned}
X_0 &= A_f - \frac{1}{A_f}\Big((\lambda_c^2 + t_c^2) + (\lambda^2 + t^2)^2\Big(\frac{1}{\bar{\bar{\epsilon}}_3^2} + \frac{t_h^2}{\bar{\epsilon}_2^2\bar{\bar{\epsilon}}_2^2} - \frac{t_h}{\bar{\epsilon}_2\bar{\bar{\epsilon}}_2\bar{\bar{\epsilon}}_3}2\cos(\varphi)\Big)\Big) = 0,\\
X_1 &= \frac{1}{A_f}\Big(- \cos(2\varphi_3+\varphi)\frac{2(2\lambda t\lambda_c + t_c(\lambda^2 - t^2))}{\bar{\bar{\epsilon}}_3} - \sin(2\varphi_3+\varphi)\frac{2(-2\lambda t t_c + \lambda_c(\lambda^2 - t^2))}{\bar{\bar{\epsilon}}_3} +\\
&\quad + \cos(2\varphi_3)\frac{2(2\lambda t\lambda_c + t_c(\lambda^2 - t^2))t_h}{\bar{\epsilon}_2\bar{\bar{\epsilon}}_2} + \sin(2\varphi_3)\frac{2(-2\lambda t t_c + \lambda_c(\lambda^2 - t^2))t_h}{\bar{\epsilon}_2\bar{\bar{\epsilon}}_2}\Big) = 0,\\
X_2 &= \frac{1}{A_f}\Big(\cos(2\varphi_3+\varphi)\frac{2(-2\lambda t t_c + \lambda_c(\lambda^2 - t^2))}{\bar{\bar{\epsilon}}_3} - \sin(2\varphi_3+\varphi)\frac{2(2\lambda t\lambda_c + t_c(\lambda^2 - t^2))}{\bar{\bar{\epsilon}}_3} -\\
&\quad - \cos(2\varphi_3)\frac{2(-2\lambda t t_c + \lambda_c(\lambda^2 - t^2))t_h}{\bar{\epsilon}_2\bar{\bar{\epsilon}}_2} - \sin(2\varphi_3)\frac{2(2\lambda t\lambda_c + t_c(\lambda^2 - t^2))t_h}{\bar{\epsilon}_2\bar{\bar{\epsilon}}_2}\Big) = 0.
\end{aligned}
\tag{2.15}
$$

From this point on, my aim is to show how the SOI influences the rigid flat band conditions. For this very reason let us first investigate these conditions in the system without SOI and external magnetic field.

2.3 Rigid flat band conditions for the system without external magnetic and SOI

I fixed the arbitrary value of zero for the energy eigenvalue, i.e. the position of the flat band, when calculating the flat band conditions in this case. This means that the flat band will appear on the horizontal axis and consequently while calculating the flat band conditions $\bar{\epsilon}_i = \epsilon_i$ $(i = 1, 2, 3, 4)$ holds.

In this case $X_1(\lambda, \lambda_c = 0, \varphi_3 = 0) = 0, X_2(\lambda, \lambda_c = 0, \varphi_3 = 0) = 0$ gives the same condition, therefore the conditions for the flat bands can be summarized in two expressions. These are the following:

$$
\begin{aligned}
X_0(\lambda, \lambda_c = 0, \varphi_3 = 0) &= \frac{(\epsilon_1 - t^2(\frac{\epsilon_4}{\epsilon_f} + \frac{\epsilon_2}{\epsilon_2^2 - t_h^2}))^2 - t^4(\frac{\epsilon_4}{\epsilon_f} - \frac{t_h}{\epsilon_2^2 - t_h^2})^2 - t_c^2}{\epsilon_1 - \epsilon_4\frac{t^2}{\epsilon_f} - \epsilon_2\frac{t^2}{\epsilon_2^2 - t_h^2}} = 0,\\
X_1(\lambda, \lambda_c = 0, \varphi_3 = 0) &= \frac{2t^2 t_c(\frac{\epsilon_4}{\epsilon_f} - \frac{t_h}{\epsilon_2^2 - t_h^2})}{\epsilon_1 - \epsilon_4\frac{t^2}{\epsilon_f} - \epsilon_2\frac{t^2}{\epsilon_2^2 - t_h^2}} = 0,
\end{aligned}
\tag{2.16}
$$

where $\epsilon_f = \epsilon_3\epsilon_4 - t_f^2$. These conditions in this specific system are an example of the general $X_j(\{h_i\}) = 0$ conditions introduced in Eq.(2.3) .

The $X_1(\lambda, \lambda_c = 0, \varphi_3 = 0) = 0$ from Eq.(2.16) can be reduced to:

$$
\frac{\epsilon_4}{\epsilon_f} - \frac{t_h}{\epsilon_2^2 - t_h^2} = 0. \tag{2.17}
$$

From Eq.(2.17) we calculate t_f. From Eq.(2.16) $X_0(\lambda, \lambda_c = 0, \varphi_3 = 0) = 0$ condition we

get the value of t_c:

$$t_{f|_{1,2}} = \pm\frac{\sqrt{-\epsilon_4(\epsilon_2^2 - t_h^2) + \epsilon_3\epsilon_4 t_h}}{\sqrt{t_h}}, \quad t_{c|_{1,2}} = \pm\frac{(\epsilon_2 + t_h)(\epsilon_1(\epsilon_2 - t_h) - t^2)}{\sqrt{(\epsilon_2^2 - t_h^2)^2}}. \quad (2.18)$$

From Eq.(2.18) we have the flat band conditions for the system without SOI and external magnetic field. These I refer to as the rigid conditions providing flat bands, since they simultaneously fix the value of two hopping matrix elements t_f, t_c. This seems to set a great difficulty in the way of engineering flat bands.

These solutions for the flat band conditions for the system without SOI and magnetic field are in agreement with literature [64].

2.3.1 The results of deviating from the rigid flat band conditions

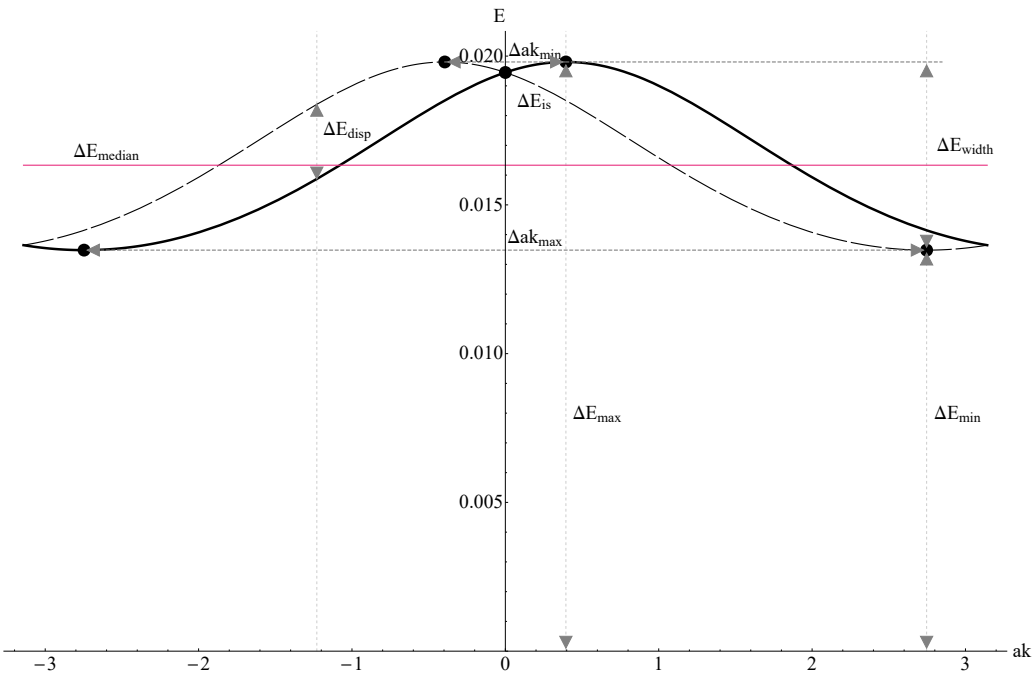

Figure 2.4: Band structure with the flat band on the horizontal axis, and the two dispersive bands, achieved by setting $\lambda/t = 0.2$. Different E quantities are shown, which we will use to describe how the SOI is able to alter the flat band (see Fig.2.5). These quantities are given in t units. The Hamiltonian parameters used for the calculation are in A.4/ Table A.1.

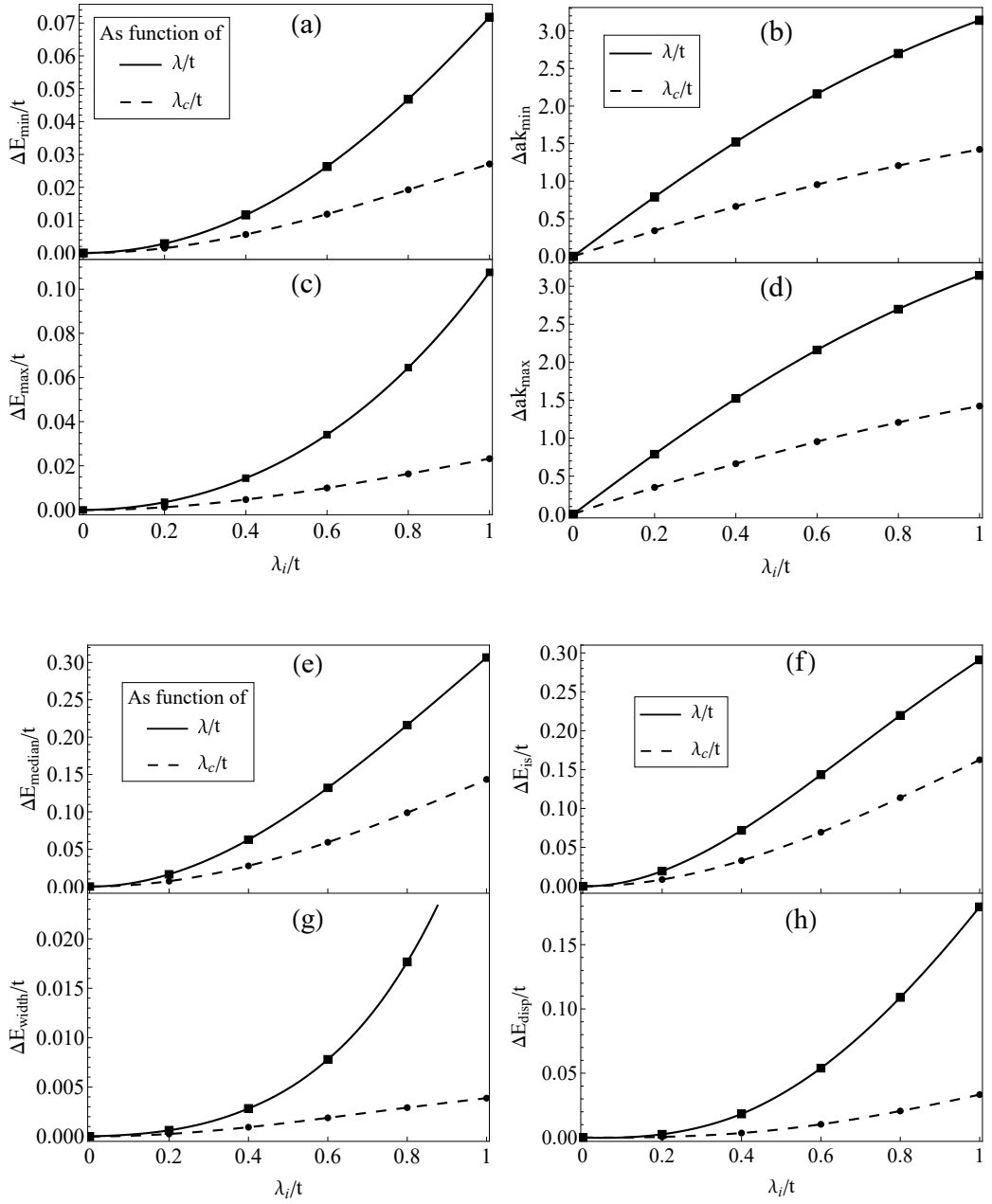

Figure 2.5: (a) Minimum- (ΔE_{min}), (b) maximum E values (ΔE_{max}) of the dispersive band, (c) The distance between the positions of the two minimum- (Δak_{min}), (d) the two maximum(Δak_{max}) of the two dispersive bands. (e) The position of the median (ΔE_{median}), (f) the width of the dispersive band (ΔE_{width}) (g) The position of the intersection point (ΔE_{is})of the two dispersive band and (h) the maximal distance between the bands (ΔE_{disp}). The figures are as the fuction of λ_i/t: λ_c/t in the case of the dashed line, and λ/t in the case of the solid line.

To demonstrate the rigidity of the flat band conditions deduced in Section 2.3 I show how changing two different parameters can change the acquired flat band into dispersive bands. In the former Section I provided strict restrictions for two of the hopping couplings t_c and t_f (Eq.(2.18)), which I refer to as the rigid flat band conditions.

I first show that considering a non zero spin-orbit coupling strength the formerly shown flat band, which we described in the absence of spin-orbit coupling, turns into two dispersive bands. These dispersive bands are not double degenerate, which is the result of SOI in the system. The spin splitting of the bands in the presence of SOI is a well-documented phenomenon (see Section 1.3). Fig.2.4 shows the two dispersive bands.

Fig.2.5 shows how the properties of the dispersive bands as the function of λ and λ_c. Minimum-, and maximum energy values; the distance between the two minimum-, and maximum of the two dispersive bands; the location of the median; the width of the dispersive band; the position of the intersection point-; and the maximal distance between the bands are shown. The quantities presented are explained on Fig.2.4.

The flat band can also cease to exist if we do not consider SOI in the system. By changing the value of the Hamiltonian parameters, given by the flat band conditions, we also arrive to a dispersive band. In this case the dispersive band is double degenerate. On Fig.2.6 there is a dispersive band pictured by changing t_c value by 8.62%.

Fig.2.7 shows the changes of the depicted properties of the dispersive bands (see $\Delta\bar{E}_{median}, \Delta\bar{E}_{max}, \Delta\bar{E}_{min}$ on Fig.2.6), namely the distance of the median-, maximum and minimum of the dispersive band from the formerly existing flat band as function Δt_c.

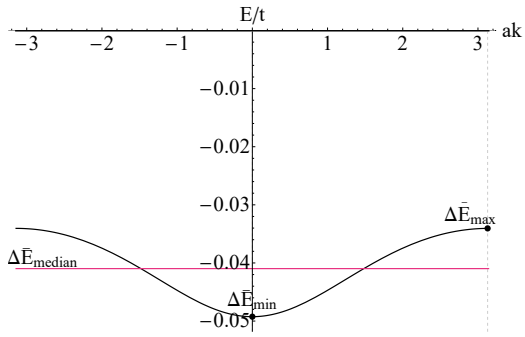

Figure 2.6: Band structure with the flat band on the horizontal axis and the dispersive band without SOI, only changing the t_c value given by flat band conditions by 8.62%. The line in the middle shows the median of the band. The $\Delta\bar{E}$ values are there to describe how altering t_c effects the flat band. The $\Delta\bar{E}$ values are in t units. The Hamiltonian parameters used for the calculation are in A.4/ Table A.1.

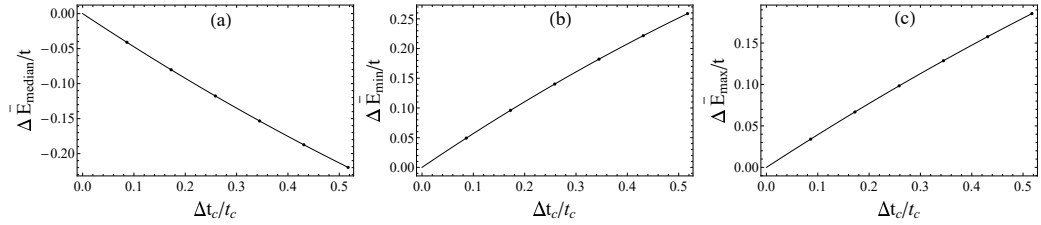

Figure 2.7: Describes how the flat band, which was originally located on the horizontal axis changes to a double degenerate dispersive band, after the value of t_c is changed by Δt_c. The presented cases: the distance between the flat band and (a) the median- ($\Delta \bar{E}_{median}$), (b) the maximum- ($\Delta \bar{E}_{max}$), (c) the minimum ($\Delta \bar{E}_{min}$) of the dispersive band. The Hamiltonian parameters used for the calculation are in A.4/ Table A.1.

2.4 The role of SOI in recreating the flat band at the same position of the energy axes

2.4.1 Without external magnetic field present ($B = 0$)

Now the question is if it is possible to achieve flat band structure considering there is a non zero spin-orbit coupling strength in the system. Furthermore if it is possible to achieve flat bands by changing the spin-orbit coupling strengths λ and λ_c, while the rigid flat band conditions for two hopping parameters t_c, t_f are not fulfilled.

To answer these questions, we turn our attention to the flat band conditions $X_0(\lambda, \lambda_c \neq 0, B = 0) = 0$ and $X_1(\lambda, \lambda_c \neq 0, B = 0), X_2(\lambda, \lambda_c \neq 0, B = 0) = 0$.

$$
\begin{aligned}
X_0(\lambda, \lambda_c \neq 0, B = 0) &= A_f - \frac{1}{A_f}\left((\lambda_c^2 + t_c^2) + (\lambda^2 + t^2)^2\left(\frac{1}{\bar{\bar{\epsilon}}_3^2} + \frac{t_h^2}{\bar{\epsilon}_2^2\bar{\bar{\epsilon}}_2^2} - 2\frac{t_h}{\bar{\epsilon}_2\bar{\bar{\epsilon}}_2\bar{\bar{\epsilon}}_3}\right)\right) = 0, \\
X_1(\lambda, \lambda_c \neq 0, B = 0) &= -\frac{2}{A_f}\left(2\lambda t\lambda_c + t_c(\lambda^2 - t^2)\right)\left(\frac{\epsilon_4}{\epsilon_f} - \frac{t_h}{\epsilon_2^2 - t_h^2}\right) = 0, \\
X_2(\lambda, \lambda_c \neq 0, B = 0) &= -\frac{2}{A_f}\left(2\lambda t t_c - \lambda_c(\lambda^2 - t^2)\right)\left(\frac{\epsilon_4}{\epsilon_f} - \frac{t_h}{\epsilon_2^2 - t_h^2}\right) = 0.
\end{aligned}
\tag{2.19}
$$

Since the $X_1(\lambda, \lambda_c \neq 0, B = 0) = 0, X_2(\lambda, \lambda_c \neq 0, B = 0) = 0$ shares a common multiplier, they can be summarized in a single condition:

$$
\left(\frac{\epsilon_4}{\epsilon_f} - \frac{t_h}{\epsilon_2^2 - t_h^2}\right) = 0. \tag{2.20}
$$

The condition Eq.(2.20) is also the only solution to simultaneously satisfy the $X_1(\lambda, \lambda_c \neq 0, B = 0) = X_2(\lambda, \lambda_c \neq 0, B = 0) = 0$ conditions, since complex solutions for the spin-orbit couplings are not physical. The expression Eq.(2.20) was also seen in Eq.(2.17), and

we used it to calculate the value of t_f:

$$t_{f|_{1,2}} = \pm \frac{\sqrt{-\epsilon_4(\epsilon_2^2 - t_h^2) + \epsilon_3 \epsilon_4 t_h}}{\sqrt{t_h}}. \tag{2.21}$$

This means, that the t_f value for the system with SOI remains the same as the one for the system without SOI considered.

From $X_0(\lambda, \lambda_c \neq 0, B = 0) = 0$ one obtains a λ or λ_c value. This was done numerically.

Turning our attention back to the question if it is possible to achieve flat band in the system with SOI after perturbing the rigid conditions given by the flat band conditions for the system without SOI or magnetic field (see Eq.(2.18)).

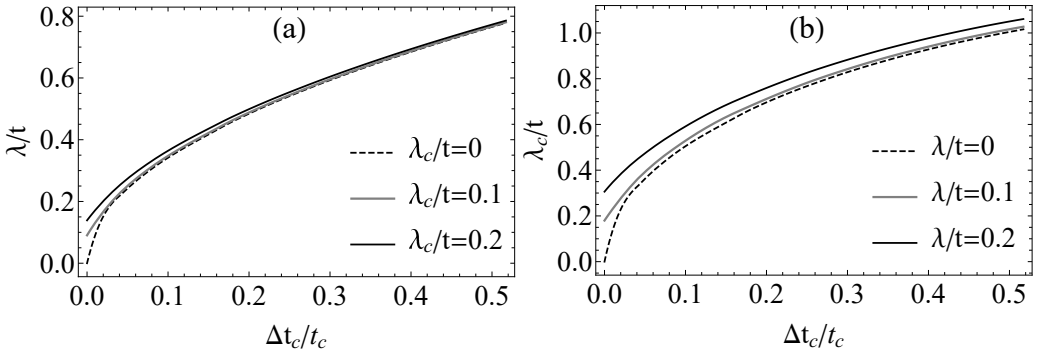

Figure 2.8: (a) The calculated λ values required to get a flat band structure in the case of three different fixed λ_c values, after modifying the t_c value defined by the flat band conditions with Δt_c (b) The calculated λ_c values required to get a flat band structure in the case of three different fixed λ values, after modifying the t_c value defined by the flat band conditions with Δt_c The parameters used for this demonstration are detailed in A.4/Table A.1.

Fig.2.8 shows the λ and λ_c values calculated from $X_0(\lambda, \lambda_c \neq 0, B = 0) = 0$ condition. With these spin-orbit coupling strengths we can obtain flat bands from the dispersive band achieved by the perturbation of the initial t_c values (see Fig.2.7). From Fig.2.8 we can observe that even 50% changes in the t_c can be compensated for with λ, λ_c values.

From Fig.2.8 one can also notice, that λ (inter-base SOI strength) possesses a better ability in compensating for the perturbed t_c values, since smaller values of λ are sufficient to achieve a flat band for the same Δt_c magnitudes.

Fig.2.9 shows $\Delta t_f/t_f$, $\Delta t_c/t_c$ values which can be compensated by λ, λ_c values. Note that the flat band condition for t_f is exactly the same as the flat band condition for t_f in the system without SOI (see Eq.(2.21),(2.18)). This is due to fixing the position of the flat band ($E = E_{inital} = 0$). In the next section I discuss how we can also relax the rigid condition for the value of t_f by not fixing the position of the flat band to its initial

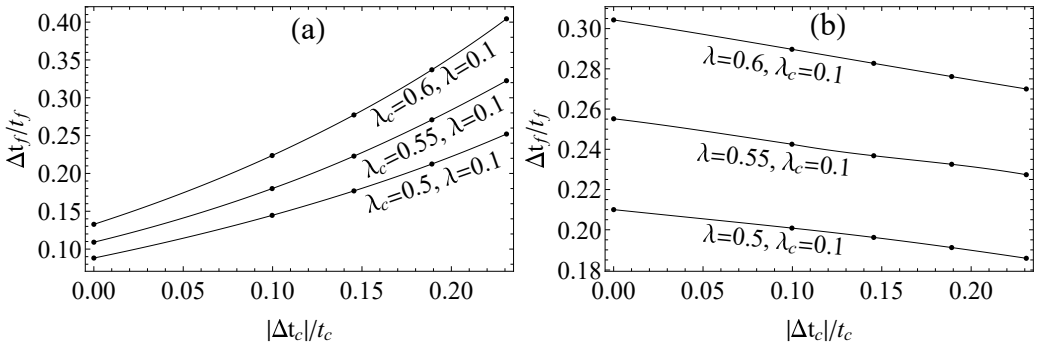

Figure 2.9: The λ, λ_c values necessary to achieve a flat band structure after changing the t_c value defined by the flat band conditions with Δt_c. The Δt_f values are achieved by modifying the t_h hopping magnitude, thus t_h is continuously changing along the solid lines, form the original t_h to $1.5t_h$. The parameters used for this demonstration are detailed in Appendix A.4/Table A.1.

position (i.e. $E \neq E_{inital}$). Hence in this case Δt_f values were achieved by changing the magnitude of t_h. The results are shown on Fig.2.9.

Changing the value of t_f through modifying t_h can be done by changing the side group connected to the pentagon (as in Fig.2.2, where the side group NH_2 is in the top (apical) part of the figure, i.e. the antenna of the unit cell).

At the same time the counter apical (as the N-N bond in Fig.2.2) t_h hopping coupling has to be also modified. In the case of polyaminotriazole, this can be achieved by doping polyaminotriazole with ClO_4 ($PATClO_4$), fluorine (PATF), HF_2 ($PATHF_2$), etc.

On Fig.2.9 it seems that greater λ_c values can compensate for greater Δt_f values in transforming the dispersive band to flat band. Increasing the SOI strength along the intercell bonds (i.e. λ_c) is possible, and usually done by introducing heavy ions on intercell bonds [72].

Finally on Fig.2.10 $\bar{\lambda} = \lambda = \lambda_c$. This case emerges if the values of λ, λ_c are small and intrinsic, i.e. spin-orbit enhancing methods discussed above (doping, heavy ion implantation) were not used and external side groups (apical atoms) are not present. The $\bar{\lambda}$ then can be tuned by external electric field (as seen in Eq.(2.4)).

2.4.2 In external magnetic field ($B \neq 0$)

The external magnetic field in the system acts through the Peierls phase factors. In the case of conducting polymers three separate phase factors were calculated $\varphi_1, \varphi_2, \varphi_3$ (see Appendix A.1). If the base of the conducting polymer is a regular pentagon all corner

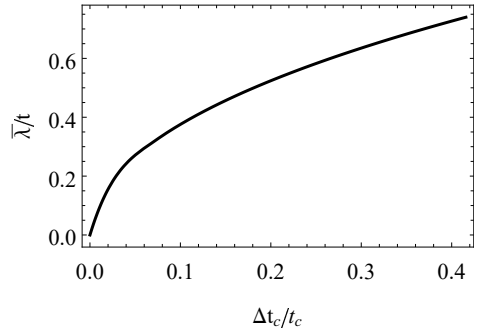

Figure 2.10: The $\bar{\lambda} = \lambda = \lambda_c$ value required to compensate the deviation of $\Delta t_c \neq 0$ from the t_c defined by the initial flat band conditions, in order to re-create the flat band at the origin of the energy axis. The Hamiltonian parameters used for the calculation are in Appendix A.4/ Table A.1.

angles are equal, thus $\varphi = 5\varphi_3$. In the case of a general pentagon $\varphi = \varphi_1 + 2\varphi_2 + 2\varphi_3$. Using the notation $\varphi_b = \varphi_1 + 2\varphi_2$ the flat band conditions for a general pentagon are:

$$\begin{aligned}
X_0 &= A_f - \frac{1}{A_f}\left((\lambda_c^2 + t_c^2) + (\lambda^2 + t^2)^2\left(\frac{1}{\bar{\bar{\epsilon}}_3^2} + \frac{t_h^2}{\bar{\epsilon}_2^2\bar{\bar{\epsilon}}_2^2} - \frac{t_h}{\bar{\epsilon}_2\bar{\bar{\epsilon}}_2\bar{\bar{\epsilon}}_3}2\cos(2\varphi_3 + \varphi_b)\right)\right) = 0,\\
X_1 &= \frac{-1}{A_f}\left(\cos(4\varphi_3 + \varphi_b)\frac{v}{\bar{\bar{\epsilon}}_3} + \sin(4\varphi_3 + \varphi_b)\frac{u}{\bar{\bar{\epsilon}}_3} - \cos(2\varphi_3)\frac{vt_h}{\bar{\epsilon}_2\bar{\bar{\epsilon}}_2} - \sin(2\varphi_3)\frac{ut_h}{\bar{\epsilon}_2\bar{\bar{\epsilon}}_2}\right) = 0,\\
X_2 &= \frac{1}{A_f}\left(\cos(4\varphi_3 + \varphi_b)\frac{u}{\bar{\bar{\epsilon}}_3} - \sin(4\varphi_3 + \varphi_b)\frac{v}{\bar{\bar{\epsilon}}_3} - \cos(2\varphi_3)\frac{ut_h}{\bar{\epsilon}_2\bar{\bar{\epsilon}}_2} - \sin(2\varphi_3)\frac{vt_h}{\bar{\epsilon}_2\bar{\bar{\epsilon}}_2}\right) = 0.
\end{aligned} \tag{2.22}$$

where $v = 2(2\lambda t\lambda_c + t_c(\lambda^2 - t^2))$, $u = 2(-2\lambda t t_c + \lambda_c(\lambda^2 - t^2))$ Here X_1, X_2 can be written as:

$$\begin{aligned}
X_1 = \frac{1}{A_f}(-K_g v - S_g u), \quad X_2 = \frac{1}{A_f}(K_g u - S_g v).\\
K_g = \frac{\cos(4\varphi_3 + \varphi_b)}{\bar{\bar{\epsilon}}_3} - t_h\frac{\cos(2\varphi_3)}{\bar{\epsilon}_2\bar{\bar{\epsilon}}_2}, S_g = \frac{\sin(4\varphi_3 + \varphi_b)}{\bar{\bar{\epsilon}}_3} - t_h\frac{\sin(2\varphi_3)}{\bar{\epsilon}_2\bar{\bar{\epsilon}}_2}.
\end{aligned} \tag{2.23}$$

Since for the spin-orbit couplings λ, λ_c we considered real, positive numbers, the $X_1, X_2 = 0$ conditions can be summarized in the equations $K_g = 0, S_g = 0$.

By rearranging $K_g = 0, S_g = 0$ conditions from Eq.(2.23) one gets:

$$\frac{\cos(2\varphi_3)}{\cos(4\varphi_3 + \varphi_b)} = X_\varphi, \frac{\sin(2\varphi_3)}{\sin(4\varphi_3 + \varphi_b)} = X_\varphi, \tag{2.24}$$

where $X_\varphi = \frac{\epsilon_4(\epsilon_2^2 - t_h^2)}{\epsilon_f t_h}$. Using trigonometric identities Eq.(2.24) can be fulfilled as:

$$\sin[(4\varphi_3 + \varphi_b) - 2\varphi_3] = \sin(\varphi) = 0. \tag{2.25}$$

Which for φ gives the solutions $\varphi = \pm s\pi$, where $s \in \mathbb{Z}$. Thus the possible solutions for X_φ are ± 1, where the upper sign is acquired at $s = 0$, and with that we get back the result for the system in the limit of zero external magnetic field. This way we arrive for the result in the system with external magnetic field while $X_\varphi = -1$.

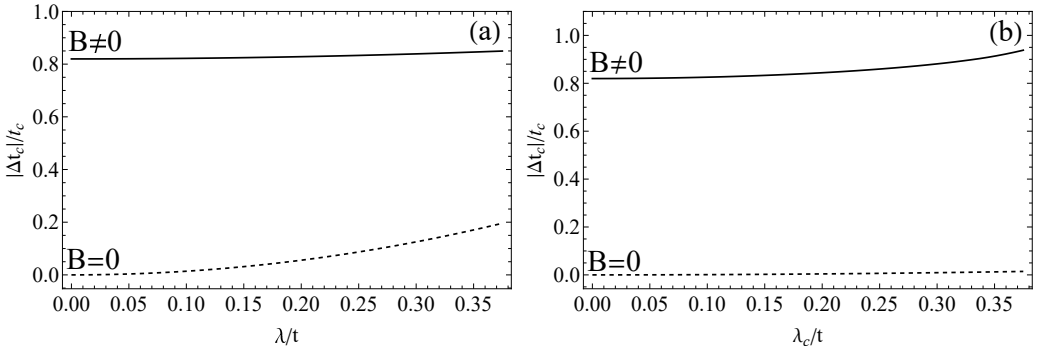

Figure 2.11: This figure shows the (a) λ and (b) λ_c values required to achieve the flat band structure, after changing the t_c value defined by the flat band conditions with Δt_c, while in the case of solid line $B \neq 0$ ($X_\varphi = -1$), in the case of dashed line $B = 0$ ($X_\varphi = 1$) holds. The parameters used for this demonstration are detailed in Appendix A.4/Table A.2.

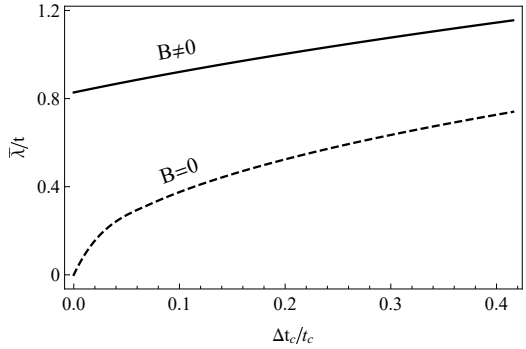

Figure 2.12: This figure shows the $\bar{\lambda}$ values required to achieve the flat band structure, after changing the t_c value defined by the flat band conditions with Δt_c, while in the case of solid line $B \neq 0$ ($X_\varphi = -1$), in the case of dashed line $B = 0$ ($X_\varphi = 1$) holds. The parameters used for this demonstration are detailed in Appendix A.4/Table A.3.

At $B \neq 0$, i.e. $X_\varphi = -1$ from Eq.(2.24), one gets the

$$\frac{\epsilon_4}{t_h}\frac{\epsilon_2^2 - t_h^2}{\epsilon_f} = -1 \tag{2.26}$$

condition.

I used condition Eq.(2.26) to compare the rigidly fixed flat band conditions in the system without external magnetic field to the present case, where external magnetic

field is present. For this purpose I calculated the value of t_f from the condition Eq.(2.26). The difference between the t_f values set by the flat band conditions in the system with-, and without external magnetic field is denoted by Δt_f. I found that there are four discreet Δt_f values; two for each t_f solution at $B = 0$ from Eq.(2.21):

$$\Delta t_f = \frac{\sqrt{t_h \epsilon_4}}{t_h} \left(\pm \sqrt{(\epsilon_2^2 + t_h(\epsilon_3 - t_h))} \pm \sqrt{(-\epsilon_2^2 + t_h(\epsilon_3 + t_h))} \right). \tag{2.27}$$

As a conclusion, when we fixed the position of the flat band E, we lost the opportunity to relax the rigid condition relating t_f. At $B = 0$, in the system with SOI the conditions for t_f remained the same (Eq.(2.21)) as in the system without SOI (Eq.(2.18)). At $B \neq 0$ these conditions changed (Eq.(2.27)), but remained similarly restrictive in quality. From the remaining $X_0 = 0$ condition we can deduce the λ or λ_c values. These results are shown on Fig.2.11.

Similarly to Fig.2.10, on Fig.2.12 I show results relating a system with only small, intrinsic $\lambda = \lambda_c$ values.

To conclude the results regarding the system at non-zero external magnetic field I found that achieving flat bands is possible at discreet φ values (see Eq.(2.25)). This consequently means that flat bands can exist at discreet B external magnetic field values, since φ is a Peierls phase factor through which the external magnetic field acts in the system. At the same time deviations from the rigidly fixed t_f value can be done by the calculated discreet Δt_f values (see Eq.(2.27)). In this case the value of t_c is no longer fixed and great deviations from the initial t_c values can be achieved by modifying the spin-orbit coupling magnitudes λ and λ_c (see Fig.2.11). One can also conclude that greater Δt_c values can be compensated for with the same SOI strengths, than in the system without external magnetic field.

2.5 The role of SOI in recreating the flat band without maintaining its former position

In the former section (Section 2.4) we analysed how we can recreate flat band bands at the same position at the energy axes ($E = E_{inital} = 0$). First I showed that changing the parameters (t_c, t_f) set by the rigid flat band conditions (see Section 2.3), results in a dispersive band (see Subsection 2.3.1). Tuning the SOI, changing it from zero to a value determined by flat band conditions helped us to achieve a flat band again at the same position on the energy scale.

Now I am going to show how the same can be done, without maintaining the position of the flat band (i.e. $E \neq E_{inital}$).

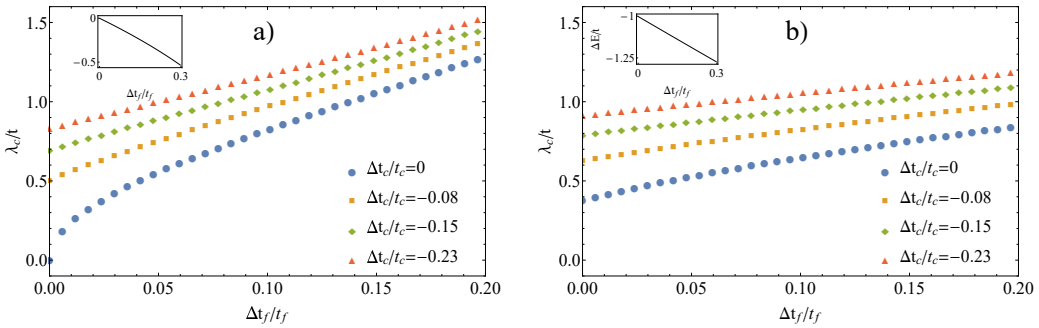

Figure 2.13: Changing both t_f and t_c from the initial their initial values determined by the rigid flat band conditions for the system without SOI we acquire a dispersive band. The λ_c values are able to compensate the common deviations of these changed parameters a) when $B = 0$, and b) in the presence of B external field. The flat band created this way reappears at ΔE position, as shown on the inset. In this case $\Delta t_c/t_c < 0$. The parameters used for this demonstration are detailed in Appendix A.4/Table A.4.

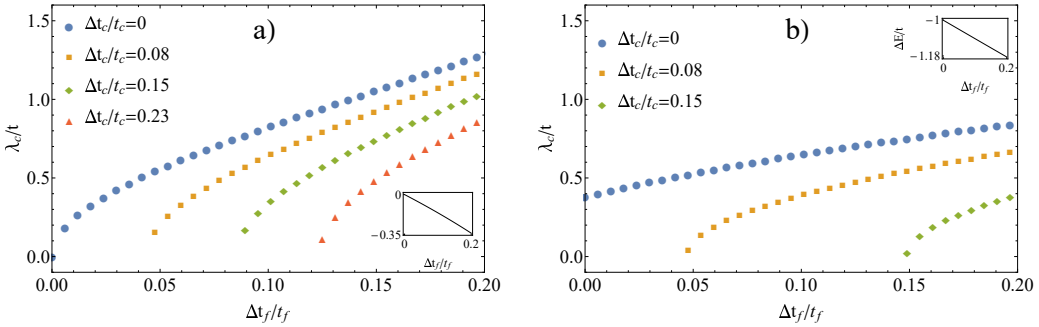

Figure 2.14: The λ_c spin orbit coupling values required to compensate the common deviations of $\Delta t_c \neq 0$ and $\Delta t_f \neq 0$ at a) $B = 0$, and b) $B \neq 0$ in order to re-create a flat band placed originally (at $\lambda = \lambda_c = B = 0$) in the origin of the energy axis $E = 0$. The flat bands acquired this way are placed at $E = \Delta E$, as shown on the inset. $\Delta t_c/t_c > 0$ and $\lambda = 0$ holds. The parameters used for this demonstration are detailed in Appendix A.4/Table A.4.

The initial t_c, t_f values, set by the rigid flat band conditions, which were obtained in Eq.(2.18) were changed by the depicted Δt_c and Δt_f values, which resulted in dispersive bands. Fig.2.13 shows $\Delta t_c/t_c < 0$ values, while Fig.2.14 shows $\Delta t_c/t_c > 0$ values which were calculated to compensate for the common deviations of t_c, t_f in recreating the flat bands.

If we consider small, intrinsic λ and λ_c, we can tune the SOI strength via external electric field. This results in the $\bar{\lambda} = \lambda = \lambda_c$ case, which I show on Fig.2.15, which was plotted at non-zero, constant external magnetic field B. From Fig.2.15 one can conclude that a wider range of Δt_c, Δt_f deviations can be compensated for (even 30%) with

relatively small $\bar{\lambda}$ values of order 10^{-1}.

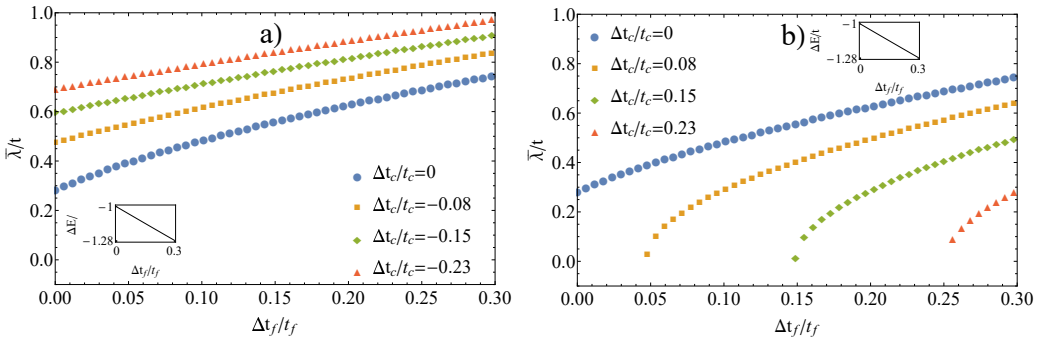

Figure 2.15: The $\lambda_c = \lambda = \bar{\lambda}$ values required to make up for the common deviations $\Delta t_c \neq 0$ and $\Delta t_f \neq 0$ at $B \neq 0$ and a) $\Delta t_c/t_c < 0$, and b) $\Delta t_c/t_c > 0$, in order to re-create a flat band placed originally (at $\bar{\lambda} = B = 0$) at $E = 0$. The flat bands acquired this way are placed at $E = \Delta E$, as shown on the inset. The parameters used for this demonstration are detailed in Appendix A.4/Table A.4.

2.6 Further comments on the physical interpretation of the acquired results

I would like to address some of the possible questions readers might ask themselves after reading this Chapter so far.

One notices, that this study was presented in a way of a mathematical description. This allowed me to show, that flat bands can be found generally in a similar, arbitrary system. As oftentimes done in the literature; flat band conditions were deduced, while simultaneously providing the positions of the flat bands on the energy scale.

Furthermore, the Hamiltonian parameters presented in Table A.1-A.4 in Appendix A.4 also show that the results concluded in this chapter does not belong to only one specific material, but instead to a broad spectrum of application. These Hamiltonian parameters have not been first introduced in my thesis, on the contrary: they are known and often used in the literature. For this reason the way these parameters influence the band structure is generally known. For example it is know how the Peierls phase factors -representing the effects of the external magnetic field on the orbital motion of itinerant electrons- affect the brand structure [58, 76, 77]. In the case of conducting polymers the influence of hopping parameters (t_i) and on-site one particle potentials (ϵ_i) were reported several times [64, 78, 79, 80]. It was also seen many times how SOI effects the band structure (most of the times causing spin-splitting of the bands, as seen 1.3.1), for example in [81, 82].

Additionally, there are terms which were taken into consideration, but not implemented in the Hamiltonian, in Eq.(2.5). Next I give the proper reasoning concerning

these terms. First -as addressed before under the text of Eq.(2.5) - the Zeeman term as a consequence of the configuration of the system provides no contribution. Since the spin of the electrons is perpendicular the external magnetic field $\vec{B}$, the scalar product $\vec{B} \cdot \vec{\sigma} = 0$.

The second terms relates to the electric dipole moment $\vec{p}$. If it is present in the system it appears as an additional term for the external magnetic field. In the studied system, if a dipole moment vector exists, it is on the plane stretched by x and y axes. The origin of $\vec{p}$ is typically inside the unit cell. Additionally, it can be noted that the magnitude of $\vec{p}$ is relatively small, in order and often below 1 debye [83]. Moreover, the applied external field $\vec{\varepsilon}$ in the presented system is perpendicular to the plane of the unit cell, thus $\vec{\varepsilon} \cdot \vec{p} = 0$, meaning that Stark terms are also not present. I would like to add, that sometimes increasing the dipole moment is done for the purpose of enriching the application possibilities of the polymer (e.g. in capacitor devices, solar energy technology). This can be achieved through the introduction of specific functional groups with large dipole moment [84]. The results obtained in this chapter remain applicable for systems with the aforementioned constellation, but the external electric field must be additionally renormalized by the attained dipole moments.

Instead of just the band flattened by the SOI, I illustrated the whole band structure for polyaminotriazole at $B = 0$ on Fig.2.16. The Hamiltonian parameters for polyaminotriazole type polymer I used for plotting Fig.2.16 are from the literature: $t_f/t = 1$ (see Ref.[78, 79]), $t_h/t = 0.93, t_c/t = 1.06, \epsilon_1/t = \epsilon_2/t = 0.33, \epsilon_3/t = 1.66, \epsilon_4/t = 0.8$ (see Ref.[85]).

In the presented system in the absence of external magnetic field and SOI, flat bands-according to the rigid flat band conditions (see Eq.(2.18)) -would appear at the fixed $t_f = 1.406$, $t_c = 1.996$ values (in t units). As it is not the case, the starting point of the band structure is one without a flat band present. At the calculated value of $\lambda/t = 0.17$ however, a flat band appears, meaning λ results in a $\Delta t_f/t_f = 0.40$, $\Delta t_c/t_c = 0.88$ relaxation of the rigid flat band conditions.

In this case, the flat band appears at $E/t = 0.35$, i.e. at the place of the third band (see Fig.2.16.a). Note, that changing a sign in the Hamiltonian parameters, generally results in the flat band appearing at a different position.

The reason why the flat bands appear is explained in this chapter as the following: From the secular equation $[F(\epsilon, \{h_i\}, trig_j(\vec{k}\vec{b}_D) = 0$, see Eq.(2.1)] of the H transformed in $\vec{k}$ space the band structure is calculated. The $X(\{h_i\})$ coefficients are defined only by the energy E and the set of Hamiltonian parameters $\{h_i\}$. The band structure $E_n(k)$ is calculated from the $F = 0$ secular equation. Since flat bands are $\vec{k}$ independent, they can be acquired when all $X_j = 0$ is met. Then the position of the flat band can be obtained by the remaining $X_0 = 0$ condition. The $X_j = 0$ requirements are achieved by tuning the set of Hamiltonian parameters $\{h_i\}$. In this clear, mathematical manner flat bands can be achieved. This mathematical description has the advantage that it can be generally applied for any arbitrary system to obtain flat bands. Consequently the presented method can be applied not just on a special, but on any given system by tuning the corresponding Hamiltonian parameters, as done before many times [86, 87].

For example in the case of a simple cubic latte in tight binding approximation

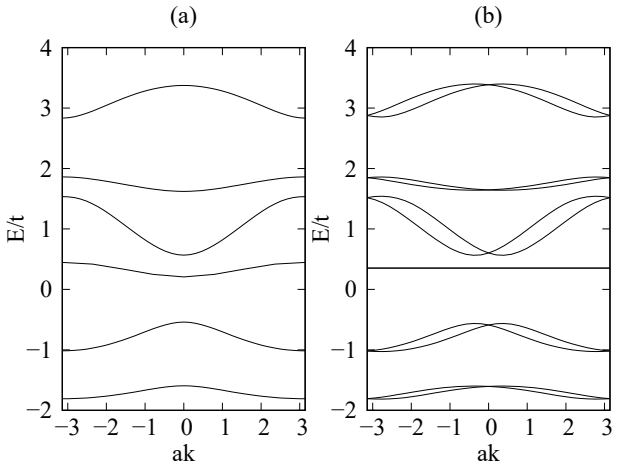

Figure 2.16: The effects of the many-body spin orbit coupling on the whole band structure. Dispersive bands are present on Plot a), where $\lambda = \lambda_c = B = 0$. At $B = 0$ $\lambda/t = 0.178$ provides a double degenerate flat band on Plot b) (see Appendix A.2). The Hamiltonian parameters used are described in the text.

from $F = 0$ we obtain the band structure $E - A_0 - A_1[cos(xk_x) + cos(yk_y) + cos(zk_z)] = 0$, while $X_0 = \epsilon - A_0, X_1 = A_1 \sim t$ holds, where t is the nearest neighbour hopping integral. Thus the flat band appears at $E = A_0$ if the flat band condition $T_1 = A_1 = 0$ is met.

The physical interpretation behind the formed flat band when all of the $X_j = 0$ flat band conditions are met can be vastly different in every case. In the presented example for the cubic lattice $X_1 = 0$ happens when there is no nearest neighbour overlap. This can be achieved by increasing the lattice constant at fixed particle number, meaning the charge carrier concentration decreases, i.e. we arrive to a low concentration, localized insulating state (for example a Wigner lattice, as the Coulomb repulsion appears without exception).

On the other hand, which makes understanding the physical phenomena behind flat bands even more complex, is the fact that there are flat bands with not localized charge carriers (see e.g. Ref.[59]). If charge carriers are localized in the flat bands, the emergence of the flat bands (i.e. meeting all $X_j = 0$ conditions) are linked to the destructive interference, often as the result of frustration or lattice geometry (see [86, 87]).

In the presented work I focused on conducting pentagon polymer chains. The flat band states for these are reported to consist of localized one-particle Wannier states, which are extended over two cells (i.e. can be given by a linear combination of extended Bloch states) [79]. For the two cell extension of the Wannier states constructive interference seems to be a viable explanation. All things considered, the most important to take away is, that no matter how we physically explain Eq.(2.3), namely the $X_j = 0$ conditions, the method explored here remains applicable.

2.7 Summary

In this chapter flat band conditions for conductive polymers with pentagon chains were obtained. The choice of the studied system is not only supported by the broad application of said polymers (see Section 1.4), but also by the fact that this way flat band conditions can be explored in a general, clear manner. Additionally, in the presented system I also had the opportunity to take into account two different spin-orbit coupling term; for the inter-cell (λ_c) and the in-cell (λ).

Despite the fact that flat bands are sought after, engineering flat-bands represents a challenging task. This is due to the rigorous flat band conditions for these systems, which are known to cause interdependencies between the Hamiltonian parameters. These can be achieved only by extensive tuning of the Hamiltonian parameters. In my study I first presented these rigid flat band conditions for two of the Hamiltonian parameters t_c and t_f.

After this I showed how the flat bands acquired by tuning the value of t_c and t_f become dispersive band in two cases. First by introducing a small spin-orbit coupling (see Fig.2.5). In the first case introducing the SOI in the system resulted in two spin-splitted dispersive bands. The spin-splitting properties of the SOI was not unexpected, it has been documented extensively in the literature (see Sect. 1.3).

Changing the t_c values defined by the flat band conditions with Δt_c also resulted in a dispersive band, which was double degenerate. I showed how introducing SOI in the system is able to transform this dispersive band back to a flat band. At first this was done while preserving the original position (E) of the flat band. In this case $20-30\%$ deviation from the t_c value was compensated by the SOI (see Fig.2.8). In the presence of magnetic field this increased to $\sim 80\%$ (see Fig.2.11). In the case of small, intrinsic SOI $\bar{\lambda} = \lambda = \lambda_c$ solutions were obtained at $B = 0$ (see Fig.2.10), and $B \neq 0$ (see Fig.2.12).

I studied how the flat band conditions change if we let the reflattened band appear at a new position on the energy scale (ΔE). Mathematically this means one less flat band conditions, which in this case was used to deduce ΔE, the new positions of the formed flat band. This way the rigid flat band conditions are not restrictive anymore. The energy of the flat band relative to the the initial flat band energy ($E/\Delta E$) changed around $10-20\%$ on an arbitrary energy scale. The formally restricted parameters t_f, t_c could be changed with around $20-30\%$ at $B = 0$ (see Fig.2.13) and the presence of external magnetic field seems to enhance the relaxing properties of SOI even more (see Fig.2.14).

These results seem to be promising from the standpoint of application in real systems. This is due to the fact that SOI can be modified with different methods. Tuning λ_c can be achieved by doping with heavy intrachain atoms. There are options which provide even continuous tuning possibilities for SOI strengths such as twisting, torsioning. Even more promisingly applied external electric field was found to be able to continuously change the strengths of SOI [69].

The contents of this chapter are based on the publications Refs.[O1, O2]. The corresponding thesis point is Thesis point 1.

Chapter 3

Spin-orbit interactions in two dimensional strongly correlated systems

This chapter is based on the publications Refs.[O3, O4, O5]. In this chapter I studied a two dimensional, itinerant, non integrable system in the presence of spin-orbit coupling, with two bands, one of which being correlated. The electrons in the correlated band interact through a Hubbard type interaction. My goal was to calculate the exact ground state wave function in order to investigate the physical properties of the system. Due to the non-integrability of the system the method based on the properties of positive semidefinite operators was applied to deduce an exact ground state (see Section 1.6).

The method has the following steps i) Transforming the Hamiltonian of the studied model in positive semidefinite form, ii) Determining the conditions of the transformation (matching equations), iii) Deducing the ground state wave function, iv) Investigating the physical properties of the ground state through calculating the ground state expectation values.

As step i) of the method the transformation of the Hamiltonian of the system can be done to the following positive semidefinite form:

$$\hat{H} = \hat{P} + C, \tag{3.1}$$

where $\hat{P}$ is a positive semidefinite operator and C is a constant. A Hamiltonian can be transformed to different PSO forms. These transformation belong to different Hamiltonian parameter space region. In step ii) one describes the conditions of the transformation. By transforming the Hamiltonian into positive semidefinite form as described in Eq.(3.1), what we gain is that we know what the smallest possible eigenvalue may be, which is in the case of positive semidefinite operators is zero. As the iii) step then, the ground state wave function $|\Psi_g\rangle$ can be written as the most general wave function, which satisfies the

$\hat{P}|\Psi_g\rangle = 0$ condition. Comparing this with Eq.(3.1) we can see that then the energy of the ground state E_g is C.

With the acquired ground state wave function in step iv) one can calculate the expectation values of the physical quantities, which stand in the focus of the attention. In the case of the presented 2D system my interest revolved around the magnetic behaviour of the system, and how the SOI can affect it (see Section 1.5). Moreover the mobility of the charge carriers influenced by SOI was also investigated, since it is also an important aspect in spinorbitronics.

Contents of Chapter 3

The structure of this Chapter is as follows: in **Section 3.1** I present the system I studied and its Hamiltonian in **Section 3.2** I take a look at the physical behaviour of the system in the light of the effects SOI has on the band structure. Here I provide the motivation to explore the exact ground state using the positive semidefinite operator method presented in **Section 3.3** and **Section 3.4**. In the latter I calculate the exact ground state wave function of the presented system at high- (Subsection 3.4.1), and low concentration (Subsection 3.4.2).

In **Section 3.5**, I show the physical quantities calculated using the exact ground state derived at high concentration: the expectation value of the spin z projection (Subsection 3.5.1) and the expectation value of the distance-dependent hopping ground state (Subsection 3.5.2). In this section I also discuss the dependence of these quantities on the strength of the spin-orbit interaction. In **Section 3.6**, I discuss the physical quantities resulting from the ground state wave function derived at low concentration.

In **Section 3.7** I expand the model introduced before, by taking next nearest-neighbour terms (i.e. plaquette diagonal hopping terms) and spin-flip on-site one-particle potentials into account. Here for the expanded model I apply the PSO method and compare the extracted ground state wave functions at low-, and high concentration to the ground state wave functions of the original model (the model without the new terms taken into account). I frame my work with the summary in **Section 3.8**.

Appendix B contains the corresponding appendices for Chapter 3. Appendix B.1 includes the transformation of the Dresselhaus- and Rashba type interactions to second quantized form. In Appendix B.2 I show the matching equations in a detailed manner, which form a system of 74 non-linear coupled equations with complex coefficients. A detailed solution to the matching equations is given in Appendix B.3. I present the restricted parameter space, where the deducted wave function represents the ground state of the studied system in Appendix B.4. In Appendix B.5 I transform the one-particle part of the Hamiltonian into $\vec{k}$-space, then I solve the secular equation of the Hamiltonian matrix to explore the band structure. In Appendix B.6, I transform the wavefunction into $\vec{k}$ -space. I calculate the ground state expectation value of the spin z component (Appendix B.6.1) and the ground state r-dependent hopping expectation value (Appendix B.6.2), which are also described in detail. In Appendix B.7 the matching equations for the expanded model and their solution are shown.

3.1 The system analysed

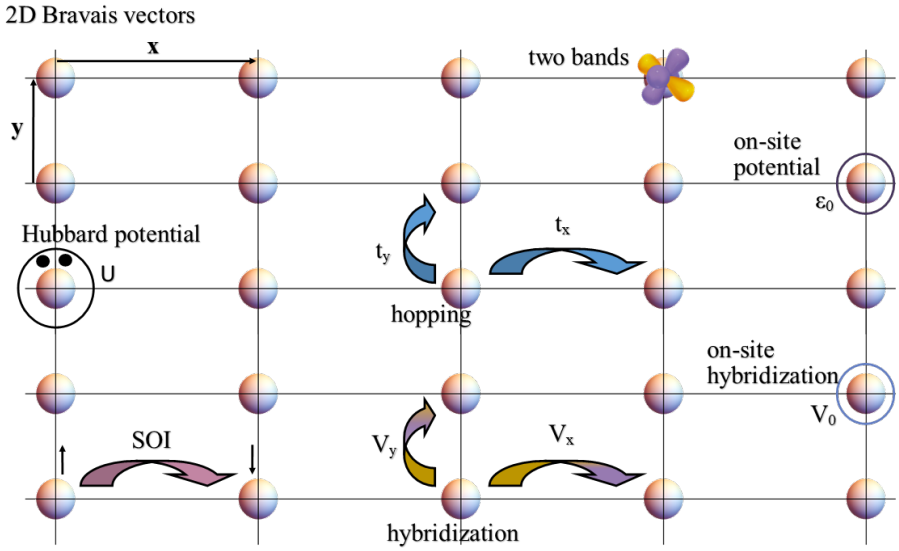

Figure 3.1: The studied system : correlated 2D surface with two bands, on-site Coulomb repulsion U and SOI, first neighbour hoppings and hybridizations, on-site potentials and hybridizations. The Bravais vectors are denoted with $\mathbf{x}$ and $\mathbf{y}$.

Correlations are know to enhance SOI [88], or vice versa, while multi-orbital treatment is important for the description of effects caused by SOI [32,33]. For this reason the studied system is a two-dimensional quadratic lattice with two bands (which I denoted by d and f), with one of them being the correlated band (band f), which does hybridise with the non correlated band (band d).

Note that the use of two bands does not diminish the applicability of the deduced results because for a multiband material the theoretical description is given usually by projecting the multiband structure in a few-band picture [89]. Thus for its relative simplicity I considered two bands.

The interaction between the electrons of the correlated band is present via the on-site Coulomb interaction ($U_f > 0$). In this system there are on-site one-particle potentials (ϵ_0), on-site (V_0)-, and nearest neighbour (V_x, V_y) hybridizations, nearest-neighbour hopping terms (t_x, t_y) present, as denoted on Fig.3.1. Given by the many-body spin–orbit interactions, I also considered spin-flip hopping terms.

The Bravais lattice vector are $\mathbf{x}$ and $\mathbf{y}$ (See Fig.3.1). In the following calculations I have taken the translational symmetry into account and used periodic boundary conditions. On a site $\mathbf{i}$ there are two orbitals ($c = d, f$), and on each orbital two electron with opposite spin projections can be present. Thus in the case of maximum system filling, there are four electrons on each site of the lattice. Electrons are not localised to a certain site, meaning I consider a lattice with itinerant electrons.

3.1.1 The Hamiltonian of the studied system

I constructed the one-particle part of the Hamiltonian based on these considerations:

$$\hat{H}_1 = \hat{V}_0 + \sum_{\mathbf{p}=\mathbf{x},\mathbf{y}} \left[\hat{V}_{\mathbf{p}} + \sum_{c=d,f} \left(\hat{H}_{c,0} + \hat{H}_{c,\mathbf{p}} \right) \right], \tag{3.2}$$

The local terms $(\hat{H}_{c,0}, \hat{V}_0)$ in H_1 (See Eq.(3.2)) are:

$$\hat{H}_{c,0} = \sum_{\mathbf{i}} \sum_{\alpha=\uparrow,\downarrow} \epsilon_c^{\alpha,\alpha} \hat{c}^\dagger_{\mathbf{i},\alpha} \hat{c}_{\mathbf{i},\alpha}, \quad \hat{V}_0 = \sum_{\mathbf{i}} \left[\left(\sum_{\alpha=\uparrow,\downarrow} V_0^{d,f,\alpha,\alpha} \hat{d}^\dagger_{\mathbf{i},\alpha} \hat{f}_{\mathbf{i},\alpha} \right) + \text{H.c.} \right]. \tag{3.3}$$

Here $\hat{c}_{\mathbf{j},\alpha}$, $(c = d, f)$ are Fermi operators. Every electron in the system gives an energy contribution in the form of an one-site one-particle potential contribution in the Hamiltonian $(\hat{H}_{c,0})$. The $\epsilon_c^{\alpha,\alpha}$ has no site index, since the the sites in the Bravais lattice are equivalent. The $\hat{V}_0$ terms contribute for the hybridisation in the system: $V_0^{d,f,\alpha,\alpha}$ contributes for the electron hopping from the orbital f on site i to the orbital d on site i, while its hermitian conjugate stands for an electron hopping from the orbital d on site i to the orbital f on site i.

In addition to the local terms, I considered the first neighbour terms:

$$\hat{H}_{c,\mathbf{p}} = \sum_{\mathbf{i}} \left[\left(\sum_{\alpha=\uparrow,\downarrow} t_{\mathbf{p}}^{c,\alpha,\alpha} \hat{c}^\dagger_{\mathbf{i}+\mathbf{p},\alpha} \hat{c}_{\mathbf{i},\alpha} \right) + t_{\mathbf{p}}^{c,\downarrow,\uparrow} \hat{c}^\dagger_{\mathbf{i}+\mathbf{p},\downarrow} \hat{c}_{\mathbf{i},\uparrow} + t_{\mathbf{p}}^{c,\uparrow,\downarrow} \hat{c}^\dagger_{\mathbf{i}+\mathbf{p},\uparrow} \hat{c}_{\mathbf{i},\downarrow} + \text{H.c.} \right],$$

$$\hat{V}_{\mathbf{p}} = \sum_{\mathbf{i}} \left[\sum_{\alpha=\uparrow,\downarrow} \left(V_{\mathbf{p}}^{d,f,\alpha,\alpha} \hat{d}^\dagger_{\mathbf{i}+\mathbf{p},\alpha} \hat{f}_{\mathbf{i},\alpha} + V_{\mathbf{p}}^{f,d,\alpha,\alpha} \hat{f}^\dagger_{\mathbf{i}+\mathbf{p},\alpha} \hat{d}_{\mathbf{i},\alpha} \right) + \text{H.c.} \right], \tag{3.4}$$

where the first term in $\hat{H}_{c,\mathbf{p}}$ describes a hopping to the $\mathbf{p}$ direction (between sites $\mathbf{i}$ and $\mathbf{i}+\mathbf{p}$), while the spin projection remains the same, while the second term in $\hat{H}_{c,\mathbf{p}}$ describes a hopping to the $\mathbf{p}$ direction with spin-flip. This latter is the result of the presence of spin-orbit coupling in the system. $\hat{V}_{\mathbf{p}}$ stands for those first neighbour hoppings, which happen with hybridization.

The inter-electronic interaction part of the Hamiltonian is represented via a Hubbard type (local Coulomb type) interaction in the correlated (f) orbital:

$$\hat{H}_{int} = \sum_{\mathbf{i}} U_f \hat{n}^f_{\mathbf{i},\uparrow} \hat{n}^f_{\mathbf{i},\downarrow}. \tag{3.5}$$

The Hamiltonian of the system with $\hat{H}_1$ presented in Eq.(3.2), $\hat{H}_{int}$ in Eq.(3.5) is:

$$\hat{H} = \hat{H}_1 + \hat{H}_{int}. \tag{3.6}$$

3.1.2 The spin-orbit coupling in the studied system

In Eq.(3.4) the spin-flip terms in $\hat{H}_{c,\mathbf{p}}$ are the result of SOI. Often SOI is represented phenomenologically [90, 91].

If there is no spin-orbit interaction, there are no hopping terms with a spin-flip, in the absence of external fields. If an electron is hopping it can change the spin projection by its orbital momentum interacting with the spin. The term of the Hamiltonian containing such spin-flip hopping contributions is $\hat{H}_{c,\mathbf{p}}$ from Eq.(3.4). In the case of a 2D dimensional square lattice, two main types of spin-orbit interactions are considered: one is the Rashba - and the other is the Dresselhaus interaction:

$$\hat{H}_{SO,c} = \sum_{\mathbf{i}} \left[\sum_{\mathbf{p}=\mathbf{x},\mathbf{y}} \left(V^{c,\mathbf{p}}_{\uparrow,\downarrow} \hat{c}^{\dagger}_{\mathbf{i}+\mathbf{p},\uparrow} \hat{c}_{\mathbf{i},\downarrow} + V^{c,\mathbf{p}}_{\downarrow,\uparrow} \hat{c}^{\dagger}_{\mathbf{i}+\mathbf{p},\downarrow} \hat{c}_{\mathbf{i},\uparrow} \right) + \text{H.c.} \right], \tag{3.7}$$

where for fixed c the $V^{c,\mathbf{x}}_{\uparrow,\downarrow} = V^c_R - iV^c_D, V^{c,\mathbf{x}}_{\downarrow,\uparrow} = -V^c_R - iV^c_D, V^{c,\mathbf{y}}_{\uparrow,\downarrow} = V^c_D - iV^c_R, V^{c,\mathbf{y}}_{\downarrow,\uparrow} = -V^c_D - iV^c_R$, and V^c_R, V^c_D are the Rashba, and Dresselhaus interaction strengths. In order to have uniform notations throughout this thesis the spin-flip terms in Eq.(3.7) will be denoted by t instead of V, for example: $V^{c,\mathbf{x}}_{\uparrow,\downarrow} = t^{c,\uparrow,\downarrow}_{\mathbf{x}}$, etc.

The Rashba type of SOI appears when a potential has some asymmetric behaviour in a direction perpendicular to the plane of the unit cell (i.e. perpendicular to the surface). I note that an electric field connected perpendicular to a surface can induce a Rashba interaction [3] and tune its magnitude as seen in Chapter 2. Dresselhaus spin-orbit interaction occurs in cases where the system does not have inversion symmetry. A more detailed explanation of the spin-orbit interaction terms can be found in Section 1.2. Deducing the second quantized form, i.e. the form of Eq.(3.7) can be found in Appendix B.1.

3.2 The effects of SOI on the band structure

To gain insight into the physical behaviour of this system, we turn our attention to the band structure, which is attained from the one-particle part of the Hamiltonian $\hat{H}_1$, transformed to $\vec{k}$-space (see Appendix B.5).

On Fig.3.2/a) I show the band structure of a system without spin-orbit coupling. The $\uparrow,\downarrow$ signs on the bands, are meant to represent the double degenerated nature of the band, caused by spin-projection degeneracy.

For simplicity, the energy values as function of $\vec{k}$ are shown at $k_y = 0$, while the first Brillouin zone is between the borders of the k_x axis. Thus the kx changes between $-\pi$ and $+\pi$, while $\vec{x}$ is the Bravais vector in the x direction. The energy values are in $t^{d,\uparrow,\uparrow}_x$ unit.

In contrast I show a system with spin-flip process present on Fig.3.2/b). The spin-flip terms appear in the form of spin-flip on-site one-particle potentials. In this case

the two bands seen Fig.3.2/a) split into two bands, thus the spin double degeneracy ceases to exist. The bands signed with ± contain the two different spin projections with different weights. As seen from Fig.3.2 introducing SOI in the system causes the energy bands to split.

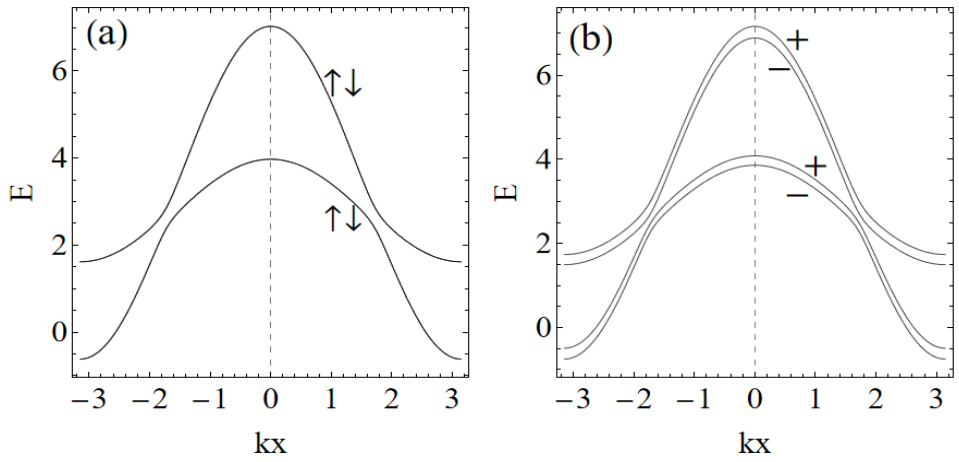

Figure 3.2: a) The band structure with no SOI present. The parameters are in $t_x^{d,\sigma,\sigma} = t_x^d$ units and each parameter only different in their σ indices are equal. The Hamiltonian parameters used for plotting are $t_x^{d,\uparrow,\uparrow} = 1.0; t_y^{d,\uparrow,\uparrow} = 1.1; \epsilon_d^{\uparrow,\uparrow} = 0.5; t_x^{f,\uparrow,\uparrow} = 1.5; t_y^{f,\uparrow,\uparrow} = 1.6; \epsilon_f^{\uparrow,\uparrow} = 0.1; V_0^{d,f,\uparrow,\uparrow} = -1.2; V_x^{d,f,\uparrow,\uparrow} = V_x^{f,d,\uparrow,\uparrow} = 0.6; V_y^{d,f,\uparrow,\uparrow} = V_y^{f,d,\uparrow,\uparrow} = 0.7$. b) SOI terms are taken into account. The same parameters were used for plot b), additionally SOI is represented in the form of spin-flip on-site potentials: $\epsilon_d^{\uparrow,\downarrow} = 0.1; \epsilon_f^{\uparrow,\downarrow} = 0.15$. The ± notations are explained in text.

Similarly to Fig.3.2, on Fig.3.3, I presented the band structure of the studied system, with the Hamiltonian seen in Eq.(3.6). In this case there is no double degeneracy present.

The behaviour of the system presented on Fig.3.3, namely the splitting of the double degenerate bands is the result of the introduced SOI (See Eq.(3.7)). This can lead to such peculiarities as magnetic phenomena on the surface [28, 34, 43, 44] or magneto-transport [92, 30]. These observations lead me to provide an in depth investigation on the studied system in the presence of spin-orbit coupling. The question is: is SOI together with the interaction between electrons able to cause magnetism in a multiband system, which is strongly correlated? Since the magnitude of SOI coupling is many order of magnitude smaller than the Hubbard coupling strengths (U), perturbation theories are not suitable to describe the system, thus exact solutions are required. Also considering, that system is not integrable a I used a special method, i.e. the method based on PSO to deduce the ground state wave functions (see Section 1.6). Accordingly to answer the question and to provide additional details of the physical properties of the system I will deduce the exact ground state wave function.

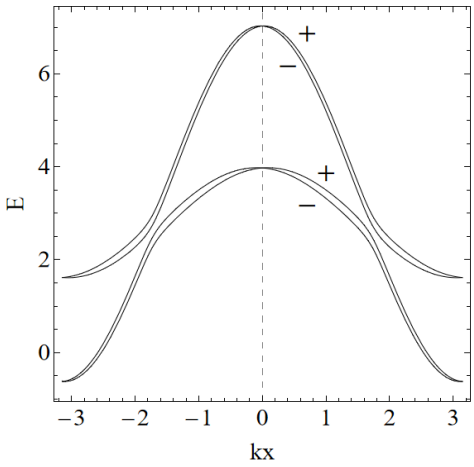

Figure 3.3: Band structure of the studied system, in the presence of spin-orbit interaction (H_{SO} from Eq.(3.7)), with $V_R^d = V_R^f = 0.05$ and $V_D^d = V_D^f = 0.02$. The nonzero $\hat{H}_1$ parameters are the same as in Fig.1a. The energy and all $\hat{H}_1$ parameters are expressed in t_x^d units. Note that $\vec{k} \cdot \vec{y} = 0$ holds.

3.3 Transformation of the Hamiltonian to positive semidefinite form

As the first step of the PSO method I transform the Hamiltonian from Eq.(3.6) to PSO form seen in Eq.(3.1). To construct $\hat{P}$ from Eq.(3.1), i.e. the positive semidifinite form of the Hamiltonian I used block operators. Since $\hat{H}$ also contains spin-flip hoppings in the presented case, the positive semidefinite operators $\hat{P}$ are defined with utilising two block operators. The reason why two block operator are needed, is that two block operators are capable of generating the terms with mixed spin indices. Each unit cell in the lattice can be thought of as a block, where I introduce two block operators connected to the site $\mathbf{i}$ of this block: $\hat{A}_i$ and $\hat{B}_i$, which I will denote as $\hat{G}$ ($G = A, B$).

In this case, the block operators act on all four sites of the unit cell $n = 1, 2, 3, 4$ (see Fig.3.4). From the notation of the block operators one notices that $\hat{G}_i$ does not contain a spin index, since its expression contains both spin indices:

$$\hat{G}_{\mathbf{i}} = \sum_{c=d,f} \sum_{\alpha=\uparrow,\downarrow} \left(g_{G,c,1,\alpha} \hat{c}_{\mathbf{i},\alpha} + g_{G,c,2,\alpha} \hat{c}_{\mathbf{i}+\mathbf{x},\alpha} + g_{G,c,3,\alpha} \hat{c}_{\mathbf{i}+\mathbf{x}+\mathbf{y},\alpha} + g_{G,c,4,\alpha} \hat{c}_{\mathbf{i}+\mathbf{y},\alpha} \right), \quad (3.8)$$

where $g_{G,c,n,\alpha}$ denotes 16 numerical coefficients for any fixed G ($c = d, f$, $\alpha = \uparrow, \downarrow$, $n = 1, 2, 3, 4$), which are the same in all blocks belonging to any site $\mathbf{i}$ as a result of the Bravais translational symmetry. In the history of the application of positive semidefinite operator method this is the first occasion, when block operators do not have spin indices, i.e. do not depend on the spin projection. The $\hat{G}_{\mathbf{i}}$ are linear combination of fermionic annihilation operators ($\hat{c}_{\mathbf{j},\alpha}$) for any $c = d, f$ and $\alpha = \uparrow, \downarrow$. These fermionic operators, defined on each of the four sites of the unit cell have the following in-cell notations: starting from

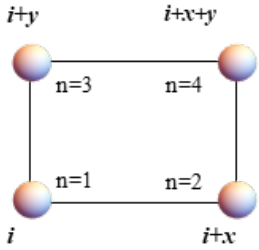

Figure 3.4: Unit cell defined at the lattice site $\mathbf{i}$ with in-cell notations of sites $n = 1, 2, 3, 4$. The Bravais vectors of the 2D lattice are denoted by $\mathbf{x}$ and $\mathbf{y}$.

site $\mathbf{i}$ clockwise, $\mathbf{i}, \mathbf{i}+\mathbf{x}, \mathbf{i}+\mathbf{x}+\mathbf{y}, \mathbf{i}+\mathbf{y}$. The sites within the block have the notations $n = 1, 2, 3, 4$ (See Fig.3.4). Note that these numbers appear in the indices of the block operators numerical coefficients.

The block operators shown in Eq.(3.8) are suitable for transforming the Hamiltonian of the system. Considering Eq.(3.1) $\hat{P}$ can be written as:

$$\begin{aligned}
&\hat{P} = \hat{P}_G + \hat{P}_1, \\
&\hat{P}_G = \sum_{\mathbf{i}} \sum_{G=A,B} \hat{G}_{\mathbf{i}} \hat{G}_{\mathbf{i}}^{\dagger}, \quad \hat{P}_1 = U_f \sum_{\mathbf{i}} \hat{P}_{\mathbf{i}}, \\
&C = \eta N - U_f N_s - \sum_{G=A,B} \sum_{\mathbf{i}} z_{\mathbf{i}}^{G}, \; U_f > 0,
\end{aligned} \tag{3.9}$$

where N is the number of electrons, N_s is the number of sites, $z_{\mathbf{i}}^{G} = \{\hat{G}_{\mathbf{i}}, \hat{G}_{\mathbf{i}}^{\dagger}\}$. η is a constant defined by the matching equations (See Appendix B.2). In Eq.(3.9) periodic boundary conditions were taken into account. The positive semidefinite operator $\hat{P}_i$ attains its smallest eigenvalue -zero- when there is at least one charge carrier on each $\mathbf{i}$ sites, since $\hat{P}_{\mathbf{i}} = \hat{n}_{\mathbf{i},\uparrow}^{f} \hat{n}_{\mathbf{i},\uparrow}^{f} - (\hat{n}_{\mathbf{i},\uparrow}^{f} + \hat{n}_{\mathbf{i},\uparrow}^{f}) + 1$.

Note that the transformation described Eq.(3.9) is one possibility to transform $\hat{H}$ to PSO form, which I will later refer to as the transformation at high concentration. This definition will be explained in Section 3.4 with the ground state wave function corresponding to this transformation.

The products of the two block operators $\hat{A}$ and $\hat{B}$ are capable of forming all the fermionic operator products that were in the original Hamiltonian (Eq.(3.6)). In these block operator products, the coefficients in front of the fermionic operator products will then be the sums of different $g_{G,c,n,\alpha}$ block operator parameter products.

These sums of different block operator products have to be equal to the known coupling constants in the Hamiltonian, standing before the corresponding fermionic operator products. These restrictions for the block operator parameters, set by the Hamiltonian couplings are the matching equations. These are discussed in detail in Appendix B.2 and their solutions are presented in Appendix B.3.

To see, how the matching equations formed, I would like to present a few examples. First, let us take the hopping term $\hat{d}_{\mathbf{i}+\mathbf{x},\uparrow}^{\dagger} \hat{d}_{\mathbf{i},\uparrow}$, which has the coupling constant $t_{\mathbf{x}}^{d,\uparrow,\uparrow}$ (see Eq.(3.4)). The corresponding term in the positive semidefinite op-

erator seen in Eq.(3.9) appears with the coefficient $-(g^*_{A,d,2,\uparrow}g_{A,d,1,\uparrow}+\ g^*_{A,d,3,\uparrow}g_{A,d,4,\uparrow}$ $+g^*_{B,d,2,\uparrow}g_{B,d,1,\uparrow}\ +g^*_{B,d,3,\uparrow}g_{B,d,4,\uparrow})$. Thus accordingly the matching equation is $-t^{d,\uparrow,\uparrow}_{\mathbf{x}} = g^*_{A,d,2,\uparrow}g_{A,d,1,\uparrow} + g^*_{A,d,3,\uparrow}g_{A,d,4,\uparrow} + g^*_{B,d,2,\uparrow}g_{B,d,1,\uparrow} + g^*_{B,d,3,\uparrow}g_{B,d,4,\uparrow}$, which is in Eq.(B.9) in Appendix B.2.

Consequently, the unknown parameters of the matching equations are the block operators, while the known quantities are the coupling strengths of the Hamiltonian. We can also see from Eq.(3.9) that the block operator products in $\sum_{\mathbf{i}}\sum_{G=A,B}\hat{G}_{\mathbf{i}}\hat{G}^\dagger_{\mathbf{i}}$ produce fermionic operator products that were not part of the original Hamiltonian. These fermionic operator products describe processes, which we have not taken into account in this system, such us second neighbour hybridizations, local spin-flip hybridizations, second neighbour hoppings, etc. Since these terms are not present in the original Hamiltonian (Eq.(3.6)) I had to eliminate them from the transformed Hamiltonian too, meaning I equated the sums of block operator parameters standing before these terms to zero. This is also the reason why I have taken two block operators $(\hat{A}, \hat{B})$ into account instead of one: only one, linear block operator would not be able to produce the terms in the Hamiltonian (as shown in Eq.(3.9)), while I also eliminate the terms which were not part of it. To exemplify the latter, let us take the fermionic operator product $\hat{d}^\dagger_{\mathbf{i}+\mathbf{x}+\mathbf{y},\uparrow}\hat{d}_{\mathbf{i},\uparrow}$, from $\sum_{\mathbf{i}}\sum_{G=A,B}\hat{G}_{\mathbf{i}}\hat{G}^\dagger_{\mathbf{i}}$ in Eq.(3.9), which has the coefficient $-(g^*_{A,d,3,\uparrow}g_{A,d,1,\uparrow}+g^*_{B,d,3,\uparrow}g_{B,d,1,\uparrow})$. The term $\hat{d}^\dagger_{\mathbf{i}+\mathbf{x}+\mathbf{y},\uparrow}\hat{d}_{\mathbf{i},\uparrow}$ describes a plaquette diagonal (second neighbour) hopping, which was not part of the original Hamiltonian, thus its coefficient has to equal to zero, providing the following matching equation: $-(g^*_{A,d,3,\uparrow}g_{A,d,1,\uparrow} + g^*_{B,d,3,\uparrow}g_{B,d,1,\uparrow}) = 0$, which is in Eq.(B.13) in Appendix B.2.

The whole system of matching equations deduced this way is presented in Appendix B.2.

There is however another way to transform the Hamiltonian to positive semidefinite operator, other than the way described in Eq.(3.9). Notice, that in Eq.(3.9), in $\hat{P}_G$ the block operators are in the following order: $\hat{G}_{\mathbf{i}}\hat{G}^\dagger_{\mathbf{i}}$. In the next transformation in Eq.(3.10) this order will change to the opposite $\hat{G}^\dagger_{\mathbf{i}}\hat{G}_{\mathbf{i}}$ and so the semidefinite transformation in Eq.(3.1) can be conducted also as:

$$\begin{aligned}
&\hat{P}^l = \hat{P}^l_G + \hat{P}^l_1,\\
&\hat{P}^l_G = \sum_{\mathbf{i}}\sum_{G=A,B}\hat{G}^\dagger_{\mathbf{i}}\hat{G}_{\mathbf{i}}, \quad \hat{P}^l_1 = \sum_i U_f\hat{n}_{if\uparrow}\hat{n}_{if\downarrow},\\
&C^l = \eta\hat{N},
\end{aligned} \tag{3.10}$$

where $\hat{n}_{if\sigma} = \hat{f}^\dagger_{if\sigma}\hat{f}_{if\sigma}$ and $\hat{n}_{if\sigma}$ is the fermionic number operator providing the number of electrons with spin projection σ on the f orbital and site i. $\hat{N} = \sum_{i\sigma}(\hat{n}_{id\sigma} + \hat{n}_{if\sigma})$, $\sigma = \uparrow\downarrow$ is the operator of the total number of electrons. Moreover, the constant C^l, seen in Eq.(3.10) can be merged with the on-site potential terms in $\hat{H}$ and with that the ground state energy can be calculated after the transformation is completed. The matching equations corresponding to this transformation are detailed in Appendix B.2.1.

In general the transformation described in Eq.(3.10) is used in low concentration, while the transformation described in Eq.(3.9) is used in high concentration. These

aspects will be explained later on in Section 3.4.

To complete the transformation and move onto the next step of the method, one has to solve the matching system of equations. In this case it means solving a system of 74 non-linear, coupled complex equations. The complete solution is described in Appendix B.3. The conditions for performing the transformation, i.e. the parameter space region, where the solution exists is described in Appendix B.4. In the possession of the solution for the matching equations I can follow up with deducing the ground state wave function.

3.4 The ground state wave function

I will divide this section to two parts. In Subsection 3.4.1 I will deduce the ground state wave function for high concentration, which belongs to the transformation introduced in Eq.(3.9). Then in Subsection 3.4.2 I will show the ground state wave function for low concentration corresponding to the positive semidefinite transformation proposed in Eq.(3.10).

3.4.1 Ground state wave function at high concentration

Many methods exist for the deduction of $|\Psi_g\rangle$ [64]. I will present the method I used in two steps. In the first step, my aim is to find the $|\chi\rangle$ wave vector, which satisfies the condition $\sum_i \left(\hat{A}_i\hat{A}_i^\dagger + \hat{B}_i\hat{B}_i^\dagger\right)|\chi\rangle = 0$:

$$\hat{P}_G|\chi\rangle = 0. \tag{3.11}$$

In this step I used the fermionic anticommutation relations $\{\hat{A}_i, \hat{A}_j\} = 0, \{\hat{A}_i^\dagger, \hat{A}_j^\dagger\} = 0$, since the block operators are sums of linear combinations of fermionic annihilation operators. This means that both $\hat{A}_i^\dagger\hat{A}_i^\dagger$ and $\hat{B}_i^\dagger\hat{B}_i^\dagger$ equals to zero. Using these properties $|\chi\rangle$ can be written as $|\chi\rangle = \Pi_i\ \hat{A}_i^\dagger\hat{B}_j^\dagger|0\rangle$, where $|0\rangle$ is the vacuum state.

Thus we have the most general wave function, which satisfies the condition Eq.(3.11). To deduce the ground state wave function besides Eq.(3.11), the condition $\hat{P}_1|\Psi_g\rangle = 0$ has to also be satisfied. This means that $\sum_i U\hat{P}_i$ acting on the wave function has to also result in zero.

Thus in the second step I place $|\chi\rangle$ into the kernel of operator $\hat{P}_1 = \sum_i U\hat{P}_i$. The kernel of an operator $\hat{O} : H \to H$ is $\ker(\hat{O}) = \left\{\mathbf{v} \in H \mid \hat{O}\mathbf{v} = \mathbf{0}\right\}$, where H is a Hilbert space. The $|\chi\rangle$ presented in the first step is not in the kernel of $\sum_i U\hat{P}_i$, since $\sum_i U\hat{P}_i$ acting on the wave vector is only zero, if there is at least one electron on each f orbital. Thus in order to acquire this goal, there has to be at least one electron on each f orbital. This can be achieved by introducing $\hat{C}^\dagger$ operator, which creates an electron on each f orbital, and with this $\hat{C}^\dagger = \Pi_{i=1}^{N_s}\hat{C}_i$,$\hat{C}_i = (\alpha_{i\uparrow}\hat{f}_{i\uparrow}^\dagger + \alpha_{i\downarrow}\hat{f}_{i\downarrow}^\dagger)$, where $\alpha_{i\downarrow}$ and $\alpha_{i\uparrow}$ are arbitrary coefficients.

This way I got the desired wave vector in the following form:

$$|\Psi_g\rangle = \left(\Pi_{i=1}^{N_s} \hat{A}_i^\dagger \hat{B}_i^\dagger\right) \hat{C}^\dagger |0\rangle. \tag{3.12}$$

Since each $\hat{A}_i^\dagger$, $\hat{B}_i^\dagger$, and $\hat{C}_i^\dagger$ creates an electron on site i, there are in total $3N_s$ electron in the system. Thus the ground state wave function contains $3N_s$ out of the maximum $4N_s$ particle number. For this reason we call this ground state the high concentration ground state, corresponding to the positive semidefinite transformation from Eq.(3.9).

The following can be seen from the wave function described by Eq.(3.12). If one expands the product, $|\Psi_g\rangle$ becomes a sum of orthogonal expressions. Moreover if even one operator is missing at an arbitrary i site, the wave function corresponding to this state is not a ground state wave function for the studied Hamiltonian. In addition the contribution of one product of the expanded expression of the right side of Eq.(3.12) does not represent a single particle wave function.

The wave function seen in Eq.(3.12) can be extended above three-quarter system filling. With the total number of particles being $N = 3N_s + N_t$, where $N_t < N_s$ holds, this wave function is

$$|\Psi_g\left(N > 3N_s\right)\rangle = \left(\Pi_{i=1}^{N_s} \hat{A}_i^\dagger \hat{B}_i^\dagger\right) \hat{C}^\dagger \hat{F}^\dagger |0\rangle, \quad \hat{F}^\dagger = \Pi_{\delta=1}^{N_t} \hat{c}^\dagger_{\delta,\vec{k}_\delta,\sigma_\delta}, \tag{3.13}$$

where $\hat{c}$ can be $\hat{d}, \hat{f}$, δ is an arbitrary site, σ_δ is an arbitrary spin projection, $\vec{k}_\delta$ is an arbitrary momentum from the first Brillouin zone.

3.4.2 Ground state wave function at low concentration

To get the low concentration solution we start with the Hamiltonian transformed to positive semidefinite operator in the way described in Eq.(3.10). I will show how I got the wave function in this case in two steps. First I found the $|\chi^l\rangle$ wave function for which $\hat{P}_G^l|\chi^l\rangle = 0$ is true. It can be seen that $|\chi^l\rangle = \Pi_{j\in\Omega}\hat{D}_j^\dagger|0\rangle$ meets this condition, if Ω is a set of sites and $\hat{D}_j^\dagger$ satisfies the anticommutation relations: $\{\hat{A}_i, \hat{D}_j^\dagger\} = 0, \{\hat{B}_i, \hat{D}_j^\dagger\} = 0$ for any $j \in \Omega$ and arbitrary i. $\hat{D}_j^\dagger$ are block operators connected to site j, while being linear combinations of fermionic creation operators. Thus $\hat{D}_j^\dagger$ has the form:

$$\hat{D}_j^\dagger = \sum_n \chi_n c_{j+r_n}^\dagger, \tag{3.14}$$

where $j \in \Omega$ and the χ_n coefficients are determined in a way to satisfy the $\{\hat{A}_i, \hat{D}_j^\dagger\} = 0, \{\hat{B}_i, \hat{D}_j^\dagger\} = 0$ conditions.

The $|\chi^l\rangle$ must also be in the kernel of $\hat{P}_1^l$, thus this need to be achieved in the second step. The $\hat{P}_1^l$ acting on the wave function provides zero only if there are no doubly filled i sites on the f orbitals. To satisfy this condition I will narrow the Ω set of indices to include only those sites from the orbital f, where there are less than two electrons on

the same site. The newly acquired set of indices will be denoted with $\bar{\Omega}$. The sought ground state wave function $|\Psi_g(N \leq N_s)\rangle$:

$$|\Psi_g(N \leq N_s)\rangle = \Pi_{j\in\bar{\Omega}} \hat{D}_j^\dagger |0\rangle \tag{3.15}$$

This wave function corresponds to quarter system filling or below ($N \leq N_s$), thus it is called low concentration.

3.5 Physical properties at high concentration

In this section I will discuss the physical properties of the ground state at high concentration (See Eq.(3.12)). We are now in the possession of the explicit, exact ground state wave functions, consequently the physical attributions can be investigated. In Section 3.2 I showed that as a result of the spin-orbit coupling in the system, the double degenerate bands become split in non degenerate components. At the end of the section I mentioned, that further examination of the properties in the light of spin-orbit coupling has to be postponed until I attain ground state wave functions of the system. After transforming the Hamiltonian to positive semidefinite form in Section 3.3 and getting the ground state wave function in Section 3.4 this further examination became possible.

3.5.1 The magnetic properties of the ground state

In this section I will study the magnetic properties of the system. The system is ferromagnetic if $\langle \hat{S}^2 \rangle \neq 0$. If this is true, it means that there has to be a projection of $\langle \hat{\vec{S}} \rangle$ which is nonzero. In order to show that the ground state of the system is indeed ferromagnetic, I calculate the expectation value of the total spin z projection. If it proves to be nonzero that implicates $\langle \hat{S}^2 \rangle \neq 0$ and clearly shows us a ferromagnetic state. To ease the calculations the expectation values will be expressed from the wave function transformed to $\vec{k}$-space. The transformation is detailed in Appendix B.6. In the $\vec{k}$-space the electrons in $\vec{k}$ state have the spin z projection $\hat{S}^z_{\vec{k}}$: the electron on the d orbital has $\hat{S}^z_{\vec{k}d}$, while the electron on the f orbital has $\hat{S}^z_{\vec{k}f}$. Thus $\hat{S}^z_{\vec{k}} = \hat{S}^z_{\vec{k}d} + \hat{S}^z_{\vec{k}f}$. Generally an electron on the orbital c with momentum $\vec{k}$ has the spin z projection:

$$\hat{S}^z_{\vec{k}c} = \frac{1}{2}\left(\hat{n}_{\vec{k}c\uparrow} - \hat{n}_{\vec{k}c\downarrow}\right), \tag{3.16}$$

where $\hat{n}_{\vec{k}c\sigma}$ are the particle number operators for the bands $c = f, d$, momentum $\vec{k}$ and $\sigma = \uparrow, \downarrow$. To acquire the total spin z projection, we have to take the sum of all the $\vec{k}$ states in the reciprocal space. Accordingly the total spin z projection:

$$\hat{S}^z = \frac{1}{N_s} \sum_{\vec{k}=1}^{N_s} \hat{S}^{\vec{k}}_z, \tag{3.17}$$

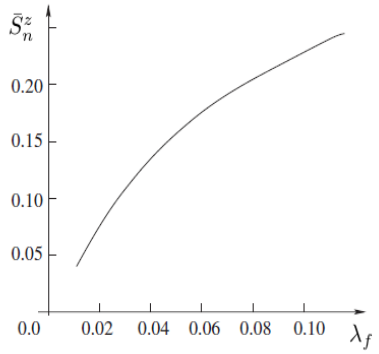

Figure 3.5: $\bar{S}_n^z$, the total spin z expectation value ($\bar{S}^z$) normalized with respect to $\bar{S}^z_{Max} = 1/2$ as function of the effective SOI of the correlated band: $\lambda_f = (|V_R^f|^2 + |V_D^f|^2)^{1/2}$. The λ_f is in $t_x^{f,\sigma,\sigma}$ units. At $\lambda_f = 0$ the ground state wave function $|\Psi_g\rangle$ from Eq.(3.12) does no longer describe the ground state, thus the plot cannot start from $\lambda_f = 0$. Still the relation $\lim_{\lambda_f \to 0} \bar{S}_n^z = 0$ holds.

where N_s is the number of sites. Using Eq.(3.17) it can be proved that $\langle \hat{S}^z \rangle > 0$, hence the ground state is identified as a ferromagnetic state. See the corresponding calculation in Appendix B.6.1. On Fig.3.5 I show the results of the numerical calculations. Here $\bar{S}^z$ (the expectation value of the total spin z projection $\hat{S}^z$, as calculated in Appendix B.6.1) is shown as a function of λ_f. The λ_f is the effective SOI coupling strength of the correlated f band, thus defined as $\lambda_f = \sqrt{(V_D^f)^2 + (V_F^f)^2}$. The Hamiltonian parameters used for Fig.3.7 are in first neighbour hopping $t_x^{f\uparrow\uparrow}$ units.

As a conclusion one can see that the magnetization of the system can be increased as we increase the SOI coupling strengths of the correlated f band. If we decreased the value of λ_f simultaneously $\bar{S}_z$ also decreases, while we stayed in the Hamiltonian parameter space, where the solution for the ground state wave function (See Eq.(3.12)) is satisfied. This indicates that the magnetization in this 2D system is due to the SOI.

The role of the Hubbard type interaction in the magnetic properties of the system is to ensure the existence of an ordered phase; without the Hubbard type interaction a disordered state would exist, which does not allow ferromagnetic order.

3.5.2 The long range hopping of the ground state

Next let us investigate how the SOI influences the mobility of the charge carriers. For this purpose I examined the r dependent hopping ($\hat{\Gamma}_r$), which I defined as:

$$\hat{\Gamma}_r = \frac{1}{N_s} \sum_j \left(\hat{c}^\dagger_{j\sigma} \hat{c}_{j+r\sigma} + \hat{c}^\dagger_{j+r\sigma} \hat{c}_{j\sigma} \right), \tag{3.18}$$

where r, is the arbitrary and fixed magnitude of the distance. From Eq.(3.18) the expectation value of the r-dependent ground state hopping can be calculated. This is done in Appendix B.6.2.

On Fig.3.6 one has $\tilde{\lambda} = (1/2) \sum_{l=d,f} \lambda_l$, where $\lambda_l = \sqrt{(V_R^l)^2 + (V_D^l)^2}$- denotes the effective SOI coupling. By increasing the SOI coupling magnitude for any orbital, Γ_r

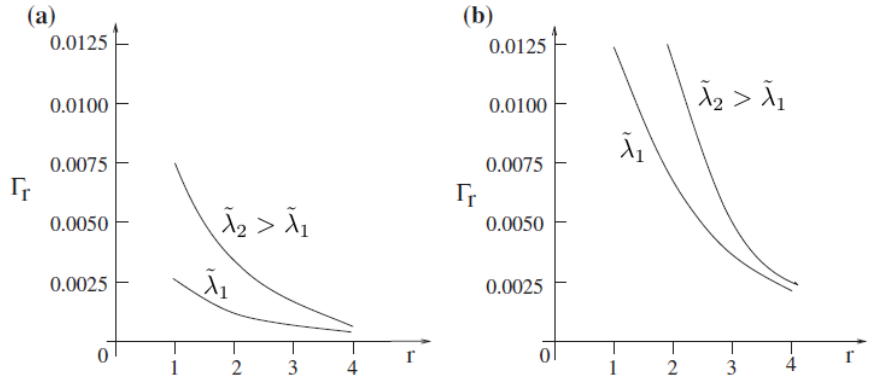

Figure 3.6: The long-range hopping ground state expectation values $\Gamma_{\vec{r}}$ as function of r, for two different, fixed effective total SOI $\tilde{\lambda} = (1/2)\sum_{l=d,f}\lambda_l$. The r values are in lattice constant units. I demonstrated $\langle\Gamma_r\rangle$ values in the case of the electrons on the d band moving in the $\vec{x}$ direction. The $\tilde{\lambda}_1 = 0.0185$, and $\tilde{\lambda}_2 = 0.0495$ are given in $t_x^{f,\sigma,\sigma}$ units. With $\tilde{\lambda}$, the $\Gamma_{\vec{r}}$ expectation value simultaneously increases, signalling a SOI dependence. On Plot a) the spin z projection is negative, and on Plot b) it points to the opposite direction (i.e it is positive).

also increases for any fixed, arbitrary r. This means, that the mobility of the electrons is enhanced if we increase the SOI strengths in the system. One also notes, that $\langle\Gamma_r\rangle$ is different for the charge carriers with spin projections pointing towards (see Fig.3.6/b))-, and opposite the direction z (see Fig.3.6/a)).

3.5.3 Interface magnetism

The results at high concentration provide a better understanding of how it is possible for the interface of two non-magnetic materials (for e.g. perovskites as $LaAlO_3$ and $SrTiO_3$) to become ferromagnetic [92] as seen in Section 1.5. Here it is stated that the breaking of inversion symmetry at interfaces results in large Rashba spin-orbit interaction on the perovskite interfaces [36].

In my model I considered itinerant, mobile electrons on a 2D lattice, in the presence of SOI. This might be a good approximation for the interface found between the non-magnetic materials presented. I showed that in the presence of the many-body spin orbit interaction a ferromagnetic ground state can be found, just as it was experimentally observed in the presented cases.

Additionally in Ref.[37] the mobility of the charge carriers on the interface was found to be tunable by the SOI strength, whose magnitude can be modulated by the application of an external electric field. This is indeed in argument with what I found for the mobility of the charge carriers as the function of SOI in Subsection 3.5.2 (see Fig.3.6). With $\tilde{\lambda}$ Γ_r simultaneously increases signalling a strong SOI strength dependence for the mobility.

3.6 Physical properties at low concentration

Opposite to the last section, where I demonstrated the physical properties of the ground state at high concentration, I will now concentrate on the physical attributes attained at low concentration (See Eq.(3.15)).

Under a quarter system filling, the ground state is highly degenerate. The non-normalized wave function in this case:

$$|\Psi(N < N_s)\rangle = \sum_{\Omega_N} \alpha_{\Omega_N} \Pi_{j\in\Omega_N} \hat{D}^{\dagger}_{j(\sigma)} |0\rangle, \tag{3.19}$$

where Ω_N is a set containing N ($N < N_s$) sites, where N_s is the total number of sites in the system. In Eq.(3.19) the sum is over all possible Ω_N configurations. $\hat{D}^{\dagger}_{j(\sigma)}$ are operators defined on a block, which have the following meaning: for touching blocks $\hat{D}^{\dagger}_{j\sigma}$ with fixed σ, and for every other non-touching block it is $\hat{D}^{\dagger}_{j}$. Every $\hat{D}^{\dagger}_{j\sigma}$ or $\hat{D}^{\dagger}_{j}$ places an electron in the system. In the case of the wave function defined in Eq.(3.19) the number of blocks is less than of the sites. Consequently, when blocks touch, every spin projection on orbital f must point to the same direction, so orbital f is not double filled. Otherwise it would increase the energy, due to the Hubbard interaction.

In this way clusters can form, with touching blocks with the same fixed spin projections. In these clusters the spin projection is fixed, but arbitrary. The spin projections of the different clusters are not correlated.

For quarter system filling, every block touches, thus the form of the non-normalized wave function becomes

$$|\Psi(N = N_s)\rangle = \Pi_{j=1}^{N_s} (\hat{f}^{\dagger}_{j\sigma} - \nu \hat{d}^{\dagger}_{j\sigma}) |0\rangle, \tag{3.20}$$

where σ is fixed. In this case the number of sites equals to that of the blocks, every cluster touches and every spin points to the same direction. This corresponds to a saturated ferromagnetic state.

The wave function in Eq.(3.20) can be easily normalized: $\langle\Psi(N = N_s)|\Psi(N = N_s)\rangle = (1 + |\nu|^2)^{N_s}$. With the normalized wave function the r-dependent ground state hopping expectation values can be calculated, which gives us information about the mobility of the electrons. For the r-dependent hopping $\hat{\Gamma}_{\vec{r}}$ I used the definition also seen in Eq.(3.18). The expectation value of $\hat{\Gamma}_{\vec{r}}$ for the ground state:

$$\langle\Gamma_{\vec{r}}\rangle = \frac{\langle\Psi(N = N_s)|\Gamma_{\vec{r}}|\Psi(N = N_s)\rangle}{\langle\Psi(N = N_s)|\Psi(N = N_s)\rangle} = 0, \tag{3.21}$$

because in the system with the wave function $\Psi(N = N_s)$ there is one electron on each site and any hopping would cause a double filled orbital, which would increase the energy.

As a result the ground state in Eq.(3.20) contains electrons localized to the sites, therefore the mobility of the electrons is zero.

3.7 Expanding the model

Next, I would like to investigate how expanding the model influences the acquired results. For this reason I have taken into account next nearest-neighbour terms (i.e. plaquette diagonal hopping terms) $\hat{H}_{n.n}$ and spin-flip on-site one-particle potentials $\hat{H}_{0,sf.}$, which were originally neglected in the starting Hamiltonian, in Eq.(3.6). This way the $\hat{H}_1$ presented in Eq.(3.2), will have two additional terms:

$$\hat{H}_{n.n} = \sum_{\mathbf{i}} \sum_{c=d,f} \sum_{\alpha} \sum_{\substack{\mathbf{p}=\mathbf{x}+\mathbf{y},\\ \mathbf{p}=\mathbf{y}-\mathbf{x}}} t_{\mathbf{p}}^{c,\alpha,\alpha} \hat{c}^{\dagger}_{\mathbf{i}+\mathbf{p},\alpha} \hat{c}_{\mathbf{i},\alpha} + \text{H.c.},$$
$$\hat{H}_{0,sf.} = \sum_{\mathbf{i}} \sum_{c=d,f} \sum_{\alpha} \epsilon_c^{\alpha,-\alpha} \hat{c}^{\dagger}_{\mathbf{i},\alpha} \hat{c}^{\dagger}_{\mathbf{i},-\alpha}. \tag{3.22}$$

Considering the new terms from Eq.(3.22) additionally, the Hamiltonian of the expanded model ($\hat{H}'$) is:

$$\hat{H}' = \hat{H} + \hat{H}_{0,sf.} + \hat{H}_{n.n}. \tag{3.23}$$

For the system with these modifications my goal was to deduce a ground state wave function at high concentration and then compare it to the one acquired- also at high concentration (see Eq.(3.12)) - for the system with the original Hamiltonian $\hat{H}$ in Eq.(3.6). In order to do this I used the method of PSOs again, but in this time the starting point was $\hat{H}'$ from Eq.(3.23). With these modification what really changes in the way I deduced the ground state wave function is in the execution of the PSO transformation itself.

As the first step of the PSO method, in the case of the expanded model I carried out the PSO transformation for $\hat{H}'$ in the way it was originally described for $\hat{H}$ in Eq.(3.9). The transformation of $\hat{H}'$ is done with block operators defined similarly as seen in Eq.(3.8), but with a new set of 32 $g'_{G,c,n,\alpha}$ parameters:

$$\hat{G}'_{\mathbf{i}} = \sum_{c=d,f} \sum_{\alpha=\uparrow,\downarrow} (g'_{G,c,1,\alpha} \hat{c}_{\mathbf{i},\alpha} + g'_{G,c,2,\alpha} \hat{c}_{\mathbf{i}+\mathbf{x},\alpha} + g'_{G,c,3,\alpha} \hat{c}_{\mathbf{i}+\mathbf{x}+\mathbf{y},\alpha} + g'_{G,c,4,\alpha} \hat{c}_{\mathbf{i}+\mathbf{y},\alpha}), \tag{3.24}$$

where $(G' = A', B')$ the block operators for the expanded model. With these block operators, the PSO transformation can be done in the form of $\hat{H}' = \hat{P}' + C'$, where

$$\hat{P}' = \hat{P}_{G'} + \hat{P}_1,$$
$$\hat{P}_{G'} = \sum_{\mathbf{i}} \sum_{G'=A,B} \hat{G}'_{\mathbf{i}} \hat{G}'^{\dagger}_{\mathbf{i}}, \quad \hat{P}_1 = U_f \sum_{\mathbf{i}} \hat{P}_{\mathbf{i}},$$
$$C' = \eta N - U_f N_s - \sum_{G=A,B} \sum_{\mathbf{i}} z_{\mathbf{i}}^{G'}, \ U_f > 0, \tag{3.25}$$

where N is the number of electrons, N_s is the number of sites, $z_{\mathbf{i}}^{G'} = \{\hat{G}'_{\mathbf{i}}, \hat{G}'^{\dagger}_{\mathbf{i}}\}$ holds, $\hat{P}_{\mathbf{i}} = \hat{n}^f_{\mathbf{i},\uparrow} \hat{n}^f_{\mathbf{i},\uparrow} - (\hat{n}^f_{\mathbf{i},\uparrow} + \hat{n}^f_{\mathbf{i},\uparrow}) + 1$.

The differences in the block operator parameters come from the additional terms

in the Hamiltonian, which enter the expression of the $g'_{G,c,n,\alpha}$ parameters through the matching equations. In this case the matching equations consist of a system of coupled, non-linear equations, with the new set of 32 $g'_{G,c,n,\alpha}$ parameters as unknown (see Eq.(3.8)) and all the nonzero Hamiltonian parameters as known. The new system of matching equations leads to the new block operator parameters. These differ from the ones obtained by solving the system of matching equations for the original $\hat{H}$ (see Appendix B.2). The new system of matching equations and their solutions are described in Appendix B.7.

After I solved the matching equations for the transformation of $\hat{H}'$, the PSO form of $\hat{H}'$ is obtained in the way as described in Eq.(3.25). In the next step I deduced the ground state wave function of the expanded model for $3N_s$ system filling $|\psi'_g\rangle$. Following the steps conducted in Subsection 3.4.1, I arrived to

$$|\psi'_g\rangle = \left(\Pi_{i=1}^{N_s} \hat{A'}_i^{\dagger} \hat{B'}_i^{\dagger}\right) \hat{C}^{\dagger}|0\rangle, \tag{3.26}$$

$\hat{C}^{\dagger} = \Pi_{i=1}^{N_s} \hat{C}_i$,$\hat{C}_i = (\alpha_{i\uparrow} \hat{f}_{i\uparrow}^{\dagger} + \alpha_{i\downarrow} \hat{f}_{i\downarrow}^{\dagger})$, where $\alpha_{i\downarrow}$ and $\alpha_{i\uparrow}$ are numerical coefficients.

One easily notices, that the high concentration ground state wave function of the system with the original Hamiltonian $\hat{H}$ (see Eq.(3.12)) and the wave function of the expanded model with the Hamiltonian $\hat{H}'$ (see Eq.(3.26)) are really similar in their structure. As a result $|\psi'_g\rangle$ is the same in its nature, namely just as $|\psi_g\rangle$. Consequently expanding the Hamiltonian with the next nearest-neighbour terms and spin-flip on-site one-particle potentials did not change qualitatively the physical properties of the ground state.

I would like to note, that $|\psi'_g\rangle$ can also be expanded above $\frac{3}{4}$-, and below quarter system filling , similarly as seen also in Eq.(3.13) and Eq.(3.15). The difference will remain to lay in the parameters of the blocks operators used to perform the PSO transformation of $\hat{H}'$.

I would like to add, that it is also possible to apply external fields ($\vec{h}$). For example, it is possible to add an external magnetic field, with the form

$$\hat{H}_h = \sum_{p,\mathbf{i}} \sum_{\alpha,\alpha'} \vec{h}_{p,\mathbf{i}} \hat{c}_{p,\mathbf{i},\alpha}^{\dagger} \vec{\sigma}_{\alpha,\alpha'} \hat{c}_{p,\mathbf{i},\alpha'}, \tag{3.27}$$

which is applied in-plane (i.e. the z vector component of the field is zero $h_z = 0$). This way the spin-flip on-site one-particle terms ($\epsilon_0^{\uparrow,\downarrow}$) will be additively renormalized by $\tilde{\epsilon}_0^{\uparrow,\downarrow} = \epsilon_0^{\uparrow,\downarrow} + h_x - ih_y$, while $\tilde{\epsilon}_0^{\uparrow,\downarrow} = (\tilde{\epsilon}_0^{\downarrow,\uparrow})^*$ holds. By introducing the terms seen in Eq.(3.27) I have not found new physical effects.

3.8 Summary

In this work I deduced exact ground state wave functions for an itinerant, strongly correlated system on a 2D, square lattice with two bands, from which one is correlated. I took into account a Hubbard type interaction and the presence of SOI. Often SOI is presented

phenomenologically in other models, but in my work SOI is represented with its structure on the level of the Hamiltonian. There are many papers investigating and proving that interfaces between non magnetic materials possess great SOI strengths, thus SOI has to be taken into account while investigating such systems [30].

In the case of 2D, non integrable systems with SOI exact method are necessary to provide reliable approximation to the physical properties and behaviour of the system.

I used the method of positive semidefinite operators to acquire an exact ground state wave function. This used method is able to provide exact results relating to the ground state regardless of the integrability and the dimensions of the investigated systems, even in the case of strongly correlated systems. The first step of the method was to transform the Hamiltonian into positive semidefinite form, which I have done with the so called block operators. To conclude this transformation I solved the matching system of equations (see Appendix B.3), which were equations containing the Hamiltonian parameters with the block operator parameters as unknowns (see Appendix B.2).

After the transformation were effectuated I determined the ground state wave functions for two different system filling, one being the low-, while the other being the high concentration. With these wave functions I finally calculated different ground state expectation values.

My main interest was the magnetic properties of the system, so accordingly I calculated the expectation value of the total spin z component. At high concentration my results support the formerly experimentally shown fact, namely that the surface of non-magnetic materials often turns ferromagnetic. This magnetization was due to the spin-orbit coupling in the correlated band in my model. The magnitude of the magnetization can be modulated by the SOI strengths, which can be changed e.g. by an electric field perpendicular to the surface. Simultaneously the SOI increases the mobility of the electrons in both bands. This results have been deduced by calculating the ground state r-dependent hopping of the charge carriers. The r-dependent hopping expectation values are different for the charge carriers with different spin projections. These results imply a possible application in spintronics.

At low concentration I showed a saturated ferromagnetic ground state for quarter system filling. In this case the ferromagnetism is not the result of SOI, though the wave function is deduced taking SOI into account, the saturated ferromagnetic ground state is the result of the Hubbard type interaction. Here the electrons are localized, the mobility is zero and all electron spin projections point to the same direction. Under a quarter system filling I have shown a paramagnetic ground state, which consists of unordered clusters.

I presented an extended model, were I have also taken next nearest-neighbour terms (i.e. plaquette diagonal hopping terms) and spin-flip on-site one-particle potentials into account. I showed that expanding the original Hamiltonian of the system, with terms which were originally neglected due to their small magnitude, the extracted ground state wave function remained qualitatively the same at both low-, and high concentration.

To my knowledge exact results for two dimensional fermionic systems with SOI were not available in the literature before. In this chapter I also showed how the 2D

model applies to the interface of two non-magnetic material, where ferromagnetism at the interface was observed. In these cases the inversion symmetry in the system is broken at the interface, thus SOI arises. Many papers reported highly mobile electron system, where SOI dependence of the mobility of charge carriers was observed. This was in agreement with the SOI strength dependent mobility of the ferromagnetic ground state of my 2D model. These results support the huge importance of taking SOI into account in understanding the ferromagnetism between non-magnetic materials.

I also note, that the fact that SOI can increase the mobility was shown experimentally in Ref.[93], where the effects of SOI on the charge carriers was investigated using external magnetic field. Another theoretical work can also be mentioned [94], where it was shown that the mobility of electrons can increase as a result of the Rashba SOI.

The contents of this chapter are based on the publications Refs.[O3, O4, O5]. The corresponding thesis point is Thesis point 2.

Chapter 4

Explanation of peculiar magnetic behaviour of gold nanograins

The contents of this chapter is based on Ref.[O6]. In this chapter, I provide possible explanation on peculiar magnetic behaviour of non-magnetic materials. These are explained with using the ferromagnetic exact ground state wave function of the 2D strongly correlated system with two bands and itinerant, spin 1/2 electrons, in the presence of SOI and a Hubbard type interaction between the electrons of the correlated band, in high concentration, which was deduced in Chapter 3.

In this chapter, I mainly concentrate on golden nanograins, which unexpectedly attain ferromagnetic properties at nanosize (~ 3 nanometers). This was observed by Hori et al. in 1999 [96], then confirmed by many experimentalist to come. On Fig.4.1 the size dependence of the nanomagnetism of golden nanograins is plotted. Though several models aim to explain it -which were briefly explored in this chapter- the source of this magnetism is not clear to this day.

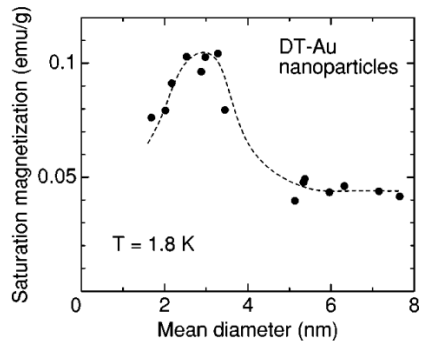

Figure 4.1: Saturation magnetization as the function of the mean diameter of the dodecane thiol (DT) capped gold nanoparticles. The experiment was conducted at low temperature by a superconducting quantum interference device magnetometer. The figure was taken from the corresponding study in Ref.[95].

Contents of Chapter 4

In **Section 4.1** I discuss the size-dependent nanomagnetism experienced in the case of Au. Theories providing possible explanations are presented and analysed in the light of the experimental findings. In Subsection 4.1.1 I explain how the model discussed in Chapter 3 at high concentration is able to explain the presented magnetic behaviour of golden nanoparticles.

At the end of this Chapter, in **Section 4.2** I provide the summary.

4.1 Nanomagnetism in case of gold nanoparticles

Nanomagnetism plays a prominent role in todays technology due to its broad applicability in the modern industry. Given these circumstances an important role of condensed matter physicist, both in experimental and theoretical fields is to better understand the subject [97]. It is not unusual to find materials possessing a nonzero net magnetic momentum at macroscopic size to behave the same way at nanosize. This can be observed for example in the case of nanocomposites [98] and magnetic ion containing nanomagnets [99]. This is usually due to magnetic domains, but domain walls in constrained geometry can also be a cause.

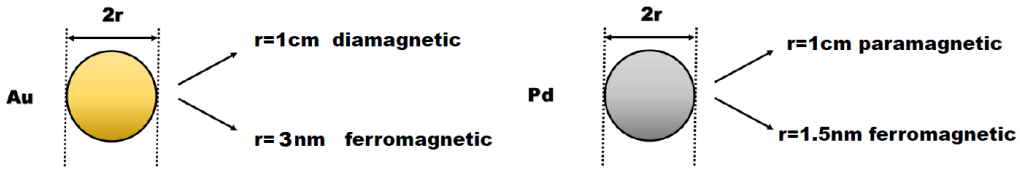

Figure 4.2: The magnetic properties of gold and palladium compared at nano-, and macro size

On the other hand, it can also happen that a material is not magnetic at macroscopic size i.e. does not possess magnetic moments, but appears to be magnetic at nanoscale. This phenomenon represents an exciting field in nanomagnetism, where the magnetic properties of a material are connected to its size. On Fig.4.2 I showed two examples, on the left hand side in the case of gold, while on the right hand side for palladium. This latter exhibits paramagnetic properties at macro size, but around 1.5 nanometers it becomes ferromagnetic. In this chapter however, I rather concentrated on gold nanograins, but later in this chapter I also briefly discuss the case of Pd nanograins.

After our research conducted for the 2D itinerant, non-integrable, strongly correlated system in the presence of SOI, which I detailed in Chapter 3 I turned my attention to the subject of nanomagnetism in the case of gold nanograins. Consequently, in the focus of my attention was gold which is diamagnetic in macroscopic form, but around 3 nanometers it is ferromagnetic [100]. It can generally be said, that 4d and 5d elements are not magnetic in macroscopic size, without external fields present [101]. From Fig.4.2 one

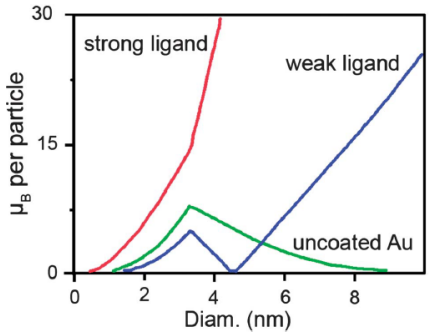

Figure 4.3: The magnetic moment of the Au nanoparticles as function of the diameter. The green line represent the uncoated, bare Au. Au nanoparticles stabilized by different protective agents are also represented. An agent inducing strong polarization is plotted with red, while in the case of blue line the agent used induces weak polarization. The source of this figure is Ref.[101].

can notice that gold was experimentally shown to be ferromagnetic at nanoscale. This was done first by Hori et al. in 1999 [96], then given it was considered a peculiar finding, several research group confirmed it [100, 102, 103].

This begs for the question, what can be the source of this ferromagnetism?

Many of the first theories aiming to explain this phenomenon theorized that the source is the ligand coating of the nanoparticles (as e.g. Refs.[104, 95, 105, 106]). These theories failed to explain how can golden nanoparticles remain ferromagnetic even when the ligand coating was removed [102, 107]. The same was observed, when the nanoparticles were obtained with photochemical methods, i.e. never contacted any type of coating agents in the first place [107]. See also Fig.4.3, where the magnetic moment of the bare golden nanoparticles can be compared to the magnetic moment of coated golden nanoparticles. The coating does influence the magnetic moments, but the studied effect remains to be present even for uncoated Au.

It was also found that for different types of ligands (dodecanethiol, tiopronin and tetralkyl ammonium) gold nanoparticles around 2 nanometers can be ferro-, para-, and diamagnetic [108]. This experiment with many other (e.g. Ref.[109]) clearly shows us that ligands on the surface can change the magnetic properties of gold nanoparticles.

From these findings it is safe to conclude that something other than the ligands is responsible for this behaviour. An other source of magnetism could be the magnetic impurities present in the nanoparticles. Reich et al. concluded experiments with x-ray photoelectron spectroscope being able to eliminate the effects of magnetic impurities Ni, Fe, Co, Mn [110]. It was concluded that the magnetism of gold nanoparticles remained qualitatively the same.

There are mean-field theories taking spin-spin type interactions into account [111]. In this case it is however not clear what the source of magnetic moments is and whether it is reasonable to neglect inter-particle correlations.

Similarly, several other theories use descriptions, where correlations between the particles are missing, e.g. one-particle representation [112], or two-particle interactions are in place [113]. On the other hand, according the literature and several published papers inter-particle correlation in the case of gold are important [114, 115, 116].

A model with inter-particle correlation was established for golden nanoparticles

in Ref.[117]. The model represents a 2D Hubbard model with itinerant, spin 1/2 electrons on a single band. Periodic boundary conditions in both direction were considered creating a closed surface. The results in Ref.[117] were investigated for a $L \times L$ square lattice, with finite, but arbitrary L. In it the method based on the properties of PSOs were used, due to the model being a 2D non integrable system. For small sample sizes a ferromagnetic ground state was found with a presented 12×12 example. This ground state was found to loose its relevance in $L \to \infty$. As a conclusion it is stated, that the reason of the decrease of the total magnetic moment is the increasing sample size. This is in fact in agreement with the experiments demonstrated in this section.

The acquired ground state belongs to low system filling. The spins in the system are arranged parallel in order to attain the lowest possible ground state energy in the presence of the Hubbard interaction. Various experiments confirm that the ground state is a coherent quantum state. One finds that the presence of the impurities in the system reduces the quantum coherence, thus the magnetic moment also decreases. This was shown in the case of Au nanoparticles, where introducing magnetic impurities (for instance Fe) reduced the ferromagnetic order [118].

4.1.1 The application of the 2D model

The presented toy model in Ref.[117] is based solely on the effects of Coulomb repulsion between the electrons, and quantum mechanical many-body behaviour. While it does describe a ferromagnetic ground state for a nano sized sample, the validity to apply it on gold specifically is questionable, since it does not take into account some of the more important properties of Au nanograins. In order, to approach the real system more accurately I applied the 2D model presented in Chapter 3 and showed why it is a good description for the surface of golden nanoparticles.

The studied 2D system in Chapter 3 had two-band structure. In the case of gold it has been shown multiple times, that the multiband property of gold is crucial. Sekiyama et al. reported after examining the valence-band electronic structures of gold, that the electrons of the 5d orbital contribute prominently to the conduction electrons in gold [115]. For this reason, I found, that not less than two bands is necessary to provide a qualitatively satisfying description; one correlated (f) and a non-correlated band (d).

The strong itinerancy and hybridization for the electrons of the 5d orbital in gold has been also reported on several accounts from theorist using relativistic methods, such as Korringa-Kohn-Rostoker method [119] and relativistic augmented-plane-wave method [120]. Moreover, without a direct evidence of 5d magnetism [115], a 2D model with itinerant, hybridized two band electron system seems to be an ideal starting point for the description of gold surface. As a result the following hybridization terms are represented in the Hamiltonian:

$$\hat{V}_0 = \sum_{\mathbf{i}} \left[\left(\sum_{\alpha=\uparrow,\downarrow} V_0^{d,f,\alpha,\alpha} \hat{d}^{\dagger}_{\mathbf{i},\alpha} \hat{f}_{\mathbf{i},\alpha} \right) + \text{H.c.} \right],$$

$$\hat{V}_{\mathbf{p}} = \sum_{\mathbf{i}} \left[\sum_{\alpha=\uparrow,\downarrow} \left(V_{\mathbf{p}}^{d,f,\alpha,\alpha} \hat{d}^{\dagger}_{\mathbf{i}+\mathbf{p},\alpha} \hat{f}_{\mathbf{i},\alpha} + V_{\mathbf{p}}^{f,d,\alpha,\alpha} \hat{f}^{\dagger}_{\mathbf{i}+\mathbf{p},\alpha} \hat{d}_{\mathbf{i},\alpha} \right) + \text{H.c.} \right]. \tag{4.1}$$

The $\hat{V}_0$ terms contribute for the hybridisation in the system: $V_0^{d,f,\alpha,\alpha}$ contributes for the electron hopping from the orbital f on site i to the orbital d on site i, while its hermitian conjugate stands for an electron hopping from the orbital d on site i to the orbital f on site i. $\hat{V}_{\mathbf{p}}$ stands for those first neighbour hoppings in the $\mathbf{p}$ direction, which happen with hybridization.

In order to represent an itinerant electron system, in addition to the hybridization terms, one also considers the first neighbour hopping terms:

$$\hat{H}_{c,\mathbf{p}} = \sum_{\mathbf{i}} \left[\sum_{\alpha=\uparrow,\downarrow} t_{\mathbf{p}}^{c,\alpha,\alpha} \hat{c}^{\dagger}_{\mathbf{i}+\mathbf{p},\alpha} \hat{c}_{\mathbf{i},\alpha} + \text{H.c.} \right], \tag{4.2}$$

where $\hat{H}_{c,\mathbf{p}}$ describes a hopping to the $\mathbf{p}$ direction (between sites $\mathbf{i}$ and $\mathbf{i}+\mathbf{p}$), while the spin projection remains the same.

Next, the most important interactions, also must be considered. It is important to take the many-body SOI in the case of gold into account, as it was observed time and again. It was shown to play a prominent role in one particle studies [112] and to explain correlation effects in gold [116].

Currently the importance of including relativistic effects is also emphasized [116], thus the mayor role of SOI enjoys special attention [121, 122, 123, 124]. As for the surface of gold, large SOI has been reported by experimentalist [124, 125].

It can also be generally said that perpendicular to a surface $\vec{\nabla} V$ potential gradient is always present, which means one can be sure, that spin-orbit interaction (See Eq.(1.7)) occurs. This also applies for the surface of gold nanograin. The SOI strength λ is usually very small ($\sim 10^{-3}$ eV). In contrast in the case of gold, large spin-orbit coupling was reported, in order of 0.1 eV [125, 126]. This makes spin-orbit essential to be taken into account for gold nanograins as well, meaning a term representing SOI is also part of the Hamiltonian. In this case, two main types of spin-orbit interactions are considered: one is the Rashba - and the other is the Dresselhaus interaction:

$$\hat{H}_{SO,c,\mathbf{p}} = \sum_{\mathbf{i}} \left[t_{\mathbf{p}}^{c,\downarrow,\uparrow} \hat{c}^{\dagger}_{\mathbf{i}+\mathbf{p},\downarrow} \hat{c}_{\mathbf{i},\uparrow} + t_{\mathbf{p}}^{c,\uparrow,\downarrow} \hat{c}^{\dagger}_{\mathbf{i}+\mathbf{p},\uparrow} \hat{c}_{\mathbf{i},\downarrow} + \text{H.c.} \right], \tag{4.3}$$

where for fixed c the $t_{\mathbf{x}}^{c,\uparrow,\downarrow} = V_R^c - iV_D^c, t_{\mathbf{x}}^{c,\downarrow,\uparrow} = -V_R^c - iV_D^c, t_{\mathbf{y}}^{c,\uparrow,\downarrow} = V_D^c - iV_R^c, t_{\mathbf{y}}^{c,\downarrow,\uparrow} = -V_D^c - iV_R^c$, and V_R^c, V_D^c are the Rashba, and Dresselhaus interaction strengths. $\hat{H}_{SO,c,\mathbf{p}}$ describes a hopping to the $\mathbf{p}$ direction with spin-flip, as the result of the presence of spin-orbit coupling in the system.

Based on these considerations the one-particle part of the Hamiltonian has the

following form

$$\hat{H}_1 = \hat{V}_0 + \sum_{\mathbf{p}=\mathbf{x},\mathbf{y}} \left[\hat{V}_{\mathbf{p}} + \sum_{c=d,f} \left(\hat{H}_{c,0} + \hat{H}_{c,\mathbf{p}} + H_{SO,c,\mathbf{p}} \right) \right], \tag{4.4}$$

where $\hat{H}_{c,0}$ is the on-site one-particle potential

$$\hat{H}_{c,0} = \sum_{\mathbf{i}} \sum_{\alpha=\uparrow,\downarrow} \epsilon_c^{\alpha,\alpha} \hat{c}^\dagger_{\mathbf{i},\alpha} \hat{c}_{\mathbf{i},\alpha}. \tag{4.5}$$

Here $\hat{c}_{\mathbf{j},\alpha}$, $(c = d, f)$ are Fermi operators. Every electron in the system gives an energy contribution in the form of an one-site one-particle potential contribution in the Hamiltonian ($\hat{H}_{c,0}$). The $\epsilon_c^{\alpha,\alpha}$ has no site index, since the the sites in the Bravais lattice are equivalent.

As stressed before in Section 4.1 the inter-particle correlations are important to take into account in the description of gold nanoparticles. Here the inter-electronic interaction part of the Hamiltonian is represented via a Hubbard type (local Coulomb type) interaction in the correlated (f) orbital:

$$\hat{H}_{int} = \sum_{\mathbf{i}} U_f \hat{n}^f_{\mathbf{i},\uparrow} \hat{n}^f_{\mathbf{i},\downarrow}. \tag{4.6}$$

In the case of fcc Au the calculated value of the Hubbard U is 7.2 eV [127]. The model describing accurately describing the studied golden nanograins H becomes

$$\hat{H} = \hat{H}_1 + \hat{H}_{int}. \tag{4.7}$$

One notices that the Hamiltonian acquired this way is the same as the Hamiltonian show in Chapter 3 Eq.(3.6), which contains and incorporates all the terms and interactions, I discussed above. In this case from the two bands in my model the correlated band f corresponds to a d-band, while the non correlated is sp type.

Since the presented system has two bands, the ground state wave function at high concentration would be a good starting point for the description, which is obtained in Chapter 3 using the method based on the properties of PSOs. As a first step one fulfils the PSO transformation of the Hamiltonian, to then get the following exact ground state:

$$|\Psi_g(N \geq 3N_s)\rangle = \left(\Pi_{i=1}^{N_s} \hat{A}_i^\dagger \hat{B}_i^\dagger \right) \hat{C}^\dagger \hat{F}^\dagger |0\rangle, \quad \hat{F} = \Pi_{\delta=1}^{N_t} \hat{c}_{\delta,\vec{k}_\delta,\sigma_\delta}, \tag{4.8}$$

where the number of particles is $N = 3N_s + N_t$, $N_t < N_s$, thus representing a system with above 3/4 system filling. Note that the wave vector corresponds to exactly 3/4 system filling, if $N = 3N_s$ ($N_t = 0$) and $\hat{F}^\dagger$ is the identity operator. Here $\hat{c}$ can be $\hat{d}, \hat{f}$, δ is an arbitrary site, σ_δ is an arbitrary spin projection, $\vec{k}_\delta$ is an arbitrary momentum from the first Brillouin zone.

The ground state above corresponds to the high concentration ground state from Chapter 3. It was also shown there, that the high concentration ground state of

the presented system is ferromagnetic (see Subsection 3.5.1). Next I will show, how this ferromagnetic ground state of the system -which accurately describes the surface of gold- can explain the ferromagnetism found at nanoscale.

The studied system is indeed a 2D lattice with periodic boundary conditions. How can a 2D model explain the ferromagnetic of nanograins? The explanation is as follows: surface effects are important for many reason, mostly because they play a significant role on the nanoparticles properties. Nanograins have a larger surface per bulk atom ratio, than macroscopic materials. To simply see this, let us consider a nanosphere with radius r. The surface (S) of the sphere is $4\pi r^2$, while the volume (V) is $4/3(\pi r^3)$. This way the ratio $S/V = 4\pi r^2/(4\pi r^3/3) = 3/r$, meaning the surface to volume ratio decreases with increasing the radius of the sphere.

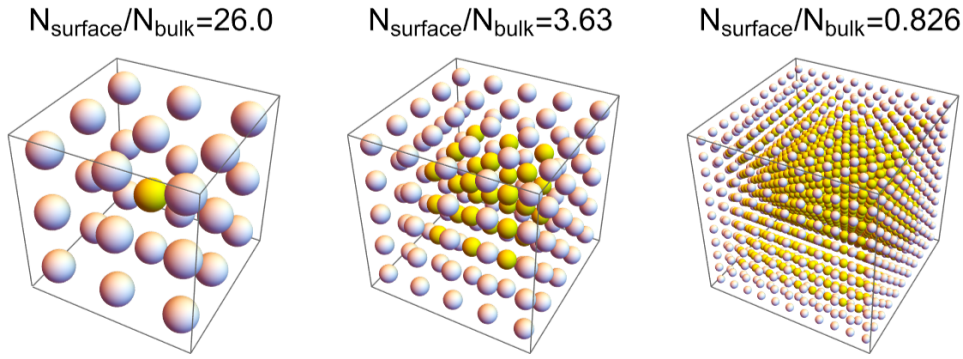

Figure 4.4: The surface-, and bulk atom ratio ($N_{surface}/N_{bulk}$), for a simple, square lattice. Note, that gold has face-centered cubic (fcc) type crystal lattice, but for the sake of a simple example a square lattice was considered. The ratio decreases with increasing sample size. The total number of atoms, $N_{total} = N_{surface} + N_{bulk}$ from left to right: 27, 125, 1331.

Consequently as the radius of the nanograin decreases, a greater portion of the atoms are found at the surface compared to those inside. I show a similar effect for a simple square lattice on Fig.4.4. In general it can be seen for a given type of lattice $N_{surface}/N_{bulk}$ does considerably increase with increasing sample size. This makes surface effects more and more dominant as the size of the sample increases, meaning at certain point the ferromagnetic ground state attained for the 2D system becomes relevant for description.

As the model in Chapter 3 corresponds to surface atoms, when the number of atoms in the volume considerably exceeds the number of atoms on the surface, i.e. the size of the nanograin grows to macroscopic size, the deduced ground state loses its relevance. This means, that the ferromagnetic state will no longer be the ground state of the system.

This model is also in agreement with one can observe on Fig.4.3. Here experimental data from several research group was collected [128] and plotted. The line for bare golden nanoparticles, i.e. the green line on Fig.4.3 can be divided to two parts: curve i)

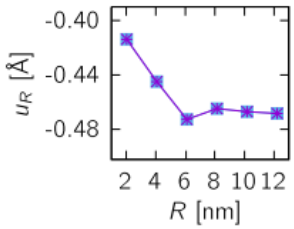

Figure 4.5: Displacement of the crystalline Au surface from ideal fcc lattice positions as the function of the diameter. The source of this figure is Ref.[129].

the portion of the curve, which belongs to smaller diamaters than the attained maximum (the position of the maximum being between 3-4 nanometers) and curve ii) the portion of the curve, which belongs to greater diameters than the attained maximum.

The curve ii) can be explained with the theory demonstrated in this section. Starting from the larger diameter to the diameter, where the maximum magnetic momentum is attained, the number of the surface atoms relative to the bulk atoms increases, thus surface effects become more relevant. This way the results for the two dimensional model become prominent, consequently a ferromagnetic state is achieved.

One can theorize that the explanation of the observed trend in curve i) is the fact, that decreasing the sample size results in a system, where one can not clearly differentiate between bulk and surface atoms anymore. This statement can be supported with the following remarks: generally the area immediate to the surface of a nanoparticle is strongly affected by the presence of the surface, which leads to the local change in the atom bindings. This phenomena is called the surface relaxation [130]. On Fig.4.5, the displacement of the surface of golden nanoparticles from the ideal fcc lattice positions of the bulk atom is plotted. The surface relaxation, i.e. the displacement of the surface starts to decrease with the decrease of the sample size below ~ 5 nanometers. This further signals that the difference between the bulk and surface atoms becomes a less prominent.

An other explanation for the trend of curve i) is as follows: if one takes a sample with a small number of atoms, the surface of this nanosized sample does not necessarily resemble a continuous, closed surface described in my 2D model, making then its results, i.e. the ferromagnetic ground state not relevant.

As mentioned before, and seen on Fig.4.3 the ligand on the golden nanograins does effect the magnetic moments. This can also be explained by the presented 2D model in the following way; the ligand on the surface can influence the SOI strength in the system. Changing the SOI strength affects the magnetic moments, as seen in Subsection 3.5.1 on Fig.3.5, where it can be noticed that increasing the effective SOI strength lead to the increase of the spin z projection expectation value as well. On Fig.4.6 a plot similar to Fig.3.5 is shown. Here the total spin z expectation value normalized with respect to the maximal spin z value is plotted as function of the Rashba spin orbit coupling strength of the correlated band. This supports the idea, that the Rashba SOI is able influence the magnetic moments in the system.

One notes, that this description is likely valid in the case of palladium nanograins, where similar effect have been reported [131, 132, 133, 134, 135] (see Fig.4.2). In

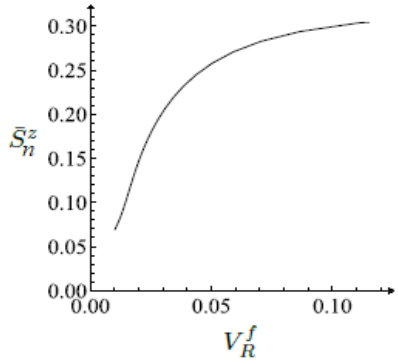

Figure 4.6: $\bar{S}_n^z$, the total spin z expectation value normalized with respect to $\bar{S}_{Max}^z = 1/2$ as function of the Rashba SOI of the correlated band V_R^f. V_R^f is in $t_x^{f,\sigma,\sigma}$ units.

the case of other non-magnetic metallic compounds, which exhibit similar behaviour, the theory described in this chapter would explain this magnetic phenomenon.

One can also note that ferromagnetic gold nanoparticle clusters behave superparamagnetic [136]. This can be related to the collective behaviour of the net magnetic moments of the gold nanoparticles within the clusters, thus the presented model and its results are not related to this phenomenon.

4.2 Summary

In this chapter a possible explanation for the size dependent ferromagnetism experienced in the case of golden nanograins was provided, using the ferromagnetic ground state wave function from Chapter 3. I drew a parallel between the surface of golden nanograins and the 2D strongly correlated, itinerant, spin 1/2 electrons on lattice, with two bands. The comparison proved to be accurate, since every aspect of the studied model applied to the surface of golden nanograins (hybridization, SOI, two-band description, etc.).

The ferromagnetic ground state was acquired for a two dimensional system with periodic boundary conditions. One indeed finds that a ferromagnetic state occurs in Au nanograins when they reach nanosize, where the majority of the particles is on the surface, thus surface effects become dominant. I also theorized that the role of the protective agents on the surface of the nanograins in the observed magnetism can be linked to their influence in the SOI strength of the surface. This was in agreement with what I found in the case of my model, where SOI strength was shown to affect the total spin z projection in the system.

The contents of this chapter is based on Ref.[O6]. The corresponding thesis point is Thesis point 3.

Chapter 5

Summary

In this dissertation I presented the influence of the many-body spin-orbit coupling on different many-body quantum systems. I performed exact calculations in the presence of SOI, first in the case of organic conducting polymer chains and then in the case of a 2D strongly correlated, non-integrable system. The results were compared to several experiments relating the effects of SOI on surfaces and interfaces, and with them theories explaining peculiar magnetic phenomena was established.

In Chapter 2 I studied flat band conditions for conducting polymers with pentagon chains. Engineering flat bands is an important task in modern condensed matter physics, due to their capability to be moved towards a wide variety of ordered phases. The choice of the studied system is not only supported by the broad application of said polymers (See Section 1.4), but also by the fact, that the description based on them allows us to explore flat band conditions in a general, clear manner. Additionally, in the presented system I also had the opportunity investigate the effects of taking into account two different spin-orbit coupling term; for the inter-cell (λ_c) and the in-cell (λ).

Despite the fact that flat bands are sought after, engineering flat-bands is challenging. This is due to the rigorous flat band conditions, which are known to cause interdependencies between the Hamiltonian parameters. These can be achieved only by extensive tuning of the Hamiltonian parameters. In my study I first presented these rigid flat band conditions for two of the Hamiltonian hopping parameters; the inter-cell hopping strength t_c and the hopping strength along the antenna of the pentagon unit cell t_f.

Next I showed how the flat bands acquired by tuning the value of t_c and t_f become dispersive band in two scenarios. First by introducing a small spin-orbit coupling (See Fig.2.5). In this case introducing the SOI in the system resulted in two spin-splitted dispersive bands. The spin-splitting properties of the SOI was not unexpected, it has been documented extensively in the literature (See Section 1.3).

Changing the t_c values defined by the flat band conditions with Δt_c also resulted in a dispersive band, which was double degenerate. My goal in this work was to show,

how SOI is able to relax the strict flat band conditions leading to flat bands, thus my next step was to show how introducing SOI in the system is able to transform this dispersive band back to a flat band. At first this was done while preserving the original position (E) of the flat band. In this case $20-30\%$ deviation from the t_c value was compensated by the SOI (See Fig.2.8). In the presence of magnetic field this increased to $\sim 80\%$ (See Fig.2.11). In the case of small, intrinsic SOI $\bar{\lambda} = \lambda = \lambda_c$ solutions were obtained at $B = 0$ (See Fig.2.10), and $B \neq 0$ (See Fig.2.12).

I studied how the flat band conditions change if we let the reflattened band appear at a new position on the energy scale (ΔE). Mathematically this means one less flat band conditions, which in this case was used to deduce ΔE, the new positions of the formed flat band. This way the rigid flat band conditions are not restrictive anymore. The energy of the flat band relative to the the initial flat band energy ($E/\Delta E$) changed around $10-20\%$ on an arbitrary energy scale. The formally restricted parameters t_f, t_c could be changed with around $20-30\%$ at $B = 0$ (See Fig.2.13) and the presence of external magnetic field seems to enhance the relaxing properties of SOI even more (See Fig.2.14).

These results seem to be promising from the standpoint of application in real systems. This is due to the fact that SOI can be modified with different methods. Tuning λ_c can be achieved by doping with heavy intrachain atoms. There are options which provide even continuous tuning possibilities for SOI strengths such as twisting, torsioning. Even more promisingly applied external electric field was found to be able to continuously change the strengths of SOI [69].

This chapter is based on publications Refs.[O1, O2]. See the list of own publication related to the dissertation in the chapter titled Own publications. The thesis point related to this chapter is the following:

1. I investigated flat band conditions for conductive polymers with pentagon chains in the presence of SOI. The band structure of the studied system was obtained from the secular equation of the diagonalized matrix of the one-particle part of the Hamiltonian transformed to k-space. First, I showed, that without SOI the flat bands conditions cause rigid interdependencies between the Hamiltonian parameters for two of the Hamiltonian hopping parameters; the inter-cell hopping strength t_c and the hopping strength along the antenna of the pentagon unit cell t_f. I showed how changing these parameters from the value defined by the flat band conditions cause the flat bands to become dispersive bands. Then I presented how SOI can reflatten the dispersive bands and thus relax the rigid flat band conditions.

   (a) At first this was done while preserving the original position of the flat band on the energy scale (E). In this case 20-30% deviation from the t_c value was compensated by the SOI. In the case of small, intrinsic SOI $\bar{\lambda} = \lambda = \lambda_c$ solutions were obtained at $B = 0$ and $B \neq 0$.

   (b) I studied how the flat band conditions change if we let the reflattened band appear at a new position on the energy scale (ΔE). In this case

one has one less flat band condition, which is used to deduce ΔE, the new positions of the formed flat band. This way the rigid flat band conditions are not restrictive anymore. The energy of the flat band relative to the initial flat band energy ($E/\Delta E$) changed around 10-20% on an arbitrary energy scale. The formally restricted parameters t_f, t_c could be changed with around 20-30% at B=0 and the presence of external magnetic field enhances the relaxing properties of SOI even more.

In the third chapter I deduced exact ground state wave functions for an itinerant, non-integrable strongly correlated system on a 2D, square lattice with two bands, from which one is correlated. I have taken into account a Hubbard type interaction and the presence of SOI. To my knowledge exact results for two dimensional fermionic systems with SOI were not available in the literature before. Often SOI is presented phenomenologically in other models, but in my work SOI is represented with its structure on the level of the Hamiltonian. In the case of 2D, non integrable systems with SOI exact method are necessary to provide reliable approximation to the physical properties and behaviour of the system.

I used the method of positive semidefinite operators to acquire an exact ground state wave function. This method is able to provide exact results relating to the ground state regardless of the integrability and the dimensions of the investigated systems, even in the case of strongly correlated systems. The first step of the method was to transform the Hamiltonian into positive semidefinite form, which I have done with the so called block operators. To conclude this transformation I solved the matching system of equations (see Appendix B.3), which were equations containing the Hamiltonian parameters with the block operator parameters as unknowns (see Appendix B.2).

After the transformation were effectuated I determined the ground state wave functions at two different system filling, one being the low concentration -, while the other being the high concentration. With these wave functions I finally calculated different ground state expectation values.

My main interest was the magnetic properties of the system, so accordingly I calculated the expectation value of the total spin z component. At high concentration I showed, that the ground state is ferromagnetic. This magnetization was due to the spin-orbit coupling in the correlated band in my model. The magnitude of the magnetization can be modulated by the SOI strengths, which can be changed for e.g. by an electric field perpendicular to the surface. Simultaneously the SOI increases the mobility of the electrons in both bands. This results have been deduced by calculating the ground state r-dependent hopping of the charge carriers. The r-dependent hopping expectation values are different for the carriers with different spin projections. These results imply a possible application in spintronics.

In this chapter I also showed how the 2D model applies to the interface of two non-magnetic material, where ferromagnetism at the interface was observed. In these cases the inversion symmetry in the system is broken at the interface, thus SOI arises. Many papers reported highly mobile electron system, where SOI dependence of the

mobility of carriers was observed. This was in agreement with the SOI strength dependent mobility of the ferromagnetic ground state of my 2D model. These results support the huge importance of taking SOI into account in understanding the ferromagnetism between non-magnetic materials.

At low concentration I showed a saturated ferromagnetic ground state for quarter system filling. In this case the ferromagnetism is not the result of SOI, though the wave function is deduced taking SOI into account, the saturated ferromagnetic ground state is the result of the Hubbard type interaction. Here the electrons are localized, the mobility is zero and all electron spin projections point to the same direction. Under a quarter system filling I have shown a paramagnetic ground state, which consists of unordered clusters.

In this chapter I also presented an extended model, were I have also taken next nearest-neighbour terms (i.e. plaquette diagonal hopping terms) and spin-flip on-site one-particle potentials into account. I showed that expanding the original Hamiltonian of the system, with terms which were originally neglected due to their small magnitude, the extracted ground state wave function remained qualitatively the same at both low-, and high concentration.

This chapter is based on the publications Refs.[O3, O4, O5]. The thesis point related to this chapter is the following:

2. I studied a 2D, itinerant, strongly correlated, many-body system, with two bands, one of which contained the strongly correlated charge carriers. I took first neighbour hoppings and hybridizations, on-site potentials and hybridizations, Hubbard type interaction in the correlated band and SOI into account.

   (a) I calculated the band structure of the studied system, by first transforming the one-particle part of the Hamiltonian to k-space, then solving the secular equation of the diagonalized one-particle Hamiltonian matrix. I showed that SOI causes the bands to split, ceasing the spin projection double degeneracy of the bands.

   (b) I used the method based on the properties of positive semidefinite operators to deduce the exact ground state wave functions of the system at low-, and high concentration. I calculated ground state expectation values at high concentration and with them I showed that the deduced ground state is ferromagnetic, by calculating the total spin z expectation value. For the r-dependent hopping I showed that it increases with increasing SOI, moreover it has a spin projection dependency.

In the fourth chapter a possible explanation for the size dependent ferromagnetism experienced in the case of golden nanograins was provided, using the ferromagnetic ground state wave function from Chapter 3. I drew a parallel between the surface of golden nanograins and the 2D strongly correlated, itinerant, spin 1/2 electrons on lattice, with two bands. The comparison proved to be accurate, since every aspect of the

studied model applied to the surface of golden nanograins (hybridization, SOI, two-band description, etc.).

The ferromagnetic ground state was acquired for a two dimensional system with periodic boundary conditions. One indeed finds that a ferromagnetic state occurs in Au nanograins when they reach nanosize, where the majority of the particles is on the surface, thus surface effects become dominant. I also theorized that the role of the protective agents on the surface of the nanograins in the observed magnetism can be linked to their influence in the SOI strength of the surface. This was in agreement with what I found in the case of my model, where SOI strength was shown to affect the total spin z projection in the system.

This chapter is based on publication Ref.[O6]. The thesis point related to this chapter is the following:

3. Using the ferromagnetic ground state wave function at high concentration, I provided a possible explanation for the size dependent ferromagnetism experienced in the case of golden nanograins. The surface of golden nanograins was modelled with the 2D strongly correlated, itinerant, spin 1/2 electrons on lattice, with two bands, SOI and periodic boundary conditions. The ferromagnetism occurs in Au nanograins when they reach nano size, where the majority of the particles is on the surface, thus surface effects become dominant and the ferromagnetic ground state of the 2D model becomes relevant. In this model, I explained the effects on the magnetism of the protective agents on the surface of the nanograins through their influence on the SOI strength. I found in the case of my model, that the SOI strength affects the total spin z projection in the system.

Chapter 6

Magyar nyelvű összefoglaló

Ebben a disszertációban a sokrészecskés spin-pálya kölcsönhatás (SOI) különböző sokrészecskés kvantumrendszerekre gyakorolt hatását vizsgáltam. Egzakt számításokat végeztem a spin-pálya kölcsönhatás jelenlétében; először vezető szerves polimerek-, majd egy kétdimenziós, erősen korrelált, nem integrálható rendszer esetében. Az eredményt több, a SOI felületekre és interfészekre gyakorolt hatását vizsgáló kísérlettel hasonlítottam össze, és ezekkel speciális mágneses jelenségeket magyarázó elméleteket állítottam fel.

A 2. fejezetben az ötszög bázisú vezető polimerláncokra vonatkozó lapos sáv kondíciókat tanulmányoztam. A lapos sávok előállítása a modern szilárdtestfizika egy kiemelkedő fontosságú feladata, aminek az oka, hogy ezen rendszerek könnyedén közelebb mozdíthatóak különböző rendezett fázisokhoz. Ebből kifolyóan a tanulmányozott rendszer széles körben alkalmazható, ezen felül pedig lehetőséget nyújt arra, hogy a lapos sáv kondíciókat általánosan és érthető módon tanulmányozni lehessen. Ezen felül a rendszerben lehetőségem volt tanulmányozni két spin-pálya kölcsönhatás tagot; a cellák közöttit (λ_c) és cellán belülit (λ).

Minden lapos sávok létrehozása való törekvés ellenére, az előállítás továbbra is nehézségeket okoz. Ennek az oka a lapos sáv kondíciók, melyek a Hamilton operátor paraméterek közötti összefüggésekhez vezetnek. Ezeket csak a Hamilton-paraméterek nagymértékű hangolásával lehet megvalósítani. A vizsgálatom során bemutattam a merev lapos sáv kondíciókat, amelyek két hopping paraméterre vonatkoznak; a cellák közötti hoppingra t_c, valamint az ötszögű egységcella antennájának mentén t_f.

Ezt követően megmutattam, hogy a lapos sávok melyeket a Hamilton operátor paraméterek hangolásával kaptam meg, hogyan változnak diszperzív sávvá két esetben. Először a változás oka a SOI bevezetése a rendszerbe. Ebben az esetben a SOI két olyan diszperzív sávot hozott létre melyek többé nem voltak a spin vetület szerint duplán degeneráltak. Ez a tulajdonsága a SOI-nak nem volt váratlan, ugyanis korábban széles körben publikált jelenségnek számít a szakirodalomban.

A t_c értékek Δt_c-vel megváltoztatva szintén diszperzív sávot kaptam, ami ezúttal spin vetület szerint duplán degenerált volt. A célom az volt, hogy bemutassam, hogy

hogyan képes a SOI a merev és szigorú lapos sáv kondíciókon enyhíteni, így ezek után megmutattam, hogy a SOI képes a diszperzív sávot ismét lapos sávvá alakítani. Először ezt a lapos sáv pozíciójának (E) az energiaskálán való rögzítése mellett szemléltettem. Ebben az esetben a lapos sáv kondíciók által meghatározott t_c értékektől való $20-30\%$ eltérést is képes voltam SOI értékekkel kompenzálni. A mágneses tér jelenlétében ez az eltérés akár $\sim 80\%$-t is elért. Kis nagyságú, belső eredetű SOI esetén a $\bar{\lambda} = \lambda = \lambda_c$ eredményeket mutattam meg $B = 0$ és $B \neq 0$ esetben.

Azt tanulmányoztam, hogy hogyan változnak a lapos sáv kondíciók, ha a laposított sávnak megengedjük, hogy az energiaskálán egy új pozícióban jelenjen meg (ΔE). Ez matematikailag azt jelenti, hogy eggyel kevesebb lapos sáv kondíciót kapunk, ugyanis egy kondíciót arra használok, hogy ΔE-t, az lapos sáv helyzetét határozzam meg. Így a lapos sáv kondíciók nem lesznek többé megszorítók. A lapos sáv energiája az eredeti lapos sáv energiájához viszonyítva ($E/\Delta E$) egy tetszőleges energiaskálán $\sim 10-20\%$ változást mutatott. A korábban rögzített paraméterek t_f, t_c esetén $20-30\%$ változást lehetett elérni $B = 0$ esetén és a külső mágneses tér jelenléte tovább növelte a SOI laposító hatását.

Ezek az eredmények ígéretesnek bizonyulnak a valós rendszerekben való alkalmazhatóság szempontjából. Ennek az oka, hogy a SOI értékét különböző módokon meg lehet változtatni. A λ_c értékét hangolni lehet nehéz atom szennyezők cellák közti behelyezésével. Vannak olyan lehetőségek is, amelyek lehetővé teszik a SOI nagyságának folytonos változtatását, mint pl. csavarás. Ennél is ígéretesebb, hogy a külső elektromos tér képes a SOI értékének folytonos változtatására [69].

Ennek a fejezetnek az alapját a következő publikációk képezik: [O1, O2]. A disszertációhoz kapcsolódó saját publikációknak a listáját az Own publications nevű fejezetben tüntettem fel. A fejezethez kapcsolódó tézispont a következő:

1. Lapos sáv kondíciókat vizsgáltam ötszög, vezetők polimerláncok esetén, SOI jelenlétében. A vizsgált rendszer sávszerkezetét a Hamilton operátor egyrészecske járulékának k-térbe transzformált, diagonalizált mátrixának szekuláris egyenletéből kaptam meg. Először is megmutattam, hogy SOI nélkül a lapos sáv kondíciók merev, a Hamilton operátor paraméterek között létrejövő összefüggésekhez vezetnek két Hamilton hopping paraméter esetében; a cellák közötti hopping nagyság t_c-, és az ötszögű egységcella antennája mentén létrejött hopping erősség t_f esetén. Megmutattam, hogy ezeknek a paramétereknek a lapos sáv kondíciók által meghatározott értékről történő megváltoztatása hogyan eredményezi a lapos sávok diszperzív sávokká válását. Ezt követően bemutattam, hogy a SOI hogyan tudja visszalaposítani a diszperzív sávokat és ezáltal lazítani a merev lapos sáv kondíciókat.

   (a) Először abban az esetben, amikor a lapos sáv megőrizte az eredeti helyzetét az energiaskálán (E-t). Ebben az esetben a SOI képes volt kompenzálni a t_c értéktől való $20-30\%$-os eltérést. Kis nagyságú, belső SOI esetén $\bar{\lambda} = \lambda = \lambda_c$ megoldásokat kaptam meg $B = 0$ és $B \neq 0$

esetben.

(b) Megvizsgáltam, hogyan változnak a lapos sáv kondíciók, ha hagyjuk az újralapított sávot az energiaskála új pozíciójában megjelenni (ΔE). Ebben az esetben egy lapos sáv feltétellel kevesebb van, amiből kiszámítottam ΔE-t, a kialakult lapos sáv új pozícióját. Így a merev lapos sáv feltételek már nem jelentenek megszorítást többé. A lapos sáv energiája a kezdeti lapos sáv energiájához viszonyítva ($E/\Delta E$) $10-20\%$ körül változott egy tetszőleges energiaskálán. A korábban megszorított t_f, t_c paraméterek $20-30\%$-kal változtathatók $B = 0$-nál, és a külső mágneses tér jelenléte még jobban fokozza a SOI a lapos sáv kondíció merevségét relaxáló képességeit.

A harmadik fejezetben egzakt alapállapoti hullámfüggvényeket határoztam meg egy itineráns, kétdimenziós erősen korrelált rendszerre, mely két sávja közül az egyik tartalmazta az elektronok közötti Hubbard típusú kölcsönhatást. Ebben a rendszerben a Hubbard kölcsönhatáson kívül szintén figyelembe vettem spin-pálya kölcsönhatást. A tudomásom szerint egzakt eredmények kétdimenziós fermionikus rendszerekre spin-pálya kölcsönhatás jelenlétében nem léteztek a szakirodalomban a bemutatott munkámat megelőzően. Gyakran a spin-pálya kölcsönhatást fenomenologikusan kezelik, ezzel szemben a munkámban a SOI-t a struktúrájával a Hamilton operátor szintjén figyelembe vettem. Ahhoz, hogy kétdimenziós, nem integrálható rendszerekre esetében egzakt eredményeket lehessen szolgáltatni egy speciális módszer alkalmazására van szükség, mely képes megbízható leírást adni a rendszer fizikai tulajdonságairól.

A munkám során a pozitív szemidefinit operátorok tulajdonságain alapuló módszert alkalmaztam az egzakt alapállapoti hullámfüggvények meghatározására. Ez a módszer alkalmazható a rendszer integrálhatóságától és dimenzióinak számától függetlenül, még az erősen korrelált rendszerek esetében is.

A módszer első lépéseként a Hamilton operátort transzformáltam pozitív szemidefinit formára, amit az ún. blokkoperátorok segítségével értem el. A transzformáció elvégzésének érdekében megoldottam a fedési egyenleteket, melyek a Hamilton operátor paramétereket tartalmazzák, mint ismert állandók, az ismeretlenei pedig a blokkoperátor paraméterek.

A transzformáció elvégzése után meghatároztam az alapállapoti hullámfüggvényt két különböző rendszertöltés esetén, melyek közül az egyik az alacsony-, míg a másik a magas koncentrációs eset volt. Ezeknek a hullámfüggvényeknek a segítségével végezetül különböző alapállapoti várható értékeket számítottam ki.

Az érdeklődésem középpontjában a rendszer mágneses tulajdonságai álltak, így a rendszer teljes spinjének z komponensének várható értékét határoztam meg. A magas koncentrációs esetben ennek segítségével megmutattam, hogy az alapállapot ferromágneses. Ez a mágnesezettség a korrelált sáv spin-pálya kölcsönhatásának köszönhető.

A mágnesezettség nagysága a SOI erősségével modulálható, ami például a felületre merőleges elektromos térrel változtatható. Ezen felül a SOI növeli az elektronok mobilitását mindkét sávban. Ezt az eredményt a töltéshordozók alapállapoti r-függő ugrásának

kiszámításával vezettük le. Az r-függő hopping várható értékei eltérőek a különböző spin vetületű töltéshordozóknál. Ezek az eredmények a spintronikában való lehetséges alkalmazásra utalnak.

Ebben a fejezetben azt is bemutattam, hogy a 2D modell hogyan alkalmazható két nem mágneses anyag interfészére, ahol a határfelületen ferromágnesességet figyeltek meg. Ezekben az esetekben a rendszerben az inverziós szimmetria megtörik a felületen, így SOI van jelen. Számos publikáció számolt be nagy mobilitású elektronrendszerről, ahol a hordozók mobilitásának SOI-függését figyelték meg. Ez összhangban volt a 2D modellem ferromágneses alapállapotának SOI erősségtől függő mobilitásával. Ezek az eredmények alátámasztják a SOI figyelembevételének óriási jelentőségét a nem mágneses anyagok közötti ferromágnesesség megértésében.

Alacsony koncentrációs esetben telített ferromágneses alapállapotot mutattam be egynegyed rendszertöltés esetében. Ebben az esetben a ferromágnesesség nem SOI eredménye, bár a hullámfüggvényt SOI figyelembevételével vezettem le, a telített ferromágneses alapállapot a Hubbard típusú kölcsönhatás eredménye. Itt az elektronok lokalizáltak, a mobilitás nulla, és minden elektronspin-vetület ugyanabba az irányba mutat. Egy negyed rendszertöltés alatt egy paramágneses alapállapotot mutattam be, amely rendezetlen klaszterekből áll.

Ebben a fejezetben egy kiterjesztett modellt is vizsgáltam, ahol figyelembe vettem a másodszomszéd hopping kifejezéseket (azaz a plakett átlós ugrásnak megfelelő kifejezéseket) és a spin-flip lokális egyrészecske potenciálokat is. Megmutattam, hogy a rendszer eredeti Hamilton operátorát kibővítve, a kis nagyságuk miatt eredetileg figyelmen kívül hagyott kifejezésekkel a kapott alapállapoti hullámfüggvény minőségileg azonos maradt, mind alacsony-, mind a magas koncentrációs esetben.

Ennek a fejezetnek az alapját a következő publikációk képezik: [O3, O4, O5]. A fejezethez kapcsolódó tézispont a következő:

2. Egy 2D, itineráns, erősen korrelált, kétsávos rendszert vizsgáltam, ahol a két sáv közül az egyik tartalmazta az erősen korrelált töltéshordozókat. Figyelembe vettem első szomszéd hoppingot és hibridizációt, lokális egyrészecske potenciált és hibridizációt, Hubbard típusú kölcsönhatást a korrelált sávban valamint SOI-t.

   (a) A vizsgált rendszer sávszerkezetét számítottam ki, először a Hamilton operátor egyrészecske járulékát k-térbe transzformáltam, majd megoldottam a szekuláris egyenletét a Hamilton operátor egyrészecske járulékából kapott diagonalizált mátrixnak. Megmutattam, hogy a SOI hatására a sávok felhasadnak, így megszűnik a sávok spinvetület szerinti dupla degenerációja.

   (b) A pozitív szemidefinit operátorok tulajdonságain alapuló módszerrel meghatároztam a rendszer egzakt alapállapoti hullámfüggvényeit alacsony és magas koncentrációs esetben. Magas koncentrációs esetben alapállapoti várható értékeket számoltam és ezekkel kimutattam, hogy

a levezetett alapállapot ferromágneses, a teljes spin z várható érték kiszámításának segítségével. Az r-függő hopping várható értéknél kimutattam, hogy a SOI növekedésével növekszik, ráadásul az értéke függ a spin-vetülettől.

A negyedik fejezetben a 3 fejezet ferromágneses alapállapot-hullámfüggvényének felhasználásával lehetséges magyarázatot adtam az arany nanoszemcsék esetében tapasztalható méretfüggő ferromágnesességre. Párhuzamot vontam az arany nanoszemcsék felülete és az erősen korrelált, kétdimenziós, itineráns, spin 1/2 elektronrendszer között. Az összehasonlítás pontosnak bizonyult, mivel a vizsgált modell minden aspektusa illet az arany nanoszemcsék felületére (hibridizáció, SOI, kétsávos leírás stb.).

A felhasznált ferromágneses alapállapotot egy kétdimenziós rendszerre, periodikus peremfeltételekkel határoztam meg. Valóban azt találjuk, hogy az Au nanoszemcsék esetén ferromágneses állapot lép fel, amikor elérik a nanoméretet, ahol a részecskék többsége a felületen van, így a felületi hatások válnak dominánssá. Azt feltételeztem továbbá, hogy a nanoszemcsék felületén lévő bevonatok szerepe a megfigyelt mágnesességben összefüggésbe hozható a felület SOI erősségére gyakorolt hatásukkal. Ez egybevágott azzal, amit a modellem esetében tapasztaltam, ahol azt mutattam, hogy a SOI erőssége befolyásolja a teljes spin z vetületet a rendszerben.

Ennek a fejezetnek az alapját a következő publikációk képezik: Ref.[O6]. A fejezethez kapcsolódó tézispont a következő:

3. A ferromágneses, nagy koncentrációs esetben kapott alapállapoti hullámfüggvény felhasználásával lehetséges magyarázatot adtam az arany nanoszemcsék esetében tapasztalható méretfüggő ferromágnesességre. Az arany nanoszemcsék felületét a 2D erősen korrelált, kétsávos itineráns, spin 1/2 elektronokra modelleztem, SOI jelenlétében és periodikus határfeltételekkel felhasználásával. A ferromágnesesség az Au nanoszemcsékben akkor lép fel, amikor azok elérik a nano méretet, ahol a részecskék nagy része a felszínen van, így a felületi hatások dominálnak és a 2D modell ferromágneses alapállapota válik relevánssá. A modellben a nanoszemcsék felületén lévő bevonatok hatását a mágnesezettségre a SOI erősségére gyakorolt hatásukkal magyaráztam. A modellem esetében azt tapasztaltam, hogy a SOI erőssége befolyásolja a rendszer teljes spin z vetületet a rendszerben.

Appendices

Appendix A

Appendices for Chapter I

A.1 The calculation of the Peierls factors

The external magnetic field in the system acts through the Peierls phase factors, which describes the effects of the external magnetic field on the orbital motion of the carriers. It is connected to the hopping matrix elements via

$$t_{j\leftarrow i}(B) = t_{j\leftarrow i}(0)e^{i\frac{2\pi}{\phi_0}\int_i^j \vec{A}\vec{dl}} = t_{j\leftarrow i}(0)e^{i\varphi_{ji}}, \tag{A.1}$$

where $\phi_0 = \frac{hc}{e}$. Here $t_{j\leftarrow i}(0)$ are the hopping couplings in the system without the magnetic field, φ_{ji} are the so called Peierls factors. One can calculate the Peierls factors, by fixing a specific choice of gauge. Since $B = rot(\vec{A})$, we want B to be constant and point to the z direction. Thus $A_x = -By, A_y = A_z = 0$. We turn our attention to calculating the exact φ_{ji} for each bond. One can easily calculate $\varphi_{56} = 0$, since the scalar product is zero ($\vec{A} \perp \vec{dl}$), φ_{47} is also 0, because $y = 0$ (see Fig.2.1).

$$\begin{aligned}
\varphi_{3\leftarrow 2} &= \frac{2\pi}{\phi_0}(-By_2), \varphi_{3\leftarrow 2} = \varphi_1, \\
\varphi_{4\leftarrow 3} &= \frac{2\pi B}{\phi_0}\frac{|y_2|b_2}{2}, \varphi_{2\leftarrow 1} = \varphi_{4\leftarrow 3} = \varphi_2, \\
\varphi_{5\leftarrow 4} &= \frac{2\pi}{\phi_0}B\frac{y_1 b}{4}, \quad \varphi_{5\leftarrow 4} = \varphi_{1\leftarrow 5} = \varphi_3.
\end{aligned} \tag{A.2}$$

Here

$$\varphi = \varphi_1 + 2\varphi_2 + 2\varphi_3 = \frac{2\pi}{\phi_0}\phi, \tag{A.3}$$

where $\phi = BS$, the flux through the unit cell, $S = |y_2|b_1 + 2\frac{|y_2|b_2}{2} + 2\frac{y_1 b}{4}$.

In the presence of constant external magnetic field, pointing to z direction,

the hoppings coupling strengths are multiplied by the formerly calculated Peierls phase factors. In summary the phase factor attaching to hopping terms present in the Hamiltonian (as seen in Eq.(2.6)):

$$\varphi_1 = \frac{2\pi}{\phi_0}(-By_2), \quad \varphi_2 = \frac{2\pi}{\phi_0}B\frac{|y_2|b_2}{2}, \quad \varphi_3 = \frac{2\pi}{\phi_0}B\frac{y_1 b}{4}. \tag{A.4}$$

A.2 The secular equation of M

The secular equation of the diaganolized matrix of the one-particle part of the Hamiltonian **M** has the form seen in expression Eq.(2.12), i.e. $\det(\mathbf{M}-E\mathbf{I}) = C(A+iV)(A-iV) = 0$. Where the form of A:

$$\begin{aligned} A = A_f \quad &- \quad \frac{1}{A_f}\left(\lambda_c e^{i(\phi_k-2\phi_3)} + 2\lambda t\xi\right)\left(\lambda_c e^{-i(\phi_k-2\phi_3)} + 2\lambda t\xi^*\right) - \\ &- \quad \frac{1}{A_f}\left(t_c e^{i(\phi_k-2\phi_3)} - (t^2-\lambda^2)\xi\right)\left(t_c e^{-i(\phi_k-2\phi_3)} - (t^2-\lambda^2)\xi^*\right). \end{aligned} \tag{A.5}$$

Here the ξ is

$$\xi = \left(\frac{\epsilon_4}{\epsilon_f}e^{i\phi} - \frac{t_h}{\epsilon_2^2 - t_h^2}\right). \tag{A.6}$$

The V from Eq.(2.12) is

$$\begin{aligned} V = \quad &- \quad \frac{1}{A_f}\left(\lambda_c e^{i(\phi_k-2\phi_3)} + 2\lambda t\xi\right)\left(t_c e^{-i(\phi_k-2\phi_3)} - (t^2-\lambda^2)\xi^*\right) - \\ &- \quad \frac{1}{A_f}\left(-\lambda_c e^{-i(\phi_k-2\phi_3)} - 2\lambda t\xi^*\right)\left(t_c e^{i(\phi_k-2\phi_3)} - (t^2-\lambda^2)\xi\right). \end{aligned} \tag{A.7}$$

A.3 The flat band conditions derived from the $(A-iV)$ expression

The expression can be written as:

$$(A - iV) = X_0 + Y_1\cos(\varphi_k) + Y_2\sin(\varphi_k) = 0, \tag{A.8}$$

where X_0 is the same as seen in (2.22). At the same time Y_1, Y_2:

$$\begin{aligned} Y_1 = \frac{1}{A_f}\Bigg(&- \cos(7\varphi_3)\frac{2(2\lambda t\lambda_c + t_c(\lambda^2-t^2))}{\bar{\bar{\epsilon}}_3} + \sin(7\varphi_3)\frac{2(-2\lambda t t_c + \lambda_c(\lambda^2-t^2))}{\bar{\bar{\epsilon}}_3} + \\ &+ \cos(2\varphi_3)\frac{2(2\lambda t\lambda_c + t_c(\lambda^2-t^2))t_h}{\bar{\epsilon}_2\bar{\bar{\epsilon}}_2} - \sin(2\varphi_3)\frac{2(-2\lambda t t_c + \lambda_c(\lambda^2-t^2))t_h}{\bar{\epsilon}_2\bar{\bar{\epsilon}}_2}\Bigg) = 0, \end{aligned}$$

$$Y_2 = \frac{1}{A_f}\Bigg(-\cos(7\varphi_3)\frac{2(-2\lambda t t_c + \lambda_c(\lambda^2 - t^2))}{\bar{\bar{\epsilon}}_3} - \sin(7\varphi_3)\frac{2(2\lambda t\lambda_c + t_c(\lambda^2 - t^2))}{\bar{\bar{\epsilon}}_3} + \\ + \cos(2\varphi_3)\frac{2(-2\lambda t t_c + \lambda_c(\lambda^2 - t^2))t_h}{\bar{\epsilon}_2\bar{\bar{\epsilon}}_2} + \sin(2\varphi_3)\frac{2(2\lambda t\lambda_c + t_c(\lambda^2 - t^2))t_h}{\bar{\epsilon}_2\bar{\bar{\epsilon}}_2}\Bigg) = 0. \tag{A.9}$$

Using the same notation as in Eg.2.23 this expression becomes:

$$Y_1 = \frac{1}{A_f}(-Kv + Su) = 0, \quad Y_2 = \frac{1}{A_f}(-Ku - Sv) = 0. \tag{A.10}$$

Since v, u contains the non zero Hamilton operator parameters, which we considered to be real numbers, the only solution for these conditions remains the be $K = S = 0$, which are in agreement with the solutions derived from the $(A + iV)$ expression.

A.4 Hamiltonian parameters used for the figures

Table A.1							
Parameters calculated from the rigid flat band conditions for the system without SOI		The unrestricted parameters					
t_c	t_f	ϵ_1	ϵ_2	ϵ_3	ϵ_4	t	t_h
1.16	2.29	0.17	0.49	0.22	3.36	1	1.5

Table A.1: All parameters presented are given in t units, and the rigidly fixed flat band conditions have been deduced at $B = \lambda = \lambda_c = 0$.

Table A.2							
Parameters calculated from the rigid flat band conditions for the system without SOI		The unrestricted parameters					
t_c	t_f	ϵ_1	ϵ_2	ϵ_3	ϵ_4	t	t_h
2.21	0.14	0.87	1.22	0.82	0.36	1	0.9

Table A.2: All parameters presented are given in t units, and the rigidly fixed flat band conditions have been deduced at $B = \lambda = \lambda_c = 0$. Where $B \neq 0$ plots were also done, the B value was deduced from Eq.(22), i.e. $I_\varphi = X_\varphi = -1$. E.g., for $\varphi_b = 3\varphi_3$ (regular pentagon), one has at minimum B the relation $\varphi_3 = (1/5)\pi$. For more in connection with the value of B, see also Appendix A.1.

Table A.3							
Parameters calculated from the rigid flat band conditions for the system without SOI		The unrestricted parameters					
t_c	t_f	ϵ_1	ϵ_2	ϵ_3	ϵ_4	t	t_h
1.44	1.23	0.11	0.10	0.92	0.86	1	0.85

Table A.3: All parameters presented are given in t units, and the rigidly fixed flat band conditions have been deduced at $B = \lambda = \lambda_c = 0$.

Table A.4							
Parameters calculated from the rigid flat band conditions for the system without SOI		The unrestricted parameters					
t_c	t_f	ϵ_1	ϵ_2	ϵ_3	ϵ_4	t	t_h
1.31	1.68	0.65	0.49	1.4	0.86	1	2

Table A.4: All parameters presented are given in t units, and the rigidly fixed flat band conditions have been deduced at $B = \lambda = \lambda_c = 0$. Where $B \neq 0$ plots were also done, the B value was deduced from Eq.(2.25), i.e. $I_\varphi = X_\varphi = -1$. E.g., for $\varphi_b = 3\varphi_3$ (regular pentagon), one has at minimum B the relation $\varphi_3 = (1/5)\pi$. For more in connection with the value of B, see also Appendix A.1.

Appendix B

Appendices for Chapter II

B.1 SOI in second quantized formalism

As other terms in the Hamiltonian I also need the SOI in second quantized formalism. In order to deduce these I will further form the H_R and H_D spin-orbit terms, as seen in first quantized forms in Eq.(1.9) and Eq.(1.10). Consequently I will transform these terms into k-space:

$$H_R = \beta_R(\sigma_x k_y - \sigma_y k_x), \quad H_D = \alpha_D(\sigma_y k_y - \sigma_x k_x). \tag{B.1}$$

A general first quantized one particle operator, $\hat{L}_{\beta\alpha}(\vec{k})$ can be transformed into second quantized form the following way:

$$\hat{L} = \sum_{\alpha\beta} \int \frac{d^D k}{(2\pi)^D} \hat{\psi}^+_\beta(\vec{k}) \hat{L}_{\beta\alpha} \hat{\psi}_\alpha(\vec{k}), \tag{B.2}$$

where D is dimension, which in our case $D = 2$, $\hat{\psi}_\alpha(\vec{k})$ is the field operator with fermionic creation operators. The basis is a set of single particle wave function, which are arbitrarily chosen as plane waves:

$$\begin{aligned} \hat{\psi}_\alpha(\vec{k}) &= \sum_i \varphi_i(\vec{k}) \hat{c}_{i\alpha}, \\ \varphi_i(\vec{k}) &= \frac{1}{2\pi} e^{-i(k_x r_{ix} + k_y r_{iy})}, \end{aligned} \tag{B.3}$$

where r_{ix} and r_{iy} are in lattice constant units in the x- and y directions. To get the two quantities (H_R and H_D) in second quantized form in Eq.(B.1), let us calculate $L_{Dy} = \sigma_y k_y \beta_D$, $L_{Dx} = \sigma_x k_x \beta_D$, $L_{Ry} = \sigma_x k_y \alpha_R$, $L_{Ry} = \sigma_y k_x \alpha_R$ in this form. The solution I will

show through an example, namely the transformation of $\hat{L}_{Dy}$ to second quantized form:

$$\hat{L}_{Dy} = \sum_{i,j}\sum_{\alpha\beta} \hat{c}^{+}_{j\beta}\sigma_y\hat{c}_{i\alpha}\beta_D \frac{\mathbf{1}}{\boldsymbol{(2\pi)^2}} \int_{-\boldsymbol{\pi}}^{\boldsymbol{\pi}} \boldsymbol{dk_x} \int_{-\boldsymbol{\pi}}^{\boldsymbol{\pi}} \boldsymbol{dk_y e^{ik_x(x_j-x_i)} e^{ik_y(y_j-y_i)} k_y}. \quad \text{(B.4)}$$

First I will calculate the integral written in bold from Eq.(B.4) :

$$\begin{aligned}
&\frac{1}{(2\pi)^2}\int_{-\pi}^{\pi} dk_x \int_{-\pi}^{\pi} dk_y e^{ik_x(x_j-x_i)} e^{ik_y(y_j-y_i)} k_y = \\
&= \underbrace{\Big[\frac{1}{2\pi}\int_{-\pi}^{\pi} dk_x e^{ik_x(x_j-x_i)}\Big]}_{\delta_{x_j,x_i}} \Big[\frac{1}{2\pi}\int_{-\pi}^{\pi} dk_y e^{ik_y(y_j-y_i)} k_y\Big] = \\
&= \delta_{x_j,x_i}\Big[\frac{1}{2\pi} e^{ik_y(y_j-y_i)} \frac{[ik_y(y_j-y_i)]k_y - 1}{[ik_y(y_j-y_i)]^2}\Big]_{-\pi}^{\pi} = \\
&= \delta_{x_j,x_i}\Big[\frac{1}{2\pi} e^{ik_y(y_j-y_i)} \frac{-1}{[ik_y(y_j-y_i)]^2}\Big]_{-\pi}^{\pi} \Big[\frac{1}{2\pi} e^{ik_y(y_j-y_i)} \frac{k_y}{ik_y(y_j-y_i)}\Big]_{-\pi}^{\pi} = \\
&= \delta_{x_j,x_i}\Big[\frac{1}{\pi(y_j-y_i)]^2} \frac{e^{i\pi(y_j-y_i)} - e^{-i\pi(y_j-y_i)}}{2}\Big]\Big[\frac{1}{i(y_j-y_i)]^2} \frac{e^{-i\pi(y_j-y_i)} + e^{i\pi(y_j-y_i)}}{2}\Big] = \\
&= \delta_{x_j,x_i}\Big[\frac{i}{\pi(y_j-y_i)]^2} \underbrace{\sin[(y_j-y_i)\pi]}_{=0}\Big]\Big[\underbrace{\frac{1}{i(y_j-y_i)]^2} \cos[(y_j-y_i)\pi]}_{=\frac{1}{i}\cos\pi = i}\Big]. \qquad \text{(B.5)}
\end{aligned}$$

Last I used that y_i and y_j are in lattice constant units, thus the difference between them is a whole number. Moreover I have taken only the first neighbour contributions into account and for this reason $y_j - y_i = 1$. This also means that for y δ_{y_j,y_i+1} is met. Based on these considerations similar integrals can be written for the other first quantized spin-orbit couplings. In the next step I will summarize by α, β:

$$\begin{aligned}
\hat{L}_{Dy} &= \sum_{\alpha,\beta}\sum_{i,j} \hat{c}^{+}_{j\beta} i\sigma_y \hat{c}_{i\alpha} \beta_D \delta_{x_j,x_i}\delta_{y_j,y_i+1} \\
&= \sum_i \beta_D (\hat{c}^{+}_{x_i,y_i+1,\uparrow}\hat{c}_{x_i,y_i+1,\downarrow} - \hat{c}^{+}_{x_i,y_i+1,\downarrow}\hat{c}_{x_i,y_i,\uparrow}) = \\
&= \sum_i \underbrace{\beta_D}_{V_D} (\underbrace{\hat{c}^{+}_{i+y,\uparrow}\hat{c}_{i,\downarrow}}_{t_y^{\uparrow,\downarrow}} - \underbrace{\hat{c}^{+}_{i+y,\downarrow}\hat{c}_{i,\uparrow}}_{t_y^{\downarrow,\uparrow}}). \qquad \text{(B.6)}
\end{aligned}$$

In the last line I signed the corresponding couplings strengths. Here $t_y^{\uparrow,\downarrow}$ and $t_y^{\downarrow,\uparrow}$ are the couplings of the spin-flip hoppings; coefficients before the operator products in the Hamiltonian from Eq.(B.6). Similarly to L_{Dy}, we now can calculate the L_{Dx}, L_{Rx}, L_{Ry} terms. These are the following:

$$\hat{L}_{Dx} = \sum_i V_D(-i\underbrace{\hat{c}^{+}_{i+x,\downarrow}\hat{c}_{i,\uparrow}}_{t_x^{\downarrow,\uparrow}}) - i\underbrace{\hat{c}^{+}_{i+x,\uparrow}\hat{c}_{i,\downarrow}}_{t_x^{\uparrow,\downarrow}}),$$

$$\hat{L}_{Rx} = \sum_i V_R(\underbrace{\hat{c}^+_{i+x,\downarrow}\hat{c}_{i,\uparrow}}_{t_x^{\downarrow,\uparrow}}) + \underbrace{\hat{c}^+_{i+x,\uparrow}\hat{c}_{i,\downarrow}}_{t_x^{\uparrow,\downarrow}}),$$
$$\hat{L}_{Ry} = \sum_i V_R(i\underbrace{\hat{c}^+_{i+y,\downarrow}\hat{c}_{i,\uparrow}}_{t_y^{\downarrow,\uparrow}}) + i\underbrace{\hat{c}^+_{i+y,\uparrow}\hat{c}_{i,\downarrow}}_{t_y^{\uparrow,\downarrow}}). \quad \text{(B.7)}$$

In (B.7) under the products of different c operators I wrote the matching hopping coupling strengths (the coefficients which multiply the same products in the Hamiltonian). Let us investigate two cases. If $V_R = 0 : t_y^{\uparrow,\downarrow} = V_D$; $t_y^{\downarrow,\uparrow} = -V_D$; $t_x^{\uparrow,\downarrow} = -iV_D$; $t_x^{\downarrow,\uparrow} = -iV_D$. If $V_D = 0 : t_y^{\uparrow,\downarrow} = iV_R$; $t_y^{\downarrow,\uparrow} = iV_R$; $t_x^{\uparrow,\downarrow} = -V_R$; $t_x^{\downarrow,\uparrow} = V_R$. Comparing this to hopping terms in the Hamiltonian (3.5), there is a interdependence between the hopping terms and the Rashba-, and Dresselhaus couplings (V_R and V_D), which is the following:

$$t_x^{c,\uparrow,\downarrow} = V_R^c - iV_D^c, \quad t_y^{c,\uparrow,\downarrow} = V_D^c - iV_R^c,$$
$$t_x^{c,\downarrow,\uparrow} = -V_R^c - iV_D^c, \quad t_y^{c,\downarrow,\uparrow} = -V_D^c - iV_R^c, \quad \text{(B.8)}$$

where $c = f, d$.

B.2 The system of matching equations

B.2.1 At low concentration

There are 74 equations, which at low concentration are the following:

The are 16 equations relating two first neighbour hoppings; 8 for each $c = d, f$ orbits and $\sigma = \uparrow, \downarrow$, from which 4 is related to a non spin-flip hopping and 4 four spin-flip hoppings ($\sigma \neq \sigma'$):

$$t_x^{c,\sigma,\sigma} = a^*_{2,c,\sigma}a_{1,c,\sigma} + a^*_{3,c,\sigma}a_{4,c,\sigma} + b^*_{2,c,\sigma}b_{1,c,\sigma} + b^*_{3,c,\sigma}b_{4,c,\sigma},$$
$$t_y^{c,\sigma,\sigma} = a^*_{4,c,\sigma}a_{1,c,\sigma} + a^*_{3,c,\sigma}a_{2,c,\sigma} + b^*_{4,c,\sigma}b_{1,c,\sigma} + b^*_{3,c,\sigma}b_{2,c,\sigma},$$

$$t_x^{c,\sigma,\sigma'} = a^*_{2,c,\sigma}a_{1,c,\sigma'} + a^*_{3,c,\sigma}a_{4,c,\sigma'} + b^*_{2,c,\sigma}b_{1,c,\sigma'} + b^*_{3,c,\sigma}b_{4,c,\sigma'},$$
$$t_y^{c,\sigma,\sigma'} = a^*_{4,c,\sigma}a_{1,c,\sigma'} + a^*_{3,c,\sigma}a_{2,c,\sigma'} + b^*_{4,c,\sigma}b_{1,c,\sigma'} + b^*_{3,c,\sigma}b_{2,c,\sigma'}. \quad \text{(B.9)}$$

Next are the 16 diagonal (second neighbour) hopping equations: 8 for each $c = d$ and f orbits. These equal to zero, since they were not considered in the original Hamiltonian Eq.(3.6).

$$t_{x+y}^{c,\sigma,\sigma} = a^*_{3,c,\sigma}a_{1,c,\sigma} + b^*_{3,c,\sigma}b_{1,c,\sigma} = 0, \qquad t_{y-x}^{c,\sigma,\sigma} = a^*_{4,c,\sigma}a_{2,c,\sigma} + b^*_{4,c,\sigma}b_{2,c,\sigma} = 0,$$
$$t_{x+y}^{c,\sigma,\sigma'} = a^*_{3,c,\sigma}a_{1,c,\sigma'} + b^*_{3,c,\sigma}b_{1,c,\sigma'} = 0, \quad t_{y-x}^{c,\sigma,\sigma} = a^*_{4,c,\sigma}a_{2,c,\sigma'} + b^*_{4,c,\sigma}b_{2,c,\sigma'} = 0. \quad \text{(B.10)}$$

Following are the first neighbour, non-spin-flip hybridizations which contribute to 8 equa-

tions ($c \neq c'$):

$$V_x^{c,c',\sigma,\sigma} = a^*_{2,c,\sigma}a_{1,c',\sigma} + a^*_{3,c,\sigma}a_{4,c',\sigma} + b^*_{2,c,\sigma}b_{1,c',\sigma} + b^*_{3,c,\sigma}b_{4,c',\sigma},$$
$$V_y^{c,c',\sigma,\sigma} = a^*_{4,c,\sigma}a_{1,c',\sigma} + a^*_{3,c,\sigma}a_{2,c',\sigma} + b^*_{4,c,\sigma}b_{1,c',\sigma} + b^*_{3,c,\sigma}b_{2,c',\sigma}. \quad \text{(B.11)}$$

Corresponding to the first neighbour, spin-flip hybridization terms there are 8 equations, each equals to zero, since they were not present in the original Hamiltonian.

$$V_x^{c,c',\sigma,\sigma'} = a^*_{2,c,\sigma}a_{1,c',\sigma'} + a^*_{3,c,\sigma}a_{4,c',\sigma'} + b^*_{2,c,\sigma}b_{1,c',\sigma'} + b^*_{3,c,\sigma}b_{4,c',\sigma'} = 0,$$
$$V_y^{c,c',\sigma,\sigma'} = a^*_{4,c,\sigma}a_{1,c',\sigma'} + a^*_{3,c,\sigma}a_{2,c',\sigma'} + b^*_{4,c,\sigma}b_{1,c',\sigma'} + b^*_{3,c,\sigma}b_{2,c',\sigma'} = 0. \quad \text{(B.12)}$$

The next 16 equations are the diagonal (second neighbour) hybridization, which are also zero.

$$V_{x+y}^{c,c',\sigma,\sigma} = a^*_{3,c,\sigma}a_{1,c',\sigma} + b^*_{3,c,\sigma}b_{1,c',\sigma} = 0,$$
$$V_{y-x}^{c,c',\sigma,\sigma} = a^*_{4,c,\sigma}a_{2,c',\sigma} + b^*_{4,c,\sigma}b_{2,c',\sigma} = 0,$$
$$V_{x+y}^{c,c',\sigma,\sigma'} = a^*_{3,c,\sigma}a_{1,c',\sigma'} + b^*_{3,c,\sigma}b_{1,c',\sigma'} = 0,$$
$$V_{y-x}^{c,c',\sigma,\sigma'} = a^*_{4,c,\sigma}a_{2,c',\sigma'} + b^*_{4,c,\sigma}b_{2,c',\sigma'} = 0. \quad \text{(B.13)}$$

The are 4 on-site hybridization equations. From these two represent spin-flip terms, which we will eliminate by making these expressions equal to zero. The first two non-spin-flip terms are on the other hand present in the original Hamiltonian:

$$\begin{aligned} V_0^{d,f,\sigma,\sigma} = \quad & a^*_{1,d,\sigma}a_{1,f,\sigma} + a^*_{2,d,\sigma}a_{2,f,\sigma} + a^*_{3,d,\sigma}a_{3,f,\sigma} + a^*_{4,d,\sigma}a_{4,f,\sigma} + \\ + \quad & b^*_{1,d,\sigma}b_{1,f,\sigma} + b^*_{2,d,\sigma}b_{2,f,\sigma} + b^*_{3,d,\sigma}b_{3,f,\sigma} + b^*_{4,d,\sigma}b_{4,f,\sigma}, \\ V_0^{d,f,\sigma,\sigma'} = \quad & a^*_{1,d,\sigma}a_{1,f,\sigma'} + a^*_{2,d,\sigma}a_{2,f,\sigma'} + a^*_{3,d,\sigma}a_{3,f,\sigma'} + a^*_{4,d,\sigma}a_{4,f,\sigma'} + \\ + \quad & b^*_{1,d,\sigma}b_{1,f,\sigma'} + b^*_{2,d,\sigma}b_{2,f,\sigma'} + b^*_{3,d,\sigma}b_{3,f,\sigma'} + b^*_{4,d,\sigma}b_{4,f,\sigma'} = 0. \end{aligned} \quad \text{(B.14)}$$

In Eq.(B.14) there are no on-site terms for fd indices, since $(V_0^{d,f,\sigma,\sigma})^* = V_0^{f,d,\sigma,\sigma}$ and $(V_0^{d,f,\sigma,\sigma'})^* = V_0^{f,d,\sigma,\sigma'}$.

The 6 equations below are for the on-site potentials. The 4 terms without spin-flip; 2 for each orbits $c = d, f$ do contribute to the Hamiltonian in my model. The last two; one for each orbits $c = d, f$ on the other hand represents spin-flip on-site potential which I considered to be zero.

$$\begin{aligned} \tilde{\epsilon}_c^{\sigma,\sigma} = \quad & a^*_{1,c,\sigma}a_{1,c,\sigma} + a^*_{2,c,\sigma}a_{2,c,\sigma} + a^*_{3,c,\sigma}a_{3,c,\sigma} + a^*_{4,c,\sigma}a_{4,c,\sigma} + \\ + \quad & b^*_{1,c,\sigma}b_{1,c,\sigma} + b^*_{2,c,\sigma}b_{2,c,\sigma} + b^*_{3,c,\sigma}b_{3,c,\sigma} + b^*_{4,c,\sigma}b_{4,c,\sigma}. \end{aligned} \quad \text{(B.15)}$$

In Eq.(B.15) $\tilde{\epsilon}_c^{\sigma,\sigma} = \epsilon_c^{\sigma,\sigma} - \eta$, $c = d, f$, $\sigma = \uparrow, \downarrow$.

$$\begin{aligned} \epsilon_c^{\uparrow,\downarrow} = \quad & a^*_{1,c,\uparrow}a_{1,c,\downarrow} + a^*_{2,c,\uparrow}a_{2,c,\downarrow} + a^*_{3,c,\uparrow}a_{3,c,\downarrow} + a^*_{4,c,\uparrow}a_{4,c,\downarrow} + \\ + \quad & b^*_{1,c,\uparrow}b_{1,c,\downarrow} + b^*_{2,c,\uparrow}b_{2,c,\downarrow} + b^*_{3,c,\uparrow}b_{3,c,\downarrow} + b^*_{4,c,\uparrow}b_{4,c,\downarrow} = 0. \end{aligned} \quad \text{(B.16)}$$

In Eq.(B.16) $(\epsilon_c^{\uparrow\downarrow})^* = \epsilon_c^{\downarrow\uparrow}$. The unknowns of the system of the equations are the block

parameters, and the known quantities are the Hamiltionian coupling strengths. I would like to point out, that coupling strengths which are not part of the original Hamiltonian i.e. Eq.(3.6) appear in this system of equations, because the products of block operators in the transformed Hamiltonian produce them. As seen in Eq.(B.10),Eq(B.12, B.13), Eq.(B.14),Eq.(B.16) I eliminated these equations by considering them to be zero.

B.2.2 At high concentration

At high concentration the right side of the equations remains the same for all of the 74 equations introduced formerly. All on the left hand side on the other hand, renormalizes with a negative sign ($\bar{t} = -t, \bar{V} = -V$) except for the on-site potentials without spin-flip ($\epsilon_c^{\sigma,\sigma}$). Additionally in the place of $\epsilon_c^{\sigma,\sigma}$ also a renormalized term ($\bar{\epsilon}_c^{\sigma,\sigma}$) will appear, where $\bar{\epsilon}_c^{\sigma,\sigma} = \epsilon_c^{\sigma\sigma} + U_c$, and $c = d, f$, while $U_d = 0$ and $U_f > 0$.

B.3 The solution for the matching equations

The matching equations shown in Appendix B.2 are mathematically identical at the low and high concentrations. For this reason I will demonstrate the solutions at the low concentration. For the high concentration system, the same solutions is appropriate if we replace the Hamiltonian coupling constants with the renormalized coupling constants shown in Appendix B.2.2.

To solve the system matching equations we will start with the least complicated equations. In this case these are related to terms eliminating the diagonal hoppings (B.10) and diagonal hybridization (B.13). This leads to the following 32 equations: 16 for the term without hybridization; 8 for each orbits $c = d, f$ and 16 for the terms with hybridization ($c' = d, f$, $c' \neq c$):

$$\begin{aligned}
&a^*_{3,c,\sigma} a_{1,c,\sigma} = -b^*_{3,c,\sigma} b_{1,c,\sigma}, \quad && a^*_{3,c,\sigma} a_{1,c',\sigma} = -b^*_{3,c,\sigma} b_{1,c',\sigma}, \\
&a^*_{3,c,\sigma} a_{1,c,\sigma'} = -b^*_{3,c,\sigma} b_{1,c,\sigma'}, \quad && a^*_{3,c,\sigma} a_{1,c',\sigma'} = -b^*_{3,c,\sigma} b_{1,c',\sigma'}, \\
&a^*_{4,c,\sigma} a_{2,c,\sigma} = -b^*_{4,c,\sigma} b_{2,c,\sigma}, \quad && a^*_{4,c,\sigma} a_{2,c',\sigma} = -b^*_{4,c,\sigma} b_{2,c',\sigma}, \\
&a^*_{4,c,\sigma} a_{2,c,\sigma'} = -b^*_{4,c,\sigma} b_{2,c,\sigma'}, \quad && a^*_{4,c,\sigma} a_{2,c',\sigma'} = -b^*_{4,c,\sigma} b_{2,c',\sigma'}.
\end{aligned} \tag{B.17}$$

At this point I will introduce four arbitrary parameters x, y, z, v. With these defining equations, Eq.(B.17) can be satisfied.

$$\begin{aligned}
&\frac{a^*_{3,d,\uparrow}}{b^*_{3,d,\uparrow}} = -\frac{b_{1,d,\downarrow}}{a_{1,d,\downarrow}} = x, \quad && \frac{a^*_{3,d,\downarrow}}{b^*_{3,d,\downarrow}} = -\frac{b_{1,d,\uparrow}}{a_{1,d,\uparrow}} = y, \\
&\frac{a^*_{4,d,\uparrow}}{b^*_{4,d,\uparrow}} = -\frac{b_{2,d,\downarrow}}{a_{2,d,\downarrow}} = z, \quad && \frac{a^*_{4,d,\downarrow}}{b^*_{4,d,\downarrow}} = -\frac{b_{2,d,\uparrow}}{a_{2,d,\uparrow}} = v.
\end{aligned} \tag{B.18}$$

I now substitute Eq.(B.18) into the 32 equation which is Eq.(B.17). This way one notices, that all the $\hat{A}$ parameters are interdependent with the $\hat{B}$ parameters. Moreover,

investigating these interdependence I found that the parameters from Eq.(B.18) are also not independent, because $x = y$ and $v = z$. Based on these findings the a parameters can be written as function of the b parameters and x, v arbitrary numbers. This way one gets 16 equations:

$$\begin{aligned} a_{1,c,\sigma} &= -\frac{1}{x} b_{1,c,\sigma}, \quad a_{3,c,\sigma} = x^* b_{3,c,\sigma}, \\ a_{2,c,\sigma} &= -\frac{1}{v} b_{2,c,\sigma}, \quad a_{4,c,\sigma} = v^* b_{4,c,\sigma}. \end{aligned} \tag{B.19}$$

With Eq.(B.19) there are 42 remaining matching equations (Eq.(B.9), Eq.(B.11), Eq.(B.13)-(B.16)). I will continue with the spin-flip, hybridization ($V_x^{c,c',\sigma\sigma'\neq\sigma} = V_y^{c,c',\sigma,\sigma'\neq\sigma} = 0$)

$$\begin{aligned} V_x^{c,c',\sigma,\sigma'} &= (\frac{1}{xv^*} + 1) b^*_{2,c,\sigma} b_{1,c',\sigma'} + (xv^* + 1) b^*_{3,c,\sigma} b_{4,c',\sigma'} = 0, \\ V_y^{c,c',\sigma,\sigma'} &= (-\frac{v}{x} + 1) b^*_{4,c,\sigma} b_{1,c',\sigma'} + (-\frac{x}{v} + 1) b^*_{3,c,\sigma} b_{2,c',\sigma'} = 0, \end{aligned} \tag{B.20}$$

where $c = f, d$, $c^{'} = f, d$ $c \neq c^{'}$, $\sigma = \uparrow, \downarrow$, $\sigma^{'} = \uparrow, \downarrow$, $\sigma \neq \sigma^{'}$. There are 8 equations relating to these terms. These can be summarized as the following proportionalities:

$$\begin{aligned} \frac{b^*_{3,d,\sigma}}{b_{1,f,\sigma'}} &= -\frac{1}{xv^*} \frac{b^*_{2,d,\sigma}}{b_{4,f,\sigma'}}, \qquad \frac{b_{2,d,\sigma}}{b^*_{4,f,\sigma'}} = \frac{v}{x} \frac{b_{1,d,\sigma}}{b^*_{3,f,\sigma'}}, \\ \frac{b_{4,d,\sigma}}{b^*_{2,f,\sigma'}} &= -\frac{1}{xv^*} \frac{b_{1,d,\sigma}}{b^*_{3,f,\sigma'}}, \qquad \frac{b^*_{4,d,\sigma}}{b_{2,f,\sigma'}} = \frac{x}{v} \frac{b^*_{3,d,\sigma}}{b_{1,f,\sigma'}}. \end{aligned} \tag{B.21}$$

I introduce two further arbitrary parameters (w, u), which are defined by the two $\frac{b_{2,d,\sigma}}{b^*_{4,f,\sigma'}} = \frac{v}{x} \frac{b_{1,d,\sigma}}{b^*_{3,f,\sigma'}}$ equations, which are present in the second column of the first row in Eq.(B.21).

$$\frac{b_{2,d,\downarrow}}{b^*_{4,f,\uparrow}} = \frac{v}{x} \frac{b_{1,d,\downarrow}}{b^*_{3,f,\uparrow}} = w, \qquad \frac{b_{2,d,\uparrow}}{b^*_{4,f,\downarrow}} = \frac{v}{x} \frac{b_{1,d,\uparrow}}{b^*_{3,f,\downarrow}} = u. \tag{B.22}$$

With the parameters in Eq.(B.22) new proportionalities can be discovered in Eq.(B.21):

$$\begin{aligned} &\frac{b^*_{3,d,\uparrow}}{b_{1,f,\downarrow}} = -\frac{1}{xv^*} \frac{b^*_{2,d,\uparrow}}{b_{4,f,\downarrow}} = -\frac{u^*}{xv^*}, \ \frac{b^*_{4,d,\uparrow}}{b_{2,f,\downarrow}} = \frac{x}{v} \frac{b^*_{3,d,\uparrow}}{b_{1,f,\downarrow}} = -\frac{u^*}{|v|^2}, \ \frac{b_{4,d,\downarrow}}{b^*_{2,f,\uparrow}} = -\frac{1}{xv^*} \frac{b_{1,d,\downarrow}}{b^*_{3,f,\uparrow}} = -\frac{w}{|v|^2}, \\ &\frac{b^*_{3,d,\downarrow}}{b_{1f\uparrow}} = -\frac{1}{xv^*} \frac{b^*_{2,d,\downarrow}}{b_{4,f,\uparrow}} = -\frac{w^*}{xv^*}, \ \frac{b^*_{4,d,\downarrow}}{b_{2,f,\uparrow}} = \frac{x}{v} \frac{b^*_{3,d,\downarrow}}{b_{1,f,\uparrow}} = -\frac{w^*}{|v|^2}, \ \frac{b_{4,d,\uparrow}}{b^*_{2,f,\downarrow}} = -\frac{1}{xv^*} \frac{b_{1,d,\uparrow}}{b^*_{3,f,\downarrow}} = -\frac{u}{|v|^2}. \end{aligned} \tag{B.23}$$

These new proportionalities link the $\hat{B}$ parameters with d-, and f indices, that is links between b_f and b_d parameters. These are:

$$\begin{aligned} &b_{1,d,\uparrow} = \frac{xu}{v} b^*_{3,f,\downarrow}, \quad b_{3,d,\uparrow} = (-\frac{u}{x^*v}) b^*_{1,f,\downarrow}, \quad b_{2,d,\uparrow} = u b^*_{4,f,\downarrow}, \quad b_{4,d,\uparrow} = (-\frac{u}{|v|^2}) b^*_{2,f,\downarrow}, \\ &b_{1,d,\downarrow} = \frac{xw}{v} b^*_{3,f,\uparrow}, \quad b_{3,d,\downarrow} = (-\frac{w}{x^*v}) b^*_{1,f,\uparrow}, \quad b_{2,d,\downarrow} = w b^*_{4,f,\uparrow}, \quad b_{4,d,\downarrow} = (-\frac{w}{|v|^2}) b^*_{2,f,\uparrow}. \end{aligned}$$

(B.24)

At this point 36 matching equations remain. By substituting Eq.(B.24) in the first neighbour hopping and hybridizations one notices the following relations

$$t_x^{d,\uparrow,\uparrow} = \frac{|u|^2}{|v|^2} t_x^{f,\downarrow\downarrow}, \quad t_x^{d,\uparrow,\downarrow} = \frac{wu^*}{|v|^2} t_x^{f,\uparrow,\downarrow}, \quad t_y^{d,\downarrow,\downarrow} = \frac{|w|^2}{|v|^2} t_y^{d,\uparrow,\uparrow}, \quad t_y^{d,\downarrow,\uparrow} = \frac{uw^*}{|v|^2} t_y^{f,\downarrow,\uparrow},$$
$$t_x^{d\downarrow\downarrow} = \frac{|w|^2}{|v|^2} t_x^{d\uparrow\uparrow}, \quad t_y^{d,\uparrow,\downarrow} = \frac{wu^*}{|v|^2} t_y^{f,\uparrow,\downarrow}, \quad t_y^{d,\uparrow,\uparrow} = \frac{|u|^2}{|v|^2} t_y^{f,\downarrow,\downarrow}, \quad t_x^{d,\downarrow,\uparrow} = \frac{uw^*}{|v|^2} t_x^{f,\downarrow,\uparrow},$$
$$V_y^{f,d,\downarrow,\downarrow} = -\frac{w}{u} V_y^{fd\uparrow\uparrow}, \quad V_x^{d,f,\downarrow,\downarrow} = -\frac{w^*}{u^*} V_x^{df\uparrow\uparrow}, \quad \tilde{\epsilon}_d^{\downarrow,\downarrow} = \frac{|w|^2}{|v|^2} \tilde{\epsilon}_f^{\uparrow,\uparrow}, \quad \tilde{\epsilon}_d^{\uparrow,\uparrow} = \frac{|u|^2}{|v|^2} \tilde{\epsilon}_f^{\downarrow,\downarrow}.$$
$$V_y^{d,f,\downarrow,\downarrow} = -\frac{w^*}{u^*} V_y^{d,f,\uparrow,\uparrow}, \quad V_x^{f,d,\downarrow,\downarrow} = -\frac{w}{u} V_x^{f,d,\uparrow,\uparrow}, \tag{B.25}$$

In order to take the $\uparrow,\uparrow$ terms with equal weight as the $\downarrow,\downarrow$ terms into account, we fix $w = -u$. From now on it is enough to investigate the remaining 17 independent equations from the starting matching equations, from where the coupling strengths from Eq.(B.25) are now expressed and thus missing. The remaining 17 equations are $t_p^{f,\sigma,\sigma}$, $t_p^{f,\sigma,\sigma'}$, $V_p^{df,\uparrow,\uparrow}$, $V_p^{fd,\uparrow,\uparrow}$, $V_0^{df,\sigma,\sigma}$,$\tilde{\epsilon}_f^{\sigma,\sigma}$, $\epsilon_f^{\uparrow,\downarrow}$, where $p = x, y$. I will continue with the current form of the spin-flip on-site potential is

$$\epsilon_f^{\uparrow,\downarrow} = \frac{1+|x|^2}{|x|^2}(b_{1,f,\downarrow} b_{1,f,\uparrow}^* + |x|^2 b_{3,f,\downarrow} b_{3,f,\uparrow}^*)$$
$$+\frac{1+|v|^2}{|v|^2}(b_{2,f,\downarrow} b_{2,f,\uparrow}^* + |v|^2 b_{4,f,\downarrow} b_{4,f,\uparrow}^*) = 0. \tag{B.26}$$

Eq.(B.26) is the last coupling strengths ($\epsilon_f^{\uparrow,\downarrow}$, spin-flip on-site potential), which is zero i.e. was not part of the original Hamiltonian. Therefore I will continue solving this system of equations by eliminating this term, by making each parenthesis in $\epsilon_f^{\uparrow,\downarrow}$ equal to zero:

$$(b_{1,f,\downarrow} b_{1,f,\uparrow}^* + |x|^2 b_{3,f,\downarrow} b_{3,f,\uparrow}^*) = 0, \quad (b_{2,f,\downarrow} b_{2,f,\uparrow}^* + |v|^2 b_{4,f,\downarrow} b_{4,f,\uparrow}^*) = 0. \tag{B.27}$$

The last 16 equations contain 8 unknowns at this point, which are the $b_{n,f,\sigma}$, where $n = 1, 2, 3, 4$, $\sigma = \uparrow, \downarrow$. I will use Eq.(B.27) to link four-out of the 8 unknowns-with the other four:

$$b_{4,f,\uparrow} = (-\frac{1}{v^*} e^{i\varphi_4}) b_{2,f,\uparrow}, \quad b_{4,f,\downarrow} = (\frac{1}{v^*} e^{i\varphi_4}) b_{2,f,\downarrow},$$
$$b_{3,f,\uparrow} = (-\frac{1}{x^*} e^{i\varphi_3}) b_{1,f,\uparrow}, \quad b_{3,f,\downarrow} = (\frac{1}{x^*} e^{i\varphi_3}) b_{1,f,\downarrow}. \tag{B.28}$$

Here φ_3 and φ_4 are arbitrary phase factors. Note that with Eq.(B.28) $\epsilon_f^{\uparrow,\downarrow} = 0$ is met. Substituting Eq.(B.28) into the remaining 16 equations, gives us the matching equations left to solve as function of the four unknown block operator parameters $b_{1,f,\uparrow}, b_{1,f,\downarrow}, b_{2,f,\uparrow}, b_{2,f,\downarrow}$. Next, one notices that from these the following proportionalities can be created between

the Hamiltonian coupling strengths:

$$\begin{aligned}
&\frac{t_x^{f,\downarrow,\uparrow}}{t_y^{f,\downarrow,\uparrow}} = \frac{v(1+xv*)}{v^*(x-v)}e^{i\varphi_4}, \qquad \frac{V_x^{d,f,\uparrow,\uparrow}}{(V_x^{f,d,\uparrow,\uparrow})^*} = \frac{vx^*(1+xv^*)}{xv^*(1+x^*v)}e^{i(\varphi_4-\varphi_3)},\\
&\frac{t_x^{f,\uparrow,\downarrow}}{t_y^{f,\uparrow,\downarrow}} = \frac{v(1+xv*)}{v^*(v-x)}e^{i\varphi_4}, \qquad \frac{V_y^{d,f,\uparrow,\uparrow}}{(V_y^{f,d,\uparrow\uparrow})^*} = -\frac{v^*x^*(x-v)}{xv(x^*-v^*)}e^{-i(\varphi_3+\varphi_4)},\\
&V_0^{d,f,\uparrow,\uparrow} = V_0^{d,f,\downarrow,\downarrow}.
\end{aligned} \tag{B.29}$$

In the light of Eq.(B.29) from the 16 equations 11 remains independent. These are the equation of $t_x^{f,\uparrow,\uparrow}, t_y^{f,\uparrow,\uparrow}, t_x^{f,\downarrow,\downarrow}, t_y^{f,\downarrow,\downarrow}, t_x^{f,\uparrow,\downarrow}, t_x^{f,\downarrow,\uparrow}, V_x^{d,f,\uparrow,\uparrow}, V_y^{d,f,\uparrow,\uparrow}, \tilde{\epsilon}_f^{\uparrow,\uparrow}, \tilde{\epsilon}_f^{\downarrow,\downarrow}$ and $V_0^{d,f,\uparrow,\uparrow}$. At this point I will use the relations between the SOI coupling strengths and other Hamiltonian coupling strengths, which were introduced in Eq.(B.8). These are derived in Appendix B.1. Comparing these relations with the $t_p^{c,\sigma,\sigma'}$ ratios in Eq.(B.29), it turns out that $t_x^{c,\downarrow,\uparrow} = -(V_R^c + iV_D^c) = -(t_x^{c,\uparrow,\downarrow})^*$, for every V_R^c és V_D^c $(c = f, d)$. For this, in Eq.(B.29) the following is true:

$$\varphi_3 = \varphi_4, \qquad \left(1+\frac{1}{xv^*}\right) = \left(1+\frac{1}{xv^*}\right)^*. \tag{B.30}$$

Also from Eq.(B.8) it is apparent, that

$$\frac{t_y^{c,\uparrow,\downarrow}}{t_x^{c,\uparrow,\downarrow}} = \frac{V_D^c - iV_R^c}{V_R^c - iV_D^c}, \qquad \frac{t_y^{c,\downarrow,\uparrow}}{t_x^{c,\downarrow,\uparrow}} = \frac{-V_D^c - iV_R^c}{-V_R^c - iV_D^c} = \frac{V_D^c + iV_R^c}{V_R^c + iV_D^c}. \tag{B.31}$$

In Eq.(B.31) the numerator and the denominator has the same absolute value, thus these fraction mean phase factors. Now if we compare this to Eq.(B.29), we find that $\frac{v-x}{1+v^*x}$ must be also a phase factor: $\frac{v-x}{1+v^*x} = e^{i\varphi}$. From this I will express x:

$$x = \frac{v - e^{i\varphi}}{e^{i\varphi}v^* + 1} \tag{B.32}$$

I substitute this into the right side of the second equation of Eq.(B.30):

$$1 + \frac{1}{xv^*} = \frac{|v|^2 + 1}{|v|^2 - v^*e^{i\varphi}} \tag{B.33}$$

Since from the second equation of Eq.(B.30) we know that $1 + \frac{1}{xv^*}$ is a real number, we know that Eq.(B.33) must also be real, meaning that the phase factor of v must be then:

$$v = |v|e^{i\varphi} \tag{B.34}$$

Using this relation in the definition of x, seen in Eq.(B.32) and Eq.(B.33):

$$x = e^{i\varphi}\frac{|v|-1}{|v|+1}, \qquad 1 + \frac{1}{xv^*} = \frac{|v|^2+1}{|v|^2-|v|} \tag{B.35}$$

Setting Eq.(B.31) and Eq.(B.29) side by side, I determined the phase factor for the spin-

flip hopping fractions to be:

$$\frac{t_y^{c,\uparrow,\downarrow}}{t_x^{c,\uparrow,\downarrow}} = e^{-i(\varphi+\varphi_4)} = e^{-i\theta}, \qquad \frac{t_y^{c,\downarrow,\uparrow}}{t_x^{c,\downarrow,\uparrow}} = -e^{-i(\varphi+\varphi_4)} = -e^{-i\theta}. \tag{B.36}$$

Next I simplify the coefficient on the left hand side in Eq.(B.29) using the expressions concluded for v (Eq.(B.34)) and x (Eq.(B.35)):

$$\frac{v-x}{1+xv^*} = e^{i\varphi}, \quad 1+\frac{1}{xv^*} = \frac{|v|^2+1}{|v|^2-|v|}, \quad \frac{xv}{x-v} = e^{i\varphi}\frac{|v|(1-|v|)}{1+|v|^2}. \tag{B.37}$$

From the structure of SOI coupling strengths, i.e. from Eq.(B.8) one can also notice, that $t_x^{c,\downarrow,\uparrow} = -(t_x^{c,\uparrow,\downarrow})^*$. Using this relations with Eq.(B.36) and Eq.(B.37) the fractions of Hamiltonian coupling strengths seen in Eq.(B.29) become:

$$\begin{aligned} &V_0^{d,f,\downarrow,\downarrow} = -\frac{w^*}{u^*}V_0^{d,f,\uparrow,\uparrow},\ (V_y^{f,d,\uparrow,\uparrow})^* = -e^{2i(\varphi+\varphi_4)}V_y^{d,f,\uparrow,\uparrow},\ (V_x^{d,f,\uparrow,\uparrow})^* = V_x^{f,d,\uparrow,\uparrow}, \\ &t_y^{f,\uparrow,\downarrow} = e^{-i(\varphi+\varphi_4)}t_x^{f,\uparrow,\downarrow}, \qquad t_y^{f,\downarrow,\uparrow} = -e^{-i(\varphi+\varphi_4)}t_x^{f,\downarrow,\uparrow}, \qquad t_x^{c,\downarrow,\uparrow} = -(t_x^{c,\uparrow,\downarrow})^*. \end{aligned} \tag{B.38}$$

With the relations in Eq.(B.38) leaves us with ten independent matching equations, which are the equations of $t_x^{f,\sigma,\sigma}$,$t_y^{f,\sigma,\sigma}$,$V_p^{d,f,\uparrow,\uparrow}$,$p = x, y, 0$,$\tilde{\epsilon}_f^{\sigma,\sigma}$. Now we consider $b_{2,f,\downarrow}$ to be

$$b_{2,f,\downarrow} = \frac{b_{2,f,\uparrow}^* b_{1,f,\uparrow}}{b_{1,f,\downarrow}^*}, \tag{B.39}$$

and with this $t_x^{f,\uparrow,\uparrow} = t_x^{f,\downarrow,\downarrow}, t_y^{f,\uparrow,\uparrow} = t_y^{f,\downarrow,\downarrow}$ is met. To satisfy the condition $\epsilon_f^{\uparrow,\uparrow} = \epsilon_f^{\downarrow,\downarrow}$, where

$$\tilde{\epsilon}_f^{\sigma,\sigma} = 2(1+|v|^2)\Big[\frac{2}{(|v|-1)^2}|b_{1,f,\sigma}|^2 + \frac{1}{|v|^2}|b_{2,f,\sigma}|^2\Big], \tag{B.40}$$

I fix the value of $b_{2,f,\uparrow}$ as:

$$|b_{2,f,\uparrow}|^2 = \frac{2|v|^2}{(|v|-1)^2}|b_{1,f,\downarrow}|^2, \rightarrow\ b_{2,f,\uparrow} = \frac{|v|\sqrt{2}}{|(|v|-1)|}b_{1,f,\downarrow}e^{i\gamma}, \tag{B.41}$$

where γ is a now arbitrary phase. With this from Eq.(B.39) I now express $b_{2,f,\downarrow}$:

$$b_{2,f,\downarrow} = \frac{|v|\sqrt{2}}{|(|v|-1)|}b_{1,f,\uparrow}e^{-i\gamma}. \tag{B.42}$$

Two block operator parameters: $b_{2,f,\uparrow}, b_{2,f,\downarrow}$ are as functions of $b_{1,f,\uparrow}, b_{1,f,\downarrow}$ now (see Eq.(B.41) and Eq.(B.42)). With this two unknowns remain $(b_{1,f,\uparrow}, b_{1,f,\downarrow})$, with 7 matching equations. From the expression of $\tilde{\epsilon}_f^{\uparrow,\uparrow} = \epsilon_f^{\uparrow,\uparrow} - \eta$

$$\tilde{\epsilon}_f^{\uparrow,\uparrow} = 4\frac{(1+|v|^2)}{(|v|-1)^2}\Big[|b_{1,f,\uparrow}|^2 + |b_{1,f,\downarrow}|^2\Big], \tag{B.43}$$

the value of η can be expressed:

$$\eta = \epsilon_f^{\uparrow,\uparrow} - 4\frac{(1+|v|^2)}{(|v|-1)^2}(|b_{1,f,\downarrow}|^2 + |b_{1f\uparrow}|^2). \tag{B.44}$$

I will now substitute the expressed block operator parameters $(b_{2,f,\uparrow}, b_{2,f,\downarrow})$ into the remaining 6 matching equations:

$$\begin{aligned}
t_x^{f,\uparrow,\uparrow} &= \frac{\sqrt{2}(1+|v|^2)}{(|v|-1)^2}(b_{1,f,\downarrow}^* b_{1,f,\uparrow} e^{-i\gamma} + b_{1,f,\uparrow}^* b_{1,f,\downarrow} e^{i\gamma}),\\
t_y^{f,\uparrow,\uparrow} &= \frac{\sqrt{2}(1+|v|^2)}{(|v|-1)^2} e^{-i\chi}(b_{1,f,\downarrow}^* b_{1,f,\uparrow} e^{-i\gamma} - b_{1,f,\uparrow}^* b_{1,f,\downarrow} e^{i\gamma}),\\
t_x^{f,\uparrow,\downarrow} &= \frac{\sqrt{2}(1+|v|^2)}{(|v|-1)^2} e^{-i\gamma}(|b_{1,f,\downarrow}|^2 - |b_{1,f,\uparrow}|^2),\\
V_x^{d,f,\uparrow,\uparrow} &= e^{i\chi}\frac{\sqrt{2}(1+|v|^2)}{(|v|-1)^2}\frac{u^*}{|v|}(b_{1,f,\uparrow}^2 e^{-i\gamma} + b_{1,f,\downarrow}^2 e^{i\gamma}),\\
V_y^{d,f,\uparrow,\uparrow} &= \frac{\sqrt{2}(1+|v|^2)}{(|v|-1)^2}\frac{u^*}{|v|}(b_{1,f,\uparrow}^2 e^{-i\gamma} - b_{1,f,\downarrow}^2 e^{i\gamma}),\\
V_0^{d,f,\uparrow,\uparrow} &= 8e^{i\chi}\frac{u^*}{|v|}\frac{(1+|v|^2)}{(1-|v|)^2} b_{1,f,\uparrow} b_{1,f,\downarrow},
\end{aligned} \tag{B.45}$$

where $\chi = \varphi + \varphi_4$. I will now determine $b_{1,f,\uparrow}$ and $b_{1,f,\downarrow}$ from the fourth and fifth equations of Eq.(B.45). By adding and subtracting aforementioned equations we get:

$$\begin{aligned}
b_{1,f,\uparrow}^2 &= \frac{(|v|-1)^2 e^{i\gamma}}{2\sqrt{2}(1+|v|^2)}\frac{|v|}{u^*}(V_x^{d,f,\uparrow,\uparrow} e^{-i\chi} + V_y^{d,f,\uparrow,\uparrow}),\\
b_{1,f,\downarrow}^2 &= \frac{(|v|-1)^2 e^{-i\gamma}}{2\sqrt{2}(1+|v|^2)}\frac{|v|}{u^*}(V_x^{d,f,\uparrow,\uparrow} e^{-i\chi} - V_y^{d,f,\uparrow,\uparrow}).
\end{aligned} \tag{B.46}$$

Let us write u in polar form: $u = |u|e^{i\phi_u}$. Doing the same for part of the left side of the equations in Eq.(B.46), we get:

$$\begin{aligned}
(V_x^{d,f,\uparrow,\uparrow} e^{-i\chi} + V_y^{d,f,\uparrow,\uparrow}) &= |V_x^{d,f,\uparrow,\uparrow} e^{-i\chi} + V_y^{d,f,\uparrow,\uparrow}| e^{i\delta_\uparrow},\\
(V_x^{d,f,\uparrow,\uparrow} e^{-i\chi} - V_y^{d,f,\uparrow,\uparrow}) &= |V_x^{d,f,\uparrow,\uparrow} e^{-i\chi} - V_y^{d,f,\uparrow,\uparrow}| e^{i\delta_\downarrow},
\end{aligned} \tag{B.47}$$

These will be used to write the last two remaining unknown block operators, $b_{1,f,\uparrow}$ and $b_{1,f,\downarrow}$ seen in Eq.(B.46) also in polar form:

$$\begin{aligned}
b_{1,f,\uparrow} &= \sqrt{\frac{(|v|-1)^2}{2\sqrt{2}(1+|v|^2)}\frac{|v|}{|u|}}\sqrt{|V_x^{d,f,\uparrow,\uparrow} e^{-i\chi} + V_y^{d,f,\uparrow,\uparrow}|}\ e^{i(\gamma+\phi_u+\delta_\uparrow)/2},\\
b_{1,f,\downarrow} &= \sqrt{\frac{(|v|-1)^2}{2\sqrt{2}(1+|v|^2)}\frac{|v|}{|u|}}\sqrt{|V_x^{d,f,\uparrow,\uparrow} e^{-i\chi} - V_y^{d,f,\uparrow,\uparrow}|}\ e^{i(-\gamma+\phi_u+\delta_\downarrow)/2},
\end{aligned} \tag{B.48}$$

At this point I will substitute $b_{1,f,\uparrow}$ and $b_{1,f,\downarrow}$ from Eq.(B.48) into the leftover matching

equations (See Eq.(B.45)). I will start with the two terms relating to first neighbour hopping on f orbit, which are the first two lines from Eq.(B.45):

$$t_x^{f,\uparrow,\uparrow} = \frac{2\sqrt{2}(1+|v|^2)}{(|v|-1)^2} Re(b^*_{1,f,\downarrow} b_{1,f,\uparrow} e^{-i\gamma}),$$
$$t_y^{f,\uparrow,\uparrow} = \frac{2\sqrt{2}(1+|v|^2)}{(|v|-1)^2} (ie^{-i\chi}) Im(b^*_{1,f,\downarrow} b_{1,f,\uparrow} e^{-i\gamma}). \tag{B.49}$$

From Eq.(B.48) $Re(b^*_{1,f,\downarrow} b_{1,f,\uparrow} e^{-i\gamma})$ and $Im(b^*_{1,f,\downarrow} b_{1,f,\uparrow} e^{-i\gamma})$ can be deduced:

$$Re(b^*_{1,f,\downarrow} b_{1,f,\uparrow} e^{-i\gamma}) = V_{1/2} \frac{(|v|-1)^2}{2\sqrt{2}(1+|v|^2)} \frac{|v|}{|u|} \cos\frac{\delta_\uparrow - \delta_\downarrow}{2},$$
$$Im(b^*_{1,f,\downarrow} b_{1,f,\uparrow} e^{-i\gamma}) = V_{1/2} \frac{(|v|-1)^2}{2\sqrt{2}(1+|v|^2)} \frac{|v|}{|u|} (ie^{-i\chi}) \sin\frac{\delta_\uparrow - \delta_\downarrow}{2}, \tag{B.50}$$

where $V_{1/2} = \sqrt{|V_x^{d,f,\uparrow,\uparrow} e^{-i\chi} + V_y^{d,f,\uparrow,\uparrow}|} \sqrt{|V_x^{d,f,\uparrow,\uparrow} e^{-i\chi} - V_y^{d,f,\uparrow,\uparrow}|}$. With Eq.(B.50) the hopping terms from Eq.(B.49) then becomes:

$$t_x^{f,\uparrow,\uparrow} = \frac{|v|}{|u|} V_{1/2} \cos\frac{\delta_\uparrow - \delta_\downarrow}{2},$$
$$t_y^{f,\uparrow,\uparrow} = (ie^{-i\chi}) \frac{|v|}{|u|} V_{1/2} \sin\frac{\delta_\uparrow - \delta_\downarrow}{2}. \tag{B.51}$$

The next matching equation is the spin-flip hopping term of the hybridized orbit, the third line from Eq.(B.45):

$$t_x^{f,\uparrow,\downarrow} = \frac{e^{-i\gamma}}{2} \frac{|v|}{|u|} (|V_x^{d,f,\uparrow,\uparrow} e^{-i\chi} - V_y^{d,f,\uparrow,\uparrow}| - |V_x^{d,f,\uparrow,\uparrow} e^{-i\chi} + V_y^{d,f,\uparrow,\uparrow}|). \tag{B.52}$$

The last matching equation is the term relating the spin-flip on-site hybridization from the last line of Eq.(B.45):

$$V_0^{d,f,\uparrow,\uparrow} = 2\sqrt{2} e^{i(\chi + \frac{\delta_\uparrow + \delta_\downarrow}{2})} V_{1/2}. \tag{B.53}$$

Lastly, the magnitude of the ratio of u and v, $|v/u|$ can be calculated from $t_x^{f,\uparrow,\downarrow}$ (See Eq.(B.52))

$$\frac{|v|}{|u|} = \frac{t_x^{f,\uparrow,\uparrow}}{\sqrt{|V_x^{d,f,\uparrow,\uparrow} e^{-i\chi} - V_y^{d,f,\uparrow,\uparrow}||V_x^{d,f,\uparrow,\uparrow} e^{-i\chi} + V_y^{d,f,\uparrow,\uparrow}|} \cos\frac{\delta_\uparrow - \delta_\downarrow}{2}}. \tag{B.54}$$

The last condition I will use to ensure the $t_x^{f,\uparrow,\uparrow} = 1$ condition, because I will use $t_x^{f,\uparrow,\uparrow}$ as a unit, in which all the hamiltonian parameters are given, when calculating the different expectation values (See for example Table **??**). This can be done, as u,v are arbitrary complex number.

B.4 Parameter space region, in which the solutions emerge

Note that the parameter space, in which the results concluded for the matching equations is restricted. To investigate these restrictions first let us turn to Eq.(B.25). The equations in Eq.(B.25) form interdependence between the hopping coupling strengths in the following way: $t_p^d = |\frac{u}{v}|^2 t_p^f$, where $p = x, y$.

Similarly we found link between the hybridization and hopping couplings in Eq.(B.54). The are related to V_p^{df} and V_p^{fd}, and similarly have to form $V_p^{df} = |\frac{u}{v}| t_p^f$, where $p = x, y$. These two interdependences can be summarized as:

$$t_{i,i+r}^{c,c'} = k^{\delta_{c,d}+\delta_{c',d}} t_{i,i+r}^{c,c'}. \tag{B.55}$$

In Eq.(B.55) I used the following notations: $t_{i,i+r}^{c,c'}$ = are hoppings, if $c = c'$; $t_{i,i+r}^{c,c'}$ = are hybridizations, if $c \neq c'$. Eq.(B.55) is the strictest restriction for the Hamiltonian parameters there is. This however, does not mean a strict restriction for the couplings, because these links were experimentally shown before for two-band systems [137], and for this reason other theoretical works also used these results [65]. Consequently these relation do not represent special constraints.

There are other relations between Hamiltonian parameters, such as the link between the on-site potentials for d and f electrons. This also narrows the parameter space region where the solution is present. These restrictions, as they were calculated in Eq.(B.25) and Eq.(B.44):

$$\epsilon_d^{\uparrow,\uparrow} - \epsilon_f^{\uparrow,\uparrow} = \sqrt{2}\Big[\frac{|u|}{|v|} - \frac{|v|}{|u|}\Big](|V_x^{d,f,\uparrow,\uparrow} e^{-i\chi} - V_y^{d,f,\uparrow,\uparrow}| + |V_x^{d,f,\uparrow,\uparrow} e^{-i\chi} + V_y^{d,f,\uparrow,\uparrow}|). \tag{B.56}$$

If we chose the $\epsilon_f^{\uparrow,\uparrow}$ as the origin of the energy scale, in the above expression only $\epsilon_d^{\uparrow,\uparrow}$ remains. An on-site potential can be modified by changing an external electrical field applied to the surface, and this way it is possible to meet the value of $\epsilon_d^{\uparrow,\uparrow}$ determined by Eq.(B.56).

The last restriction was introduced in Eq.(B.52) and links the $\hat{H}$ parameters that appear in $b_{1,f,\uparrow}$ with $t^{f\uparrow,\downarrow}$. This restriction can also be experimentally achieved, by external electric field.

Eq.(B.53) seems to constrain the possible $V_0^{d,f,\uparrow,\uparrow}$ values which also implies parameters space restriction. However the magnitude of on-site hybridization can be modified via doping on the surface [138], meaning that the right magnitude can be achieved by changing the concentration of impurities introduced to the system.

B.5 Transforming the one-particle part of the Hamiltonian in $\vec{k}$-space

To transform $\hat{H}_1$ to $\vec{k}$-space, I will use, that $\hat{c}_{\vec{j},\sigma} = \frac{1}{\sqrt{N_{cs}}} \sum_{\vec{k}} e^{(-i\vec{k}\vec{j})} \hat{c}_{\vec{k},\sigma}$, $c = d, f$, $\sigma = \uparrow, \downarrow$.

$$\hat{H}_1 = \sum_{\vec{k}} \sum_{\sigma,\sigma'} [\epsilon^{\sigma,\sigma'}_{d,\vec{k}} \hat{d}^{\dagger}_{\vec{k},\sigma} \hat{d}_{\vec{k},\sigma'} + \epsilon^{\sigma,\sigma'}_{f,\vec{k}} \hat{f}^{\dagger}_{\vec{k},\sigma} \hat{f}_{\vec{k},\sigma'} + V^{\sigma,\sigma'}_{d,f,\vec{k}} \hat{d}^{\dagger}_{\vec{k},\sigma} \hat{f}_{\vec{k},\sigma'} + V^{\sigma,\sigma'\,*}_{d,f,\vec{k}} \hat{f}^{\dagger}_{\vec{k},\sigma} \hat{d}_{\vec{k},\sigma'}]. \quad \text{(B.57)}$$

I introduce $\vec{v}$ column vector, and $\mathbf{W}$ matrix

$$\vec{v} = \begin{pmatrix} \hat{d}_{\vec{k},\uparrow} \\ \hat{f}_{\vec{k},\uparrow} \\ \hat{d}_{\vec{k},\downarrow} \\ \hat{f}_{\vec{k},\downarrow} \end{pmatrix}, \quad \mathbf{W} = \begin{pmatrix} \epsilon^{\uparrow,\uparrow}_{d,\vec{k}} & V^{\uparrow,\uparrow}_{d,f,\vec{k}} & \epsilon^{\uparrow,\downarrow}_{d,\vec{k}} & 0 \\ V^{\uparrow,\uparrow\,*}_{d,f,\vec{k}} & \epsilon^{\uparrow,\uparrow}_{f,\vec{k}} & 0 & \epsilon^{\uparrow,\downarrow}_{f,\vec{k}} \\ \epsilon^{\uparrow,\downarrow\,*}_{d,\vec{k}} & 0 & \epsilon^{\downarrow,\downarrow}_{d,\vec{k}} & V^{\downarrow,\downarrow}_{d,f,\vec{k}} \\ 0 & \epsilon^{\uparrow,\downarrow\,*}_{f,\vec{k}} & V^{\downarrow,\downarrow\,*}_{d,f,\vec{k}} & \epsilon^{\downarrow,\downarrow}_{f,\vec{k}} \end{pmatrix}. \quad \text{(B.58)}$$

Then the one-particle part of the Hamiltonian can be written as:

$$\hat{H}_1 = \sum_{\vec{k}} (\hat{d}^{\dagger}_{\vec{k}\uparrow}, \hat{f}^{\dagger}_{\vec{k}\uparrow}, \hat{d}^{\dagger}_{\vec{k}\downarrow}, \hat{f}^{\dagger}_{\vec{k}\downarrow}) \mathbf{W} \begin{pmatrix} \hat{d}_{\vec{k}\uparrow} \\ \hat{f}_{\vec{k}\uparrow} \\ \hat{d}_{\vec{k}\downarrow} \\ \hat{f}_{\vec{k}\downarrow} \end{pmatrix} = \sum_{\vec{k}} \vec{v}^{\dagger} \mathbf{W} \vec{v}, \quad \text{(B.59)}$$

where $\vec{v}^{\dagger}$ row vector is the conjugate transpose of $\vec{v}$ and $\epsilon^{\sigma,\sigma'}$ and $V^{\sigma,\sigma'}_{d,f,\vec{k}}$ are

$$\epsilon^{\sigma,\sigma'}_{c,\vec{k}} = \epsilon^{\sigma,\sigma'}_{c} + [t^{c,\sigma,\sigma'}_{x} e^{+i\vec{k}\vec{x}} + (t^{c,\sigma',\sigma}_{x})^* e^{-i\vec{k}\vec{x}}] + [t^{c,\sigma,\sigma'}_{y} e^{+i\vec{k}\vec{y}} + (t^{c,\sigma',\sigma}_{y})^* e^{-i\vec{k}\vec{y}}], \quad \text{(B.60)}$$

$$V^{\sigma,\sigma'}_{d,f,\vec{k}} = V^{d,f,\sigma,\sigma'}_{0} + [V^{d,f,\sigma,\sigma'}_{x} e^{+i\vec{k}\vec{x}} + (V^{f,d,\sigma',\sigma}_{x})^* e^{-i\vec{k}\vec{x}}] + [V^{d,f,\sigma,\sigma'}_{y} e^{+i\vec{k}\vec{y}} + (V^{f,d,\sigma',\sigma}_{y})^* e^{-i\vec{k}\vec{y}}].$$

B.5.1 Secular equation of W

The band structure, can be deduced from the secular equation of $\mathbf{W}$. Note, that in the absence of spin-orbit coupling (when $\epsilon^{\sigma,-\sigma}_{c,\vec{k}} = 0, c = d, f$), $\mathbf{W}$ can be divided into two independent diagonal matrices, which provide the following spectra:

$$(\epsilon^{\uparrow,\uparrow}_{d,\vec{k}} - \lambda_{\uparrow})(\epsilon^{\uparrow,\uparrow}_{f,\vec{k}} - \lambda_{\uparrow}) - |V^{\uparrow,\uparrow}_{d,f,\vec{k}}|^2 = 0, \quad (\epsilon^{\downarrow,\downarrow}_{d,\vec{k}} - \lambda_{\downarrow})(\epsilon^{\downarrow,\downarrow}_{f,\vec{k}} - \lambda_{\downarrow}) - |V^{\downarrow,\downarrow}_{d,f,\vec{k}}|^2 = 0, \quad \text{(B.61)}$$

where for $\lambda_{\uparrow}$ and $\lambda_{\uparrow}$ one has

$$\lambda_{\uparrow,1,2} = \frac{1}{2}[(\epsilon^{\uparrow,\uparrow}_{d,\vec{k}} + \epsilon^{\uparrow,\uparrow}_{f,\vec{k}}) \pm \sqrt{(\epsilon^{\uparrow,\uparrow}_{d,\vec{k}} - \epsilon^{\uparrow,\uparrow}_{f,\vec{k}})^2 + 4|V^{\uparrow,\uparrow}_{d,f,\vec{k}}|^2}],$$
$$\lambda_{\downarrow,1,2} = \frac{1}{2}[(\epsilon^{\downarrow,\downarrow}_{d,\vec{k}} + \epsilon^{\downarrow,\downarrow}_{f,\vec{k}}) \pm \sqrt{(\epsilon^{\downarrow,\downarrow}_{d,\vec{k}} - \epsilon^{\downarrow,\downarrow}_{f,\vec{k}})^2 + 4|V^{\downarrow,\downarrow}_{d,f,\vec{k}}|^2}], \quad \text{(B.62)}$$

which represent independent bands for $\sigma =\uparrow$ and $\sigma =\downarrow$.

In addition, if we consider that $\uparrow,\uparrow$ terms with the same weight as $\downarrow,\downarrow$ ($c = d, f$, $p = x, y$ $\sigma =\uparrow,\downarrow$)

$$t_p^c = t_p^{c,\sigma,\sigma}, \quad \epsilon_c = \epsilon_c^{\sigma,\sigma}, \quad V_0^{d,f} = V_0^{d,f,\sigma,\sigma}, \quad V_p^{d,f} = V_p^{d,f,\sigma,\sigma}, \tag{B.63}$$

then $\lambda_\uparrow = \lambda_\downarrow$, thus Eq.(B.61,B.62) provides the same band for both spin indices, see Fig.3.2/a). In the presence of spin-orbit coupling (i.e. $\epsilon_{c,\vec{k}}^{\sigma,-\sigma} \neq 0, c = d, f$ as seen on Fig.3.2/b)) Eq.(B.60) results in four bands, thus the spin double degeneracy seen in Eq.(B.61,B.62) ceases.

B.6 Transforming the wavefunction in $\vec{k}$-space

In order to calculate physical quantities, the ground state wave function in Eq.(3.12) will be transformed via Fourier transformation to $\vec{k}$ space, then the norm will be deduced. The original form of the wave function in $\vec{r}$ space:

$$|\psi_g\rangle = (\Pi_{i=1}^{N_{cs}} \hat{A}_i^\dagger \hat{B}_j^\dagger)\Pi_{i=1}^{N_{cs}}(\alpha_\uparrow \hat{f}_{i,\uparrow}^\dagger + \alpha_\downarrow \hat{f}_{i,\downarrow}^\dagger)|0\rangle \tag{B.64}$$

To complete the transformation, the Fourier transformed form of $\hat{A}_i^\dagger, \hat{B}_i^\dagger$, and $\hat{f}_{i\uparrow}^\dagger, \hat{f}_{i\downarrow}^\dagger$ is needed.

$$\begin{aligned}
\hat{G}_i &= \frac{1}{\sqrt{N_{cs}}} \sum_{\vec{k}} e^{-i\vec{k}\vec{r}_i} \hat{G}_{\vec{k}}, \\
\hat{c}_{i\sigma} &= \sum_{\vec{k}} e^{-i\vec{k}\vec{r}_i} \hat{c}_{\vec{k}\sigma},
\end{aligned} \tag{B.65}$$

where $c = d, f$, $\hat{G} = \hat{A}, \hat{B}$. To get the final form of $\hat{A}_{\vec{k}}$, let us start with the original definition of the block operators as seen in Eq.(3.8):

$$\begin{aligned}
\hat{A}_i = &(a_{1,d,\uparrow}\hat{d}_{i,\uparrow} + a_{2,d,\uparrow}\hat{d}_{i+x,\uparrow} + a_{3,d,\uparrow}\hat{d}_{i+x+y,\uparrow} + a_{4,d,\uparrow}\hat{d}_{i+y,\uparrow}) + \\
&+(a_{1,d,\downarrow}\hat{d}_{i,\downarrow} + a_{2,d,\downarrow}\hat{d}_{i+x,\downarrow} + a_{3,d,\downarrow}\hat{d}_{i+x+y,\downarrow} + a_{4,d,\downarrow}\hat{d}_{i+y,\downarrow}) + \\
&+(a_{1,f,\downarrow}\hat{f}_{i,\downarrow} + a_{2,f,\downarrow}\hat{f}_{i+x,\downarrow} + a_{3,f,\downarrow}\hat{f}_{i+x+y,\downarrow} + a_{4,f,\downarrow}\hat{f}_{i+y,\downarrow}) + \\
&+(a_{1,f,\uparrow}\hat{f}_{i,\uparrow} + a_{2,f,\uparrow}\hat{f}_{i+x,\uparrow} + a_{3,f,\uparrow}\hat{f}_{i+x+y,\uparrow} + a_{4,f,\uparrow}\hat{f}_{i+y,\uparrow}).
\end{aligned} \tag{B.66}$$

Now, I substitute the Fourier transformed of the $\hat{A}$ into the left side -,$\hat{d}$ and $\hat{f}$ on the right side of the former equation, then after factoring out:

$$\begin{aligned}
&\sum_{\vec{k}} e^{-i\vec{k}\vec{r}_i}\hat{A}_{\vec{k}} = \sum_{\vec{k}} e^{-i\vec{k}\ \vec{r}_i}(a_{1,d,\uparrow}\hat{d}_{\vec{k},\uparrow} + a_{2,d,\uparrow}e^{-i\vec{k}\vec{x}}\hat{d}_{\vec{k},\uparrow} + a_{3,d,\uparrow}e^{-i\vec{k}(\vec{x}+\vec{y})}\hat{d}_{\vec{k},\uparrow} + \\
&+a_{4,d,\uparrow}e^{-i\vec{k}\vec{y}}\hat{d}_{\vec{k},\uparrow} + a_{1,d,\downarrow}\hat{d}_{\vec{k},\downarrow} + a_{2,d,\downarrow}e^{-i\vec{k}\vec{x}}\hat{d}_{\vec{k},\downarrow} + a_{3,d,\downarrow}e^{-i\vec{k}(\vec{x}+\vec{y})}\hat{d}_{\vec{k},\downarrow} + a_{4,d,\downarrow}e^{-i\vec{k}\vec{y}}\hat{d}_{\vec{k},\downarrow} + \\
&+a_{1,f,\uparrow}\hat{f}_{\vec{k},\uparrow} + a_{2,f,\uparrow}e^{-i\vec{k}\vec{x}}\hat{f}_{\vec{k},\uparrow} + a_{3,f,\uparrow}e^{-i\vec{k}(\vec{x}+\vec{y})}\hat{f}_{\vec{k},\uparrow} + a_{4,f,\uparrow}e^{-i\vec{k}\vec{y}}\hat{f}_{\vec{k},\uparrow} + a_{1,f,\downarrow}\hat{f}_{\vec{k},\downarrow} +
\end{aligned}$$

$$+a_{2,f,\downarrow}e^{-i\vec{k}\vec{x}}\hat{f}_{\vec{k},\downarrow}+a_{3,f,\downarrow}e^{-i\vec{k}(\vec{x}+\vec{y})}\hat{f}_{\vec{k},\downarrow}+a_{4,f,\downarrow}e^{-i\vec{k}\vec{y}}\hat{f}_{\vec{k}\downarrow}). \tag{B.67}$$

At this point I introduce the following notations: $a_{kd\sigma}$, $a_{kf\sigma}$. Their defining equations are:

$$\begin{aligned} a_{\vec{k},d,\sigma} &= a_{1,d,\sigma}+a_{2,d,\sigma}e^{-i\vec{k}\mathbf{x}}+a_{3,d,\sigma}e^{-i\vec{k}(\mathbf{x}+\mathbf{y})}+a_{4,d,\sigma}e^{-i\vec{k}\mathbf{y}},\\ a_{\vec{k},f,\sigma} &= a_{1,f,\sigma}+a_{2,f,\sigma}e^{-i\vec{k}\mathbf{x}}+a_{3,f,\sigma}e^{-i\vec{k}(\mathbf{x}+\mathbf{y})}+a_{4,f,\sigma}e^{-i\vec{k}\mathbf{y}}. \end{aligned} \tag{B.68}$$

Using Eq.(B.68), the $\hat{A}_{\vec{k}}$:

$$\hat{A}_{\vec{k}}=\sum_{\sigma}(a_{\vec{k},d,\sigma}\hat{d}_{\vec{k},\sigma}+a_{\vec{k},f,\sigma}\hat{f}_{\vec{k},\sigma}). \tag{B.69}$$

Similarly $\hat{B}_{\vec{k}}$ can be deduced, using the steps seen in Eq.(B.65-B.69):

$$\hat{B}_i=\frac{1}{\sqrt{N_{cs}}}\sum_{\vec{k}}e^{-i\vec{k}\ \vec{r}_i}\hat{B}_{\vec{k}}. \tag{B.70}$$

Thus $\hat{B}_{\vec{k}}$:

$$\hat{B}_{\vec{k}}=\sum_{\sigma}(b_{\vec{k},d,\sigma}\hat{d}_{\vec{k},\sigma}+b_{\vec{k},f,\sigma}\hat{f}_{\vec{k},\sigma}). \tag{B.71}$$

To deduce $|\psi_g\rangle$ in the reciprocal lattice space, we will substitute the transformed block operators (See Eq.(B.69, B.71)). The resulting wave function I will denote as $|\psi_{gk}\rangle$.

$$|\psi_{gk}\rangle=\Pi_{k=1}^{N_{cs}}[(\hat{A}_k^{\dagger}\hat{B}_k^{\dagger})(\alpha_{\uparrow}\hat{f}_{k\uparrow}^{\dagger}+\alpha_{\downarrow}\hat{f}_{k\downarrow}^{\dagger})]|0\rangle. \tag{B.72}$$

The system is homogeneous, thus I used the $\alpha_{i,\sigma}=\alpha_{\sigma}$ notations. Further shaping the contents of the brackets from Eq.(B.72) by substituting $\hat{A}_{\vec{k}}$ and $\hat{B}_{\vec{k}}$:

$$\begin{aligned} &(\hat{A}_k^{\dagger}\hat{B}_k^{\dagger})(\alpha_{\uparrow}\hat{f}_{k,\uparrow}^{\dagger}+\alpha_{\downarrow}\hat{f}_{k,\downarrow}^{\dagger})=(a_{k,d,\uparrow}^{*}\hat{d}_{k,d,\uparrow}^{\dagger}+a_{k,f,\uparrow}^{*}\hat{f}_{k,d,\uparrow}^{\dagger}+a_{k,d,\downarrow}^{*}\hat{d}_{k,d,\downarrow}^{\dagger}+a_{k,f,\downarrow}^{*}\hat{f}_{k,d,\downarrow}^{\dagger})\\ &(b_{k,d,\uparrow}^{*}\hat{d}_{k,d,\uparrow}^{\dagger}+b_{k,f,\uparrow}^{*}\hat{f}_{k,d,\uparrow}^{\dagger}+b_{k,d,\downarrow}^{*}\hat{d}_{k,d,\downarrow}^{\dagger}+b_{k,f,\downarrow}^{*}\hat{f}_{k,d,\downarrow}^{\dagger})(\alpha_{k,f,\uparrow}\hat{f}_{k,d,\uparrow}^{\dagger}+\alpha_{k,f,\downarrow}\hat{f}_{k,d,\downarrow}^{\dagger}). \end{aligned} \tag{B.73}$$

After performing the multiplication in Eq.(B.73), to simplify the results, we will introduce $\gamma_{k1},\gamma_{k2},\gamma_{k3},\gamma_{k4}$:

$$\begin{aligned} \gamma_{k1} &= \alpha_{\uparrow}(a_{k,d,\uparrow}^{*}b_{k,d,\downarrow}^{*}-a_{kd\downarrow}^{*}b_{k,d,\uparrow}^{*}),\quad \gamma_{k2}=\alpha_{\downarrow}(a_{k,d,\uparrow}^{*}b_{k,d,\downarrow}^{*}-a_{k,d,\downarrow}^{*}b_{k,d,\uparrow}^{*}),\\ \gamma_{k3} &= \alpha_{\downarrow}(a_{k,d,\uparrow}^{*}b_{k,f,\downarrow}^{*}-a_{k,f,\uparrow}^{*}b_{k,d,\uparrow}^{*})-\alpha_{\uparrow}(a_{k,d,\uparrow}^{*}b_{k,f,\downarrow}^{*}-a_{k,f,\downarrow}^{*}b_{k,d,\uparrow}^{*}),\\ \gamma_{k4} &= \alpha_{\downarrow}(a_{k,d,\downarrow}^{*}b_{k,f,\uparrow}^{*}-a_{k,f,\uparrow}^{*}b_{k,d,\downarrow}^{*})-\alpha_{\uparrow}(a_{k,d,\downarrow}^{*}b_{k,f,\downarrow}^{*}-a_{k,f,\downarrow}^{*}b_{k,d,\downarrow}^{*}). \end{aligned} \tag{B.74}$$

With these notations $|\Psi_{gk}\rangle$:

$$|\Psi_{gk}\rangle=\Pi_{k=1}^{N_c}[\gamma_{k1}\hat{d}_{k,\uparrow}^{\dagger}\hat{d}_{k,\downarrow}^{\dagger}\hat{f}_{k,\uparrow}^{\dagger}+\gamma_{k2}\hat{d}_{k,\uparrow}^{\dagger}\hat{d}_{k,\downarrow}^{\dagger}\hat{f}_{k,\downarrow}^{\dagger}+\gamma_{k3}\hat{d}_{k,\uparrow}^{\dagger}\hat{f}_{k,\uparrow}^{\dagger}\hat{f}_{k,\downarrow}^{\dagger}+\gamma_{k4}\hat{d}_{k,\downarrow}^{\dagger}\hat{f}_{k,\uparrow}^{\dagger}\hat{f}_{k,\downarrow}^{\dagger}]|0\rangle. \tag{B.75}$$

The norm of the wave function in Eq.(B.75) can be easily calculated:

$$\langle \Psi_{gk} | \Psi_{gk} \rangle = \Pi_k [|\gamma_{k1}|^2 + |\gamma_{k2}|^2 + |\gamma_{k3}|^2 + |\gamma_{k4}|^2]. \tag{B.76}$$

B.6.1 The ground state total spin z expectation value

Transforming the wave function in $\vec{k}$ space and calculating its norm provides us with the opportunity to investigate the more important physical properties. Let us start with calculating the total spin z component of the ground state. To deduce the expectation value of $\hat{S}^z$, first I will calculate the expectation values of $\hat{n}_{k,d,\uparrow}$, $\hat{n}_{k,d,\downarrow}$, $\hat{n}_{k,f,\uparrow}$, $\hat{n}_{k,f,\downarrow}$ particle numbers. Fort this I will use the norm of the ground state wave function, i.e. Eq.(B.76):

$$\begin{aligned}
\frac{\langle \psi_{kg} | \hat{n}_{k,d,\uparrow} | \psi_{kg} \rangle}{\langle \psi_{kg} | \psi_{kg} \rangle} &= \frac{|\gamma_{k1}|^2 + |\gamma_{k2}|^2 + |\gamma_{k3}|^2}{|\gamma_{k1}|^2 + |\gamma_{k2}|^2 + |\gamma_{k3}|^2 + |\gamma_{k4}|^2}, \\
\frac{\langle \psi_{kg} | \hat{n}_{k,d,\downarrow} | \psi_{kg} \rangle}{\langle \psi_{kg} | \psi_{kg} \rangle} &= \frac{|\gamma_{k1}|^2 + |\gamma_{k2}|^2 + |\gamma_{k4}|^2}{|\gamma_{k1}|^2 + |\gamma_{k2}|^2 + |\gamma_{k3}|^2 + |\gamma_{k4}|^2}, \\
\frac{\langle \psi_{kg} | \hat{n}_{k,f,\uparrow} | \psi_{kg} \rangle}{\langle \psi_{kg} | \psi_{kg} \rangle} &= \frac{|\gamma_{k1}|^2 + |\gamma_{k3}|^2 + |\gamma_{k4}|^2}{|\gamma_{k1}|^2 + |\gamma_{k2}|^2 + |\gamma_{k3}|^2 + |\gamma_{k4}|^2}, \\
\frac{\langle \psi_{kg} | \hat{n}_{k,f,\downarrow} | \psi_{kg} \rangle}{\langle \psi_{kg} | \psi_{kg} \rangle} &= \frac{|\gamma_{k2}|^2 + |\gamma_{k3}|^2 + |\gamma_{k4}|^2}{|\gamma_{k1}|^2 + |\gamma_{k2}|^2 + |\gamma_{k3}|^2 + |\gamma_{k4}|^2}.
\end{aligned} \tag{B.77}$$

In Eq.(B.77) I take into account hat $\hat{n} = \hat{c}^\dagger \hat{c}$, thus $\hat{n}\hat{c}^\dagger = \hat{c}^\dagger$ $(c = f, d)$. Considering the expectation value of $\langle \hat{S}^z \rangle$:

$$\langle \hat{S}^z \rangle = \frac{\langle \psi_{kg} | \hat{S}^z | \psi_{kg} \rangle}{\langle \psi_{kg} | \psi_{kg} \rangle} = \frac{1}{2} \sum_{k=1}^{N_s} \frac{|\gamma_{k3}|^2 - |\gamma_{k4}|^2 + |\gamma_{k1}|^2 - |\gamma_{k2}|^2}{|\gamma_{k1}|^2 + |\gamma_{k2}|^2 + |\gamma_{k3}|^2 + |\gamma_{k4}|^2}, \tag{B.78}$$

where N_s is the number of sites.

We will now prove that the expectation value of $\hat{S}_z$ is nonzero. This means that the deduced ground state wave function indeed corresponds to a ferromagnetic state. To prove that $\hat{S}^z > 0$, I will show that the numerator of $\langle \hat{S}^z \rangle$ is greater than zero. This is enough since we already now that the denominator is a sum of positive numbers.

For $\alpha_\uparrow$ and $\alpha_\downarrow$ only the normalization condition (i.e. Eq.(B.76)) gives any restriction. Since the initial system does not have anisotropy $\alpha_\uparrow = \alpha_\downarrow = \alpha$. Then the numerator simplifies to the following term: a $|\gamma_{k3}|^2 - |\gamma_{k4}|^2$. This can be written as:

$$|\gamma_{k3}|^2 - |\gamma_{k4}|^2 = (|\gamma_{k3}| - |\gamma_{k4}|)(|\gamma_{k3}| + |\gamma_{k4}|) \tag{B.79}$$

Eq.(B.79) can only be zero, if $|\gamma_{k3}| = |\gamma_{k4}|$, that is if γ_{k3} and γ_{k4} only differs in a phase factor:

$$\gamma_{k3} = e^{i\varphi} \gamma_{k4}. \tag{B.80}$$

Turning our attention back to the defining equations of $\gamma_{k3} = \gamma_{k4}$, i.e. to Eq.(B.74), we can write these expressions as:

$$\gamma_{k3} = a_{k,f,\downarrow}A - b_{k,f,\downarrow}B, \qquad \gamma_{k4} = a_{k,f,\uparrow}A - b_{k,f,\uparrow}B, \tag{B.81}$$

where $A = (\alpha(a^*_{k,f,\downarrow} - a^*_{k,f,\uparrow})$ and $B = (\alpha(b^*_{k,f,\uparrow} - b^*_{k,f,\downarrow})$. Note that, it can be simply seen that, A and B are independent, thus Eq.(B.79) only zero, if

$$a_{k,f,\downarrow} = e^{i\varphi}a_{k,f,\uparrow}, \qquad b_{k,f,\downarrow} = e^{i\varphi}b_{k,f,\uparrow}. \tag{B.82}$$

Since Eq.(B.82) contradicts the solutions of the matching equations, these can not be simultaneously true, thus $\langle \hat{S}^z \rangle > 0$ must be true. This means that the ground state is ferromagnetic.

On Fig.3.5 the expectation values of $\hat{S}_z$ are shown. Based on Eq.(B.78) the following numeric integral was calculated:

$$\langle \hat{S}_z \rangle = \frac{1}{4\pi^2}\int_{-\pi}^{\pi} dk_x \int_{-\pi}^{\pi} dk_y \frac{1}{2}\frac{|\gamma_{k3}(k_x,k_y)|^2 - |\gamma_{k4}(k_x,k_y)|^2 + |\gamma_{k1}(k_x,k_y)|^2 - |\gamma_{k2}(k_x,k_y)|^2}{|\gamma_{k1}(k_x,k_y)|^2 + |\gamma_{k2}(k_x,k_y)|^2 + |\gamma_{k3}(k_x,k_y)|^2 + |\gamma_{k4}(k_x,k_y)|^2}, \tag{B.83}$$

where $k_x = \vec{k}\vec{x}$, $k_y = \vec{k}\vec{y}$. These values can change in the first Brillouin zone $[-\pi, \pi]$.

B.6.2 The r-dependent hopping expectation values

The $\vec{r}$-dependent ground state hopping (Γ_r) can be written as:

$$\Gamma_r = \frac{1}{N_{cs}}\sum_j (\hat{c}^\dagger_{j,\sigma}\hat{c}_{j+r,\sigma} + \hat{c}^\dagger_{j+r,\sigma}\hat{c}_{j,\sigma}) \tag{B.84}$$

To transform Γ_r to $\vec{k}$ space, I will use that $\hat{c}_{\vec{j},\sigma} = \frac{1}{\sqrt{N_{cs}}}\sum_{\vec{k}} e^{(-i\vec{k}\vec{j})}\hat{c}_{\vec{k},\sigma}$, $c = d, f$, $\sigma = \uparrow, \downarrow$:

$$\begin{aligned}
\Gamma_r = \frac{1}{N_s}\frac{1}{N_s}\sum_j\sum_{k_1}\sum_{k_2}(e^{ik_1r_j}e^{-ik_2(r_j+r)}\hat{c}^\dagger_{k_1,\sigma}\hat{c}_{k_2,\sigma} + e^{-ik_1(r_j+r)}e^{ik_2r_j}\hat{c}^\dagger_{k_1,\sigma}\hat{c}_{k_2,\sigma} = \\
\frac{1}{N_s}\sum_{k_1,k_2}\Big(\underbrace{\Big[\frac{1}{N_s}\sum_j e^{ir_j(k_1-k_2)}\Big]}_{\delta_{k_1,k_2}}\hat{c}^\dagger_{k_1,\sigma}\hat{c}_{k_2,\sigma}e^{-ik_2r} + \hat{c}^\dagger_{k_1,\sigma}\hat{c}_{k_2,\sigma}e^{ik_1r}\Big) = \\
= \frac{1}{N_s}\sum_k \hat{c}^\dagger_{k,\sigma}\hat{c}_{k,\sigma}\underbrace{(e^{ikr} + e^{-ikr})}_{2\cos(kr)} = \frac{2}{N_s}\sum_k \hat{n}_{k,\sigma}\cos(kr),
\end{aligned} \tag{B.85}$$

where in the last line, one sums over k values without indices, because of δ_{k_1,k_2}. Here $\hat{n}_{k,\sigma}$ is the fermionic number operator, $\sigma = \uparrow, \downarrow$, $c = d, f$.

To calculate the Γ_r expectation values I solved the following numerical integral:

$$\langle \Gamma_r \rangle = \frac{1}{2\pi^2} \int_{-\pi}^{\pi} \int_{-\pi}^{\pi} dk_1 dk_2 \cos((k_1+k_2)r) \frac{\langle \Psi_1 | \hat{n}_{k,d,\uparrow} | \Psi_1 \rangle}{\langle \Psi_1 | \Psi_1 \rangle}. \tag{B.86}$$

The $\langle \Gamma_r \rangle$ from Eq.(B.86) corresponds to the ground state $\vec{r}$ dependent hopping expectation value of an electron on the d orbit, with $\sigma = \uparrow$ spin. The expectation value of $n_{k,d,\uparrow}$ can be calculated as seen in Eq.(B.77).

B.7 The matching equations and their solution for the expanded model

There are 74 matching equations, with the new set of 32 $g'_{G,c,n,\sigma}$ parameters as unknown ($g' = a', b', n = 1,2,3,4, c = f, d, \sigma = \uparrow, \downarrow$) and 76 nonzero Hamiltonian parameters as known. There are in total 32 equations for the first neighbour terms. It consist of 16 first neighbour hoppings without hybridization (8 with-, and 8 without spin-flip) and 16 first neighbour hoppings with hybridization (8 with-, and 8 without spin-flip).

The 8 first neighbour hoppings without spin-flip:

$$\begin{aligned} t_x^{c,\sigma,\sigma} &= a'^*_{2,c,\sigma} a'_{1,c,\sigma} + a'^*_{3,c,\sigma} a'_{4,c,\sigma} + b'^*_{2,c,\sigma} b'_{1,c,\sigma} + b'^*_{3,c,\sigma} b'_{4,c,\sigma}, \\ t_y^{c,\sigma,\sigma} &= a'^*_{4,c,\sigma} a'_{1,c,\sigma} + a'^*_{3,c,\sigma} a'_{2,c,\sigma} + b'^*_{4,c,\sigma} b'_{1,c,\sigma} + b'^*_{3,c,\sigma} b'_{2,c,\sigma}. \end{aligned} \tag{B.87}$$

The 8 first neighbour spin-flip hoppings ($\sigma' = \uparrow, \downarrow, \sigma' \neq \sigma$):

$$\begin{aligned} t_x^{c,\sigma,\sigma'} &= a'^*_{2,c,\sigma} a'_{1,c,\sigma'} + a'^*_{3,c,\sigma} a'_{4,c,\sigma'} + b'^*_{2,c,\sigma} b'_{1,c,\sigma'} + b'^*_{3,c,\sigma} b'_{4,c,\sigma'}, \\ t_y^{c,\sigma,\sigma'} &= a'^*_{4,c,\sigma} a'_{1,c,\sigma'} + a'^*_{3,c,\sigma} a'_{2,c,\sigma'} + b'^*_{4,c,\sigma} b'_{1,c,\sigma'} + b'^*_{3,c,\sigma} b'_{2,c,\sigma'}. \end{aligned} \tag{B.88}$$

The 8 first neighbour hybridizations without spin-flip ($c' = d, f, c' \neq c$):

$$\begin{aligned} V_x^{c,c',\sigma,\sigma} &= a'^*_{2,c,\sigma} a'_{1,c',\sigma} + a'^*_{3,c,\sigma} a'_{4,c',\sigma} + b'^*_{2,c,\sigma} b'_{1,c',\sigma} + b'^*_{3,c,\sigma} b'_{4,c',\sigma}, \\ V_y^{c,c',\sigma,\sigma} &= a'^*_{4,c,\sigma} a'_{1,c',\sigma} + a'^*_{3,c,\sigma} a'_{2,c',\sigma} + b'^*_{4,c,\sigma} b'_{1,c',\sigma} + b'^*_{3,c,\sigma} b'_{2,c',\sigma}. \end{aligned} \tag{B.89}$$

The 8 first neighbour spin-flip hybridizations are zero:

$$\begin{aligned} V_x^{c,c',\sigma,\sigma'} &= a'^*_{2,c,\sigma} a'_{1,c',\sigma'} + a'^*_{3,c,\sigma} a'_{4,c',\sigma'} + b'^*_{2,c,\sigma} b'_{1,c',\sigma'} + b'^*_{3,c,\sigma} b'_{4,c',\sigma'} = 0, \\ V_y^{c,c',\sigma,\sigma'} &= a'^*_{4,c,\sigma} a'_{1,c',\sigma'} + a'^*_{3,c,\sigma} a'_{2,c',\sigma'} + b'^*_{4,c,\sigma} b'_{1,c',\sigma'} + b'^*_{3,c,\sigma} b'_{2,c',\sigma'} = 0. \end{aligned} \tag{B.90}$$

There are 16 next to nearest neighbour hopping terms without hybridization. 8 of them are without spin-flip:

$$t_{x+y}^{c,\sigma,\sigma} = a'^*_{3,c,\sigma} a'_{1,c,\sigma} + b'^*_{3,c,\sigma} b'_{1,c,\sigma}, \quad t_{y-x}^{c,\sigma,\sigma} = a'^*_{4,d,\sigma} a'_{2,c,\sigma} + b'^*_{4,c,\sigma} b'_{2,c,\sigma}. \tag{B.91}$$

The other 8 represent next to nearest neighbour hopping terms with spin-flip, which are

zero :

$$t_{x+y}^{c,\sigma,\sigma'} = a_{3,c,\sigma}'^{*} a_{1,c,\sigma'}' + b_{3,c,\sigma}'^{*} b_{1,c,\sigma'}' = 0,$$
$$t_{y-x}^{c,\sigma,\sigma'} = a_{4,c,\sigma}'^{*} a_{2,c,\sigma'}' + b_{4,c,\sigma}'^{*} b_{2,c,\sigma'}' = 0. \quad \text{(B.92)}$$

There are 16 next to nearest neighbour hopping terms with hybridization. The next 8 terms represent the next to nearest neighbour hybridization terms without spin-flip:

$$V_{x+y}^{c,c',\sigma,\sigma} = a_{3,c,\sigma}'^{*} a_{1,c',\sigma}' + b_{3,c,\sigma}'^{*} b_{1,c',\sigma}',$$
$$V_{y-x}^{c,c',\sigma,\sigma} = a_{4,c,\sigma}'^{*} a_{2,c',\sigma}' + b_{4,c,\sigma}'^{*} b_{2,c',\sigma}'. \quad \text{(B.93)}$$

The 8 next to nearest neighbour hybridization terms with spin-flip are zero:

$$V_{x+y}^{c,c',\sigma,\sigma'} = a_{3,c,\sigma}'^{*} a_{1,c',\sigma'}' + b_{3,c,\sigma}'^{*} b_{1,c',\sigma'}' = 0,$$
$$V_{y-x}^{c,c',\sigma,\sigma'} = a_{4,c,\sigma}'^{*} a_{2,c',\sigma'}' + b_{4,c,\sigma}'^{*} b_{2,c',\sigma'}' = 0. \quad \text{(B.94)}$$

And finally, the local ($\vec{r} = 0$) terms represent the remaining 16 terms. There are 8 on-site potentials:

$$\begin{aligned}
\tilde{\epsilon}_c^{\sigma,\sigma} = \;& a_{1,c,\sigma}'^{*} a_{1,c,\sigma}' + a_{2,c,\sigma}'^{*} a_{2,c,\sigma}' + a_{3,c,\sigma}'^{*} a_{3c\sigma}' + a_{4,c,\sigma}'^{*} a_{4,c,\sigma} + \\
+ \;& b_{1,c,\sigma}'^{*} b_{1,c,\sigma}' + b_{2,c,\sigma}'^{*} b_{2,c,\sigma}' + b_{3,c,\sigma}'^{*} b_{3,c,\sigma}' + b_{4,c,\sigma}'^{*} b_{4,c,\sigma}', \\
\epsilon_c^{\sigma,\sigma'} = \;& a_{1,c,\sigma}'^{*} a_{1,c,\sigma'}' + a_{2,c,\sigma}'^{*} a_{2,c,\sigma'}' + a_{3,c,\sigma}'^{*} a_{3,c,\sigma'}' + a_{4,c,\sigma}'^{*} a_{4,c,\sigma'} + \\
+ \;& b_{1,c,\sigma}'^{*} b_{1,c,\sigma'}' + b_{2,c,\sigma}'^{*} b_{2,c,\sigma'}' + b_{3,c,\sigma}'^{*} b_{3,c,\sigma'}' + b_{4,c,\sigma}'^{*} b_{4c\sigma'}' = 0.
\end{aligned} \quad \text{(B.95)}$$

Here $(\epsilon_c^{\sigma,\sigma'})^* = \epsilon_c^{\sigma',\sigma}$ holds.

Lastly, there are 8 on-site hybridizations:

$$\begin{aligned}
V_0^{c,c',\sigma,\sigma} = \;& a_{1,c,\sigma}'^{*} a_{1,c',\sigma}' + a_{2,c,\sigma}'^{*} a_{2,c',\sigma}' + a_{3,c,\sigma}'^{*} a_{3,c',\sigma} + a_{4,c,\sigma}'^{*} a_{4,c',\sigma}' + \\
+ \;& b_{1,c,\sigma}'^{*} b_{1,c',\sigma}' + b_{2,c,\sigma}'^{*} b_{2,c',\sigma}' + b_{3,c,\sigma}'^{*} b_{3,c',\sigma}' + b_{4,c,\sigma}'^{*} b_{4,c',\sigma}', \\
V_0^{c,c',\sigma,\sigma'} = \;& a_{1,c,\sigma}'^{*} a_{1,c',\sigma'}' + a_{2,c,\sigma}'^{*} a_{2,c',\sigma'}' + a_{3,c,\sigma}'^{*} a_{3,c',\sigma'} + a_{4,c,\sigma}'^{*} a_{4,c',\sigma'}' + \\
+ \;& b_{1,c,\sigma}'^{*} b_{1,c',\sigma'}' + b_{2,c,\sigma}'^{*} b_{2,c',\sigma'}' + b_{3,c,\sigma}'^{*} b_{3,c',\sigma'}' + b_{4,c,\sigma}'^{*} b_{4,c',\sigma'}' = 0.
\end{aligned} \quad \text{(B.96)}$$

Note that here $(V_0^{c,c',\alpha',\alpha})^* = V_0^{c',c,\alpha,\alpha'}$ holds.

Solving the matching equations

From Eq.(B.92), the from the conditions $t_{y\pm x}^{d,\sigma,\sigma'} = 0$ the following proportions were determined:

$$\frac{a_{3,d,\uparrow}'^{*}}{b_{3,d,\uparrow}'^{*}} = -\frac{b_{1,d,\downarrow}'}{a_{1,d,\downarrow}'} = x, \quad \frac{a_{3,d,\downarrow}'^{*}}{b_{3,d,\downarrow}'^{*}} = -\frac{b_{1,d,\uparrow}'}{a_{1,d,\uparrow}'} = y,$$
$$\frac{a_{4,d,\uparrow}'^{*}}{b_{4,d,\uparrow}'^{*}} = -\frac{b_{2,d,\downarrow}'}{a_{2,d,\downarrow}'} = z, \quad \frac{a_{4,d,\downarrow}'^{*}}{b_{4,d,\downarrow}'^{*}} = -\frac{b_{2,d,\uparrow}'}{a_{2,d,\uparrow}'} = v. \quad \text{(B.97)}$$

With them we get the $a'_{n,d,\sigma}$ parameters expressed with the $b'_{n,d,\sigma}$ parameters:

$$a'_{1,d,\uparrow} = -\frac{1}{y}b'_{1,d,\uparrow},\ a'_{1,d,\downarrow} = -\frac{1}{x}b'_{1,d,\downarrow},\ a'_{2,d,\uparrow} = -\frac{1}{v}b'_{2,d,\uparrow},\ a'_{2,d,\downarrow} = -\frac{1}{z}b'_{2,d,\downarrow},$$
$$a'^{*}_{3,d,\uparrow} = xb'^{*}_{3,d,\uparrow},\ a'^{*}_{3,d,\downarrow} = yb'^{*}_{3,d,\downarrow},\ a'^{*}_{4,d,\uparrow} = zb'^{*}_{4,d,\uparrow},\ a'^{*}_{4,d,\downarrow} = vb'^{*}_{4,d,\downarrow}. \tag{B.98}$$

Similarly for Eq.(B.94), $V^{d,f,\sigma,\sigma'}_{y\pm x} = 0$ conditions are met by introducing

$$\frac{a'_{1,f,\uparrow}}{b'_{1,f,\uparrow}} = -\frac{b'^{*}_{3,d,\downarrow}}{a'^{*}_{3,d,\downarrow}} = -\frac{1}{y},\quad \frac{a'_{1,f,\downarrow}}{b'_{1,f,\downarrow}} = -\frac{b'^{*}_{3,d,\uparrow}}{a'^{*}_{3,d,\uparrow}} = -\frac{1}{x},$$
$$\frac{a'_{2,f,\uparrow}}{b'_{2,f,\uparrow}} = -\frac{b'^{*}_{4,d,\downarrow}}{a'^{*}_{4,d,\downarrow}} = -\frac{1}{v},\quad \frac{a'_{2,f,\downarrow}}{b'_{2,f,\downarrow}} = -\frac{b'^{*}_{4,d,\uparrow}}{a'^{*}_{4,d,\uparrow}} = -\frac{1}{z}. \tag{B.99}$$

With Eq.(B.99) the $a'_{n,f,\sigma}$, $n = 1, 2$ parameters can be expressed with $b'_{n,f,\sigma}$, $n = 1, 2$ parameters:

$$a'_{1,f,\uparrow} = -\frac{1}{y}b'_{1,f,\uparrow},\ a'_{1,f,\downarrow} = -\frac{1}{x}b'_{1,f,\downarrow},\ a'_{2,f,\uparrow} = -\frac{1}{v}b'_{2,f,\uparrow},\ a'_{2,f,\downarrow} = -\frac{1}{z}b'_{2,f,\downarrow}, \tag{B.100}$$

With Eq.(B.98) and Eq.(B.100) the remaining $t^{f,\sigma,\sigma'}_{y\pm x} = 0$ conditions from Eq.(B.92) are met.

Using Eq.(B.98) and Eq.(B.100) I formed the following proportions from $t^{d,\sigma,\sigma}_{y\pm x}$, $V^{c,c',\sigma,\sigma}_{y\pm x}$

$$\frac{t^{d,\uparrow,\uparrow}_{x+y}}{V^{d,f,\uparrow,\uparrow}_{x+y}} = \frac{b'_{1,d,\uparrow}}{b'_{1,f,\uparrow}} = \alpha_{1,\uparrow},\quad \frac{t^{d,\downarrow,\downarrow}_{x+y}}{V^{d,f,\downarrow,\downarrow}_{x+y}} = \frac{b'_{1,d,\downarrow}}{b'_{1,f,\downarrow}} = \alpha_{1,\downarrow},$$
$$\frac{t^{d,\uparrow,\uparrow}_{y-x}}{V^{d,f,\uparrow,\uparrow}_{y-x}} = \frac{b'_{2,d,\uparrow}}{b'_{2,f,\uparrow}} = \alpha_{2,\uparrow},\quad \frac{t^{d,\downarrow,\downarrow}_{y-x}}{V^{d,f,\downarrow,\downarrow}_{y-x}} = \frac{b'_{2,d,\downarrow}}{b'_{2,f,\downarrow}} = \alpha_{2,\downarrow}.$$
$$\frac{t^{d,\uparrow,\uparrow}_{x+y}}{V^{f,d,\uparrow,\uparrow}_{x+y}} = \frac{b'^{*}_{3,d,\uparrow}}{b'^{*}_{3,f,\uparrow}} = \alpha^{*}_{3,\uparrow},\quad \frac{t^{d,\downarrow,\downarrow}_{x+y}}{V^{f,d,\downarrow,\downarrow}_{x+y}} = \frac{b'^{*}_{3,d,\downarrow}}{b'^{*}_{3,f,\downarrow}} = \alpha^{*}_{3,\downarrow},$$
$$\frac{t^{d,\uparrow,\uparrow}_{y-x}}{V^{f,d,\uparrow,\uparrow}_{y-x}} = \frac{b'^{*}_{4,d,\uparrow}}{b'^{*}_{4,f,\uparrow}} = \alpha^{*}_{4,\uparrow},\quad \frac{t^{d,\downarrow,\downarrow}_{y-x}}{V^{f,d,\downarrow,\downarrow}_{y-x}} = \frac{b'^{*}_{4,d,\downarrow}}{b'^{*}_{4,f,\downarrow}} = \alpha^{*}_{4,\downarrow}. \tag{B.101}$$

The $\alpha_{n,\sigma}$, $n = 1, 2, 3, 4$ parameters are considered known, since they are proportions of the know Hamiltonian parameters. With them all the block operator parameters can be expressed as function of the $b'_{n,f,\sigma}$

The $b'_{n,d,\sigma}$ coefficients expressed with $b'_{n,f,\sigma}$:

$$b'_{1,d,\uparrow} = \alpha_{1,\uparrow}b'_{1,f,\uparrow},\ b'_{2,d,\uparrow} = \alpha_{2,\uparrow}b'_{2,f,\uparrow},\ b'_{3,d,\uparrow} = \alpha_{3,\uparrow}b'_{3,f,\uparrow},\ b'_{4,d,\uparrow} = \alpha_{4,\uparrow}b'_{4,f,\uparrow},$$
$$b'_{1,d,\downarrow} = \alpha_{1,\downarrow}b'_{1,f,\downarrow},\ b'_{2,d,\downarrow} = \alpha_{2,\downarrow}b'_{2,f,\downarrow},\ b'_{3,d,\downarrow} = \alpha_{3,\downarrow}b'_{3,f,\downarrow},\ b'_{4,d,\downarrow} = \alpha_{4,\downarrow}b'_{4,f,\downarrow}. \tag{B.102}$$

The $a'_{n,d,\sigma}$ coefficients as function of

$$a'_{1,f,\uparrow} = -\frac{1}{y}b'_{1,f,\uparrow},\ a'_{2,f,\uparrow} = -\frac{1}{v}b'_{2,f,\uparrow},\ a'^*_{3,f,\uparrow} = xb'^*_{3,f,\uparrow},\ a'^*_{4,f,\uparrow} = zb'^*_{4,f,\uparrow},$$
$$a'_{1,f,\downarrow} = -\frac{1}{x}b'_{1,f,\downarrow},\ a'_{2,f,\downarrow} = -\frac{1}{z}b'_{2,f,\downarrow},\ a'^*_{3,f,\downarrow} = yb'^*_{3,f,\downarrow},\ a'^*_{4,f,\downarrow} = vb'^*_{4,f,\downarrow}. \quad \text{(B.103)}$$

Last, the $a'_{n,d,\sigma}$ parameters have the form of

$$a'_{1,d,\uparrow} = -\frac{\alpha_{1,\uparrow}}{y}b'_{1,f,\uparrow},\ a'_{2,d,\uparrow} = -\frac{\alpha_{2,\uparrow}}{v}b'_{2,f,\uparrow},\ a'^*_{3,d,\uparrow} = x\alpha^*_{3,\uparrow}b'^*_{3,f,\uparrow},\ a'^*_{4,d,\uparrow} = z\alpha^*_{4,\uparrow}b'^*_{4,f,\uparrow},$$
$$a'_{1,d,\downarrow} = -\frac{\alpha_{1,\downarrow}}{x}b'_{1,f,\downarrow},\ a'_{2,d,\downarrow} = -\frac{\alpha_{2,\downarrow}}{z}b'_{2,f,\downarrow},\ a'^*_{3,d,\downarrow} = y\alpha^*_{3,\downarrow}b'^*_{3,f,\downarrow},\ a'^*_{4,d,\downarrow} = v\alpha^*_{4,\downarrow}b'^*_{4,f,\downarrow}. \quad \text{(B.104)}$$

One notes, that with introducing the $\alpha_{n,\sigma}$ the following connection between the Hamiltonian parameters are present

$$V^{d,f,\uparrow,\uparrow}_{x+y}V^{f,d,\uparrow,\uparrow}_{x+y} = t^{d,\uparrow,\uparrow}_{x+y}t^{f,\uparrow,\uparrow}_{x+y},\quad V^{d,f,\uparrow,\uparrow}_{y-x}V^{f,d,\uparrow,\uparrow}_{y-x} = t^{d,\uparrow,\uparrow}_{y-x}t^{f,\uparrow,\uparrow}_{y-x},$$
$$V^{d,f,\downarrow,\downarrow}_{x+y}V^{f,d,\downarrow,\downarrow}_{x+y} = t^{d,\downarrow,\downarrow}_{x+y}t^{f,\downarrow,\downarrow}_{x+y},\quad V^{d,f,\downarrow,\downarrow}_{y-x}V^{f,d,\downarrow,\downarrow}_{y-x} = t^{d,\downarrow,\downarrow}_{y-x}t^{f,\downarrow,\downarrow}_{y-x}. \quad \text{(B.105)}$$

With Eq.(B.102)-(B.104) the 8 first neighbour spin-flip hybridization from Eq.(B.90), i.e. the $V^{c,c',\sigma,\sigma'}_{x} = V^{c,c',\sigma\sigma'}_{y} = 0$ conditions lead to the following expression

$$\alpha^*_{2,\downarrow}\frac{b'^*_{2,f,\downarrow}b'_{1,f,\uparrow}}{yz^*} = -\alpha^*_{3,\downarrow}b'^*_{3,f,\downarrow}b'_{4,f,\uparrow},\quad \alpha_{1,\uparrow}\frac{b'^*_{2,f,\downarrow}b'_{1,f,\uparrow}}{yz^*} = -\alpha_{4,\uparrow}b'^*_{3,f,\downarrow}b'_{4,f,\uparrow},$$
$$\alpha^*_{2,\uparrow}\frac{b'^*_{2,f,\uparrow}b'_{1,f,\downarrow}}{xv^*} = -\alpha^*_{3,\uparrow}b'^*_{3,f,\uparrow}b'_{4,f,\downarrow},\quad \alpha_{1,\downarrow}\frac{b'^*_{2,f,\uparrow}b'_{1,f,\downarrow}}{xv^*} = -\alpha_{4,\downarrow}b'^*_{3,f,\uparrow}b'_{4,f,\downarrow},$$
$$\alpha^*_{4,\downarrow}\frac{b'^*_{4,f,\downarrow}b'_{1,f,\uparrow}}{y} = \alpha^*_{3,\downarrow}\frac{b'^*_{3,f,\downarrow}b'_{2,f,\uparrow}}{v},\quad \alpha_{1,\uparrow}\frac{b'^*_{4,f,\downarrow}b'_{1,f,\uparrow}}{y} = \alpha_{2,\uparrow}\frac{b'^*_{3,f,\downarrow}b'_{2,f,\uparrow}}{v},$$
$$\alpha^*_{4,\uparrow}\frac{b'^*_{4,f,\uparrow}b'_{1,f,\downarrow}}{x} = \alpha^*_{3,\uparrow}\frac{b'^*_{3,f,\uparrow}b'_{2,f,\downarrow}}{z},\quad \alpha_{1,\downarrow}\frac{b'^*_{4,f,\uparrow}b'_{1,f,\downarrow}}{x} = \alpha_{2,\downarrow}\frac{b'^*_{3,f,\uparrow}b'_{2,f,\downarrow}}{z}. \quad \text{(B.106)}$$

I divided the two equations in each line by each other, which resulted in the conditions

$$\frac{\alpha^*_{2,\downarrow}}{\alpha_{1,\uparrow}} = \frac{\alpha^*_{3,\downarrow}}{\alpha_{4,\uparrow}},\quad \frac{\alpha^*_{2,\uparrow}}{\alpha_{1,\downarrow}} = \frac{\alpha^*_{3,\uparrow}}{\alpha_{4,\downarrow}},\quad \frac{\alpha^*_{4,\downarrow}}{\alpha_{1,\uparrow}} = \frac{\alpha^*_{3,\downarrow}}{\alpha_{2,\uparrow}},\quad \frac{\alpha^*_{4,\uparrow}}{\alpha_{1,\downarrow}} = \frac{\alpha^*_{3,\uparrow}}{\alpha_{2,\downarrow}}, \quad \text{(B.107)}$$

which can be summarised as

$$\alpha_{3,\uparrow}\alpha^*_{1,\downarrow} = \alpha^*_{3,\downarrow}\alpha_{1,\uparrow} = \alpha^*_{2,\downarrow}\alpha_{4,\uparrow} = \alpha_{2,\uparrow}\alpha^*_{4,\downarrow} = \gamma_0. \quad \text{(B.108)}$$

Here the newly introduced γ_0 is an arbitrary parameter. Besides Eq.(B.108) from Eq.(B.106) remains

$$\alpha^*_{2,\downarrow}\frac{b'^*_{2,f,\downarrow}b'_{1,f,\uparrow}}{yz^*} = -\alpha^*_{3,\downarrow}b'^*_{3,f,\downarrow}b'_{4,f,\uparrow},\quad \alpha^*_{4,\uparrow}\frac{b'^*_{4,f,\uparrow}b'_{1,f,\downarrow}}{x} = \alpha^*_{3,\uparrow}\frac{b'^*_{3,f,\uparrow}b'_{2,f,\downarrow}}{z}$$

$$\alpha^*_{2,\uparrow}\frac{b'^*_{2,f,\uparrow}b'_{1,f,\downarrow}}{xv^*}=-\alpha^*_{3,\uparrow}b'^*_{3,f,\uparrow}b'_{4,f,\downarrow},\quad \alpha^*_{4,\downarrow}\frac{b'^*_{4,f,\downarrow}b'_{1,f,\uparrow}}{y}=\alpha^*_{3,\downarrow}\frac{b'^*_{3,f,\downarrow}b'_{2,f,\uparrow}}{v}. \tag{B.109}$$

In Eq.(B.109) in both lines I carried out the following operation: I divided the first equation, with the conjugate of the second:

$$\frac{\alpha^*_{2,\downarrow}}{\alpha_{3,\uparrow}}\frac{1}{y}\frac{b'_{1,f,\uparrow}}{b'_{3,f,\uparrow}}=-\frac{\alpha^*_{3,\downarrow}}{\alpha_{4,\uparrow}}x^*\frac{b'^*_{3,f,\downarrow}}{b'^*_{1,f,\downarrow}},\quad \frac{\alpha^*_{2,\uparrow}}{\alpha_{3,\uparrow}}\frac{1}{x}\frac{b'_{1,f,\downarrow}}{b'_{3,f,\downarrow}}=-\frac{\alpha^*_{3,\uparrow}}{\alpha_{4,\downarrow}}y^*\frac{b'^*_{3,f,\uparrow}}{b'^*_{1,f,\uparrow}}. \tag{B.110}$$

From Eq.(B.108) $\frac{\alpha^*_{3,\downarrow}}{\alpha_{4,\uparrow}}=\frac{\alpha^*_{2,\downarrow}}{\alpha_{1,\uparrow}}$, and $\frac{\alpha^*_{3,\uparrow}}{\alpha_{4,\downarrow}}=\frac{\alpha^*_{2,\uparrow}}{\alpha_{1,\downarrow}}$, thus Eq.(B.110) becomes

$$\frac{\alpha_{1,\uparrow}}{\alpha_{3,\uparrow}}\frac{1}{y}\frac{b'_{1,f,\uparrow}}{b'_{3,f,\uparrow}}=-x^*\frac{b'^*_{3,f,\downarrow}}{b'^*_{1,f,\downarrow}},\quad \frac{\alpha_{1,\downarrow}}{\alpha_{3,\downarrow}}\frac{1}{x}\frac{b'_{1,f,\downarrow}}{b'_{3,f,\downarrow}}=-y^*\frac{b'^*_{3,f,\uparrow}}{b'^*_{1,f,\uparrow}}, \tag{B.111}$$

The two equations in Eq.(B.111) contains the same proportions, thus can be written as

$$-\frac{b'^*_{3,f,\downarrow}}{b'^*_{1,f,\downarrow}}=\frac{\alpha_{1,\uparrow}}{\alpha_{3,\uparrow}}\frac{1}{yx^*}\frac{b'_{1,f,\uparrow}}{b'_{3,f,\uparrow}}=u,\quad -\frac{b'_{3,f,\downarrow}}{b'_{1,f,\downarrow}}=\frac{\alpha_{1,\downarrow}}{\alpha_{3,\downarrow}}\frac{1}{xy^*}\frac{b'^*_{1,f,\uparrow}}{b'^*_{3,f,\uparrow}}=u^*, \tag{B.112}$$

where u is an arbitrary parameter. This way from Eq.(B.110) $b'_{3,f,\downarrow}$ and $b'_{3,f,\uparrow}$ can be expressed as

$$b'_{3,f,\downarrow}=-u^*b'_{1,f,\downarrow},\quad b'_{3,f,\uparrow}=\frac{\alpha_{1,\uparrow}}{\alpha_{3,\uparrow}}\frac{1}{uyx^*}b'_{1,f,\uparrow}. \tag{B.113}$$

From Eq.(B.108), and thus from Eq.(B.109) two conditions remain

$$\begin{aligned}\alpha^*_{2,\downarrow}\frac{b'^*_{2,f,\downarrow}b'_{1,f,\uparrow}}{yz^*}&=-\alpha^*_{3,\downarrow}b'^*_{3,f,\downarrow}b'_{4,f,\uparrow},\\ \alpha^*_{2,\uparrow}\frac{b'^*_{2,f,\uparrow}b'_{1,f,\downarrow}}{xv^*}&=-\alpha^*_{3,\uparrow}b'^*_{3,f,\uparrow}b'_{4,f,\downarrow}.\end{aligned} \tag{B.114}$$

After substituting Eq.(B.113) into Eq.B.114 the remaining equations become

$$\frac{b'_{1,f,\uparrow}}{b'^*_{1,f,\downarrow}}=uyz^*\frac{\alpha^*_{3,\downarrow}}{\alpha^*_{2,\downarrow}}\frac{b'_{4,f,\uparrow}}{b'^*_{2,f,\downarrow}}=-\frac{uy}{v}\frac{\alpha_{2,\uparrow}}{\alpha_{1,\uparrow}}\frac{b'_{2,f,\uparrow}}{b'^*_{4,f,\downarrow}}=w, \tag{B.115}$$

where w an arbitrary parameter. I used Eq.(B.115) to express yet other $b'_{n,f,\sigma}$ parameters

$$b'_{1,f,\downarrow}=\frac{1}{w^*}b'^*_{1,f,\uparrow},\quad b'_{4,f,\uparrow}=\frac{\alpha^*_{2,\downarrow}}{\alpha^*_{3,\downarrow}}\frac{w}{uyz^*}b'^*_{2,f,\downarrow},\quad b'_{4,f,\downarrow}=-\frac{\alpha^*_{2,\uparrow}}{\alpha^*_{1,\uparrow}}\frac{u^*y^*}{v^*w^*}b'^*_{2,f,\uparrow}. \tag{B.116}$$

Other zero Hamiltonian parameters are the local spin-flip hybridizations, as seen in Eq.(B.96). Using the form of the block operator parameters derived by the conditions $V_x^{c,c',\sigma,\sigma'}=V_y^{c,c',\sigma,\sigma'}=0$ the local spin-flip hybridization are automatically zero, i.e. $V_0^{c,c',\sigma\sigma'}=0$ is met, without any further condition. This also means, that all the zero parameters are eliminated from the starting matching equations for the expanded model. At this point all the block operator parameters are expressed via the remaining unknowns:

$b_{1,f,\uparrow}, b_{2,f,\uparrow}, b_{2,f,\downarrow}$ (see Eq.(B.113) and Eq.(B.115)).
Next the $t_x^{c,\uparrow,\uparrow} = t_x^{c,\downarrow,\downarrow}$, $t_y^{c\uparrow,\uparrow} = t_y^{c,\downarrow,\downarrow}$ conditions will be met. The $t_x^{d,\uparrow,\uparrow} = t_x^{d,\downarrow,\downarrow}$, $t_x^{f,\uparrow,\uparrow} = t_x^{f,\downarrow,\downarrow}$ conditions respectively:

$$\begin{aligned}\frac{1+yv^*}{yv^*}b'^*_{2,f,\uparrow}b'_{1,f,\uparrow}\alpha^*_{2,\uparrow}(1-\frac{\alpha_{4,\downarrow}}{\alpha_{1,\uparrow}}) + \frac{1+xz^*}{xz^*w^*}b'^*_{1,f,\uparrow}b'^*_{2,f,\downarrow}\alpha^*_{3,\downarrow}(1-\frac{\alpha_{1,\downarrow}}{\alpha_{4,\uparrow}}) = 0,\\ \frac{1+yv^*}{yv^*}b'^*_{2,f,\uparrow}b'_{1,f,\uparrow}(1-\frac{\alpha^*_{2,\uparrow}}{\alpha^*_{3,\downarrow}}) + \frac{1+xz^*}{xz^*w^*}b'^*_{1,f,\uparrow}b'^*_{2,f,\downarrow}\frac{\alpha^*_{2,\downarrow}}{\alpha^*_{3,\uparrow}}(1-\frac{\alpha^*_{3,\uparrow}}{\alpha^*_{2,\downarrow}}) = 0,\end{aligned} \tag{B.117}$$

The two conditions in Eq.(B.117) are met simultaneously if

$$\frac{1+yv^*}{yv^*}b'^*_{2,f,\uparrow}b'_{1,f,\uparrow} + \frac{1+xz^*}{xz^*w^*}b'^*_{1,f,\uparrow}b'^*_{2,f,\downarrow}\gamma_2 = 0, \tag{B.118}$$

and the form of γ_2 is

$$\gamma_2 = \frac{\alpha^*_{3,\downarrow}}{\alpha^*_{2,\uparrow}}\frac{(1-\frac{\alpha_{1,\downarrow}}{\alpha_{4,\uparrow}})}{(1-\frac{\alpha_{4,\downarrow}}{\alpha_{1,\uparrow}})} = \frac{\alpha^*_{2,\downarrow}}{\alpha^*_{3,\uparrow}}\frac{(1-\frac{\alpha^*_{3,\uparrow}}{\alpha^*_{2,\downarrow}})}{(1-\frac{\alpha^*_{2,\uparrow}}{\alpha^*_{3,\downarrow}})}. \tag{B.119}$$

The $t_y^{d,\uparrow,\uparrow} = t_y^{d,\downarrow,\downarrow}$, $t_y^{f,\uparrow,\uparrow} = t_y^{f,\downarrow,\downarrow}$ conditions become

$$\begin{aligned}\frac{v-x}{vx}b'_{2,f,\uparrow}b'^*_{1,f,\uparrow}\alpha_{2,\uparrow}(1-\frac{\alpha_{1,\downarrow}}{\alpha_{2,\uparrow}}) + \frac{y-z}{yz}w^*b'_{1,f,\uparrow}b'_{2,f,\downarrow}\alpha_{1,\uparrow}(1-\frac{\alpha_{2,\downarrow}}{\alpha_{1,\uparrow}}) = 0,\\ \frac{v-x}{vx}b'_{2,f,\uparrow}b'^*_{1,f,\uparrow}(1-\frac{\alpha^*_{3,\uparrow}}{\alpha^*_{4,\downarrow}}) + \frac{y-z}{yz}w^*b'_{1,f,\uparrow}b'_{2,f,\downarrow}\frac{\alpha_{2,\downarrow}}{\alpha_{1,\downarrow}}(1-\frac{\alpha_{1,\uparrow}}{\alpha_{2,\downarrow}}) = 0,\end{aligned} \tag{B.120}$$

The two condition is Eq.(B.120) are met simultaneously by

$$\frac{v-x}{vx}b'^*_{1,f,\uparrow}b'_{2,f,\uparrow} + \frac{(y-z)w^*}{yz}b'_{1,f,\uparrow}b'_{2,f,\downarrow}\gamma_3 = 0, \tag{B.121}$$

where γ_3 has the form

$$\gamma_3 = \frac{\alpha_{1,\uparrow}}{\alpha_{2,\uparrow}}\frac{(1-\frac{\alpha_{2,\downarrow}}{\alpha_{1,\uparrow}})}{(1-\frac{\alpha_{1,\downarrow}}{\alpha_{2,\uparrow}})} = \frac{\alpha_{2,\downarrow}}{\alpha_{1,\downarrow}}\frac{(1-\frac{\alpha_{1,\uparrow}}{\alpha_{2,\downarrow}})}{(1-\frac{\alpha^*_{3,\uparrow}}{\alpha^*_{4,\downarrow}})}. \tag{B.122}$$

From Eq.(B.108) the $\alpha_{n,\sigma}$ parameters can be written as

$$\alpha_{4,\uparrow} = \frac{\gamma_0}{\alpha^*_{2,\downarrow}}, \quad \alpha_{4,\downarrow} = \frac{\gamma^*_0}{\alpha^*_{2,\uparrow}}, \quad \alpha_{3,\uparrow} = \frac{\gamma_0}{\alpha^*_{1,\downarrow}}, \quad \alpha_{3,\downarrow} = \frac{\gamma^*_0}{\alpha^*_{1,\uparrow}}. \tag{B.123}$$

Using Eq.(B.123) γ_3 and γ_2 from Eq.(B.119) and Eq.(B.122)

$$\gamma_2 = -\frac{\gamma_0 - \alpha_{1,\downarrow}\alpha^*_{2,\downarrow}}{\gamma_0 - \alpha_{1,\uparrow}\alpha^*_{2,\uparrow}}, \quad \gamma_3 = -\frac{\alpha_{1,\uparrow} - \alpha_{2,\downarrow}}{\alpha_{1,\downarrow} - \alpha_{2,\uparrow}}, \tag{B.124}$$

if $\gamma_0 = \gamma^*_0$. is considered. One notices that from Eq.(B.118) and Eq.(B.121) introducing

$T_1 = b'^*_{2,f,\uparrow} b'_{1,f,\uparrow}$ and $T_2 = b'^*_{1,f,\uparrow} b'^*_{2,f,\downarrow}$ one gets a linear homogeneous system of equations

$$\begin{aligned} \frac{1+yv^*}{yv^*}\, T_1 + \frac{1+xz^*}{xz^*w^*}\gamma_2\, T_2 = 0, \\ \frac{v^*-x^*}{v^*x^*}\, T_1 + \frac{(y^*-z^*)w}{y^*z^*}\gamma_3^*\, T_2 = 0. \end{aligned} \tag{B.125}$$

The two unknown T_1 and T_2 has non-zero solutions only if the determinant of the system of equations in Eq.(B.125) is zero, i.e.

$$|w|^2 = \frac{\gamma_2}{\gamma_3^*}\frac{|y|^2}{|x|^2}\frac{(1+xz^*)(v^*-x^*)}{(1+yv^*)(y^*-z^*)}. \tag{B.126}$$

In the case, using the polar form of $b'_{1,f,\uparrow}$, i.e. $b'_{1,f,\uparrow} = |b'_{1,f,\uparrow}|e^{i\theta_{1,f,\uparrow}}$, one can express $b'_{2,f,\downarrow}$ as

$$b'_{2,f,\downarrow} = \omega b'_{2,f,\uparrow}, \text{where } \omega = \omega_0 e^{-2i\theta_{1,f,\uparrow}}, \omega_0 = -\frac{1+y^*v}{y^*v}\frac{zwx^*}{(1+x^*z)\gamma_2^*}. \tag{B.127}$$

For the first neighbour and on-site hybridization without spin-flip, the coupling are also spin direction independent, thus in this case, just as seen for the hopping terms the $\uparrow,\uparrow$ and $\downarrow,\downarrow$ must be equal. The hybridization without spin-flip at this point can be written as

$$\begin{aligned} V_x^{d,f,\downarrow,\downarrow} &= \frac{\alpha_{3,\downarrow}^*}{\alpha_{1,\uparrow}^*}\frac{|u|^2|y|^2}{|w|^2}\, V_x^{d,f,\uparrow,\uparrow}, \quad V_y^{d,f,\downarrow,\downarrow} = \frac{\alpha_{3,\downarrow}^*}{\alpha_{1,\uparrow}^*}\frac{|u|^2|y|^2}{|w|^2}\, V_y^{d,f,\uparrow,\uparrow}, \\ V_x^{f,d,\downarrow,\downarrow} &= \frac{\alpha_{3,\downarrow}}{\alpha_{1,\uparrow}}\frac{|u|^2|y|^2}{|w|^2}\, V_x^{f,d,\uparrow,\uparrow}, \quad V_y^{f,d,\downarrow,\downarrow} = \frac{\alpha_{3,\downarrow}}{\alpha_{1,\uparrow}}\frac{|u|^2|y|^2}{|w|^2}\, V_y^{f,d,\uparrow,\uparrow}, \\ V_0^{d,f,\downarrow,\downarrow} &= \frac{\alpha_{3,\downarrow}^*}{\alpha_{1,\uparrow}^*}\frac{|u|^2|y|^2}{|w|^2}\, V_0^{d,f,\uparrow,\uparrow}. \end{aligned} \tag{B.128}$$

From here the condition

$$|u|^2|y|^2/|w|^2 = \alpha_{1,\uparrow}/\alpha_{3,\downarrow} \tag{B.129}$$

arises.

For the next to nearest neighbour hopping also $t_{x+y}^{c,\sigma,\sigma} = t_{x+y}^{c,\sigma',\sigma'}$ and $t_{y-z}^{c,\sigma,\sigma} = t_{y-x}^{c,\sigma',\sigma'}$ must stand.

$$\begin{aligned} t_{x+y}^{f,\uparrow,\uparrow} &= \frac{(y-x)}{u^*x|y|^2}\frac{\alpha_{1,\uparrow}^*}{\alpha_{3,\uparrow}^*}|b'_{1,f,\uparrow}|^2, \quad t_{x+y}^{f,\downarrow,\downarrow} = \frac{(y-x)u}{x|w|^2}|b'_{1,f,\uparrow}|^2, \\ t_{y-x}^{f,\uparrow,\uparrow} &= \frac{(v-z)w^*}{vzu^*y^*}\frac{\alpha_{2,\downarrow}}{\alpha_{3,\downarrow}}b'_{2,f,\uparrow}b'_{2,f,\downarrow} \quad t_{y-x}^{f,\downarrow,\downarrow} = \frac{(v-z)uy}{vzw}\frac{\alpha_{2,\uparrow}}{\alpha_{1,\uparrow}}b'_{2,f,\uparrow}b'_{2,f,\downarrow}. \end{aligned} \tag{B.130}$$

Creating the proportions using Eq.(B.123) and Eq.(B.129)

$$\frac{t^{f,\uparrow,\uparrow}_{x+y}}{t^{f,\downarrow,\downarrow}_{x+y}} = \frac{\alpha_{1,\downarrow}}{\alpha_{1,\uparrow}}, \quad \frac{t^{f,\uparrow,\uparrow}_{y-x}}{t^{f,\downarrow,\downarrow}_{y-x}} = \frac{\alpha_{2,\downarrow}}{\alpha_{2,\uparrow}}, \tag{B.131}$$

which leads to $\alpha_{1,\downarrow} = \alpha_{1,\uparrow} = \alpha_1$ and $\alpha_{2,\downarrow} = \alpha_{2,\uparrow} = \alpha_1$. This considering Eq.(B.123) and that γ_0 is real leads to $\alpha_{3,\downarrow} = \alpha_{3,\uparrow} = \gamma_0/\alpha_1^*$, $\alpha_{4,\uparrow} = \alpha_{4,\downarrow} = \gamma_0/\alpha_2^*$. Thus for $|w|$ from Eq.(B.129)

$$|w| = (|u||y|\sqrt{\gamma_0})/|\alpha_1| \tag{B.132}$$

stands.

Then for $|b'_{1,f,\uparrow}| = 1/|\mu||b'_{2,f,\uparrow}|$, where $|b'_{2,f,\uparrow}|$ is a free parameter, and μ is

$$\mu = \frac{V(|\alpha_1|^2 - \gamma_0)}{|y|^2(\gamma_0 - |\alpha_2|^2)} \frac{k(1+|y|^2) - (1+|x|^2)}{k(1+V) - (1+|z|^2)\frac{|v-x|^2}{|y-z|^2}}. \tag{B.133}$$

The remaining matching equations are for the four first neighbour spin-flip hoppings, from which three is independent

$$\begin{aligned} &k\sigma^*(1+\sigma) = Z[k(1+\sigma) + X^* - \frac{|X|^2}{V}] + (V - X), \\ &\frac{X-V}{1+X}e^{i\phi_1} = V\frac{\sigma^* - Z}{V + \sigma Z}, \\ &\frac{V + ZX^*}{X - Z}e^{i\phi_2} = V\frac{(1+\sigma^*)}{\sigma - V}. \end{aligned} \tag{B.134}$$

where $\sigma = yv^*$, $X = vx^*, Z = vz^*, V = |v|^2$. In Eq.(B.134) $\sigma, k, \phi_1, \phi_2$ are arbitrary parameters, X, Y, Z are the unknowns. With them x, y, z, v parameters can be deduced.

The last unknown of the matching equations $b'_{1,f,\uparrow}$ taking Eq.(B.133) into account can be given as $b'_{1,f,\uparrow} = 1/|\mu||b'_{2,f,\uparrow}|e^{i\theta_{1,f,\uparrow}}$, where $\theta_{1,f,\uparrow}$ is an arbitrary phase factor.

The presented solution appears, when the spin-flip terms fulfill the following conditions. First

$$t_p^{f,\sigma\sigma'} = -\frac{1}{\gamma_0} t_p^{d,\sigma\sigma'}, \tag{B.135}$$

where $p = x, y$ and $\sigma \neq \sigma'$. Second the relation

$$t_p'^{c,\sigma\sigma} = \frac{1}{\gamma_0} t_p'^{c',\sigma\sigma}, \tag{B.136}$$

where $p' = x, y, y \pm x$ fixes the ratio of hopping terms without spin-flip.

Third for the first neighbour hybridization terms without spin-flip

$$V_x^{df,\uparrow\uparrow} = \frac{2\alpha_2^*}{\alpha_1\alpha_2^* + \gamma_0} t_x^{d,\uparrow,\uparrow}, \quad V_x^{fd,\uparrow\uparrow} = \frac{2\alpha_1}{\alpha_1\alpha_2^* + \gamma_0} t_x^{d,\uparrow,\uparrow},$$
$$V_y^{df,\uparrow\uparrow} = \frac{2}{\alpha_2 + \alpha_1} t_y^{d,\uparrow\uparrow}, \quad V_y^{fd,\uparrow\uparrow} = \frac{2\alpha_1\alpha_2}{\gamma_0(\alpha_2 + \alpha_1)} t_y^{d,\uparrow\uparrow}. \tag{B.137}$$

is met. Finally for the diagonal hopping terms (see Eq.(B.101))

$$\frac{t_{x+y}^{d,\sigma,\sigma}}{V_{x+y}^{d,f,\sigma,\sigma}} = \alpha_1, \quad \frac{t_{y-x}^{d,\sigma,\sigma}}{V_{y-x}^{d,f,\sigma,\sigma}} = \alpha_2, \quad \frac{t_{x+y}^{d,\sigma,\sigma}}{V_{x+y}^{f,d,\sigma,\sigma}} = \frac{\gamma_0}{\alpha_1}, \quad \frac{t_{y-x}^{d,\sigma,\sigma}}{V_{y-x}^{f,d,\sigma,\sigma}} = \frac{\gamma_0}{\alpha_2} \tag{B.138}$$

holds. The remaining Hamiltonian parameters and the 12 free parameters k, $Re(\sigma)$, $Im(\sigma)$, ϕ_1, ϕ_2, $Re(\alpha_1)$, $Im(\alpha_1)$, $Re(\alpha_2)$, $Im(\alpha_2)$, γ_0, $|b'_{2,f,\uparrow}|$, θ_2 enter the solutions presented above and with them the unknown block operator parameters can be calculated.

Own publications

[O1] N. Kucska, Zs. Gulácsi, Spin-orbit interactions may relax the rigid conditions leading to flat bands, *Physical Review B* **105**:085103, 2022. doi: 10.1103/PhysRevB.105.085103, arXiv:2110.10453

[O2] N. Kucska, Zs. Gulácsi, Flat band conditions influenced by spin-orbit interaction in the presence of external magnetic field, *Multidisciplinary Sciences*, 11(5):171-179, 2021. doi: 10.35925/j.multi.2021.5.17

[O3] N. Kucska, Zs. Gulácsi, Exact results relating spin-orbit interactions in two-dimensional strongly correlated systems, *Philosophical Magazine*, 98(18):1708-1730, 2018. doi: 10.1080/14786435.2018.1441559, arXiv:2002.05086

[O4] N. Kucska, Zs. Gulácsi, Effects of spin-orbit interaction on surfaces and interfaces, *Materials Science and Engineering*, 44(2):43-53, 2019. doi: 10.32974.mse.2019.005

[O5] N. Kucska, Zs. Gulácsi, Itinerant surfaces with spin-orbit couplings, correlations and external magnetic fields: exact results, *Philosophical Magazine Letters*, 99(3):118-125, 2019. doi: 10.1080/09500839.2019.1634291 arXiv:1912.07888

[O6] N. Kucska, Zs. Gulácsi, Nanograin ferromagnets from non-magnetic bulk materials: the case of gold nanoclusters, *International Journal of Modern Physics B*, 35(10), 2021. doi: 10.1142/S0217979221501484 arXiv:2109.07297

Bibliography

[1] L. Larrimore. Lecture notes in Physics 115 - Seminar 5, 2004.

[2] A. Manchon, H. C. Koo, J. Nitta, S.M. Frolov, and R.A. Duine. New perspectives for Rashba spin–orbit coupling. *Nature materials*, 14(9):871–882, 2015.

[3] G. Bihlmayer, O. Rader, and R. Winkler. Focus on the Rashba effect. *New journal of physics*, 17(5):050202, 2015.

[4] Y. A Bychkov and É. I. Rashba. Properties of a 2d electron gas with lifted spectral degeneracy. *JETP lett*, 39(2):78, 1984.

[5] A. Soumyanarayanan, N. Reyren, A. Fert, and C. Panagopoulos. Emergent phenomena induced by spin-orbit coupling at surfaces and interfaces. *Nature*, 539:509–517, 2016.

[6] M. Kepenekian and J. Even. Rashba and Dresselhaus couplings in halide perovskites: Accomplishments and opportunities for spintronics and spin-orbitronics. *The Journal of Physical Chemistry Letters*, 8, 2017.

[7] M. N. Baibich, J. M. Broto, A. Fert, F. Nguyen Van Dau, F. Petroff, P. Etienne, G. Creuzet, A. Friederich, and J. Chazelas. Giant magnetoresistance of (001)Fe/(001)Cr magnetic superlattices. *Phys. Rev. Lett.*, 61:2472–2475, Nov 1988.

[8] G. Binasch, P. Grünberg, F. Saurenbach, and W. Zinn. Enhanced magnetoresistance in layered magnetic structures with antiferromagnetic interlayer exchange. *Phys. Rev. B*, 39:4828–4830, Mar 1989.

[9] N.W. Ashcroft and N.D. Mermin. *Solid State Physics*. Cengage Learning, 1st edition, 1976.

[10] G. Dresselhaus. Spin-orbit coupling effects in zinc blende structures. *Phys. Rev.*, 100:580–586, 1955.

[11] M. I. D'yakonov. Spin relaxation of two-dimensional electrons in noncentrosymmetric semiconductors. *Sov. Phys. Semicond.*, 20(1):110–112, 1986.

[12] D. Leykam, A. Andreanov, and S. Flach. Artificial flat band systems: from lattice models to experiments. *Advances in Physics: X*, 3(1):1473052, 2018.

[13] S. Mukherjee, A. Spracklen, D. Choudhury, N. Goldman, P. Öhberg, E. Andersson, and R. R. Thomson. Observation of a localized flat-band state in a photonic Lieb lattice. *Phys. Rev. Lett.*, 114:245504, 2015.

[14] L. Tang, D. Song, S. Xia, S. Xia, J. Ma, W. Yan, Y. Hu, J. Xu, D. Leykam, and Z. Chen. Photonic flat-band lattices and unconventional light localization. *Nanophotonics*, 9(5):1161–1176, 2020.

[15] G. Gligoric, A. Maluckov, Lj. Hadzievski, Sergej Flach, and Boris A. Malomed. Nonlinear localized flat-band modes with spin-orbit coupling. *Phys. Rev. B*, 94:144302, 2016.

[16] C. E. Whittaker, E. Cancellieri, P. M. Walker, D. R. Gulevich, H. Schomerus, and D. et al. Vaitiekus. Exciton polaritons in a two-dimensional Lieb lattice with spin-orbit coupling. *Phys. Rev. Lett.*, 120:097401, 2018.

[17] D.-S. Ma, Y. Xu, C. S. Chiu, N. Regnault, A. A. Houck, Z. Song, and B. A. Bernevig. Spin-orbit-induced topological flat bands in line and split graphs of bipartite lattices.

Phys. Rev. Lett., 125:266403, 2020.

[18] F. Zhao, Y. Shi, L. Pan, and G. Yu. Multifunctional nanostructured conductive polymer gels: synthesis, properties, and applications. *Accounts of chemical research*, 50(7):1734–1743, 2017.

[19] K.M. Ziadan. New polymers for special applications. *Conducting polymers application "(Ed: A. de S. Gomes), Rijeka, Croatia*, 2012.

[20] Y. Shi, L. Peng, Y. Ding, Y. Zhao, and G. Yu. Nanostructured conductive polymers for advanced energy storage. *Chemical Society Reviews*, 44(19):6684–6696, 2015.

[21] G. Wegner. Polymers with metal-like conductivity—A review of their synthesis, structure and properties. *Angewandte Chemie International Edition in English*, 20(4):361–381, 1981.

[22] C. Li, H. Bai, and G. Shi. Conducting polymer nanomaterials: electrosynthesis and applications. *Chemical Society Reviews*, 38(8):2397–2409, 2009.

[23] R. Gangopadhyay and A. De. Conducting polymer nanocomposites: A brief overview. *Chemistry of materials*, 12(3):608–622, 2000.

[24] R. M. Penner and C. R. Martin. Electronically conductive composite polymer membranes. *Journal of The Electrochemical Society*, 133(2):310, 1986.

[25] C. R. Martin. Template synthesis of electronically conductive polymer nanostructures. *Accounts of chemical research*, 28(2):61–68, 1995.

[26] T. Sumida, Y. Wada, T. Kitamura, and S. Yanagida. Electrochemical preparation of macroporous polypyrrole films with regular arrays of interconnected spherical voids. *Chemical Communications*, 17:1613–1614, 2000.

[27] G. Lu and G. Shi. Electrochemical polymerization of pyrene in the electrolyte of boron trifluoride diethyl etherate containing trifluoroacetic acid and polyethylene glycol oligomer. *Journal of Electroanalytical Chemistry*, 586(2):154–160, 2006.

[28] F. Hellman, A. Hoffmann, Y. Tserkovnyak, G.S.D. Beach, E.E. Fullerton, C. Leighton, A. H. MacDonald, D. C. Ralph, D. A. Arena, H. A. Dürr, et al. Interface-induced phenomena in magnetism. *Reviews of modern physics*, 89(2):025006, 2017.

[29] Yu. M. Koroteev, G. Bihlmayer, J. E. Gayone, E. V. Chulkov, S. Blügel, P. M. Echenique, and Ph. Hofmann. Strong spin-orbit splitting on Bi surfaces. *Phys. Rev. Lett.*, 93:046403, Jul 2004.

[30] M. B. Jungfleisch, W. Zhang, J. Sklenar, W. Jiang, J. E. Pearson, J. B. Ketterson, and A. Hoffmann. Interface-driven spin-torque ferromagnetic resonance by Rashba coupling at the interface between nonmagnetic materials. *Phys. Rev. B*, 93:224419, 2016.

[31] N. Reyren, S. Thiel, A. D. Caviglia, L. Fitting Kourkoutis, G. Hammerl, C. Richter, C. W. Schneider, T. Kopp, A.-S. Rüetschi, D. Jaccard, M. Gabay, D. A. Muller, J.-M. Triscone, and J. Mannhart. Superconducting interfaces between insulating oxides. *Science*, 317(5842):1196–1199, 2007.

[32] A. Ohtomo and H.Y. Hwang. A high-mobility electron gas at the $LaAlO_3/SrTiO_3$ heterointerface. *Nature*, 427:423–426, 2004.

[33] S. Cao, M. Street, J. Wang, J. Wang, X. Zhang, Ch. Binek, and P. A. Dowben. Magnetization at the interface of Cr_2O_3 and paramagnets with large stoner susceptibility. *Journal of Physics: Condensed Matter*, 29(10):10LT01, 2017.

[34] M.J. Pechan, E.E. Fullerton, and I.K. Schuller. Sources of interface magnetization and interface anisotropy in Fe/Cu multilayers as revealed by thermal behavior. *Journal of Magnetism and Magnetic Materials*, 183(1):19–24, 1998.

[35] V. Kalappattil, R. Geng, R. Das, M. Pham, H. Luong, T. Nguyen, A. Popescu, L. M. Woods, M. Kläui, H. Srikanth, et al. Giant spin Seebeck effect through an interface organic semiconductor. *Materials Horizons*, 7(5):1413–1420, 2020.

[36] A. D. Caviglia, M. Gabay, S. Gariglio, N. Reyren, C. Cancellieri, and J.-M. Triscone. Tunable Rashba spin-orbit interaction at oxide interfaces. *Phys. Rev.*

Lett., 104:126803, 2010.

[37] M. B. Shalom, M. Sachs, D. Rakhmilevitch, A. Palevski, and Y. Dagan. Tuning spin-orbit coupling and superconductivity at the $SrTiO_3/LaAlO_3$ interface: A magnetotransport study. *Phys. Rev. Lett.*, 104:126802, 2010.

[38] J. Govenius, R. E. Lake, K. Y. Tan, and M. Möttönen. Detection of zeptojoule microwave pulses using electrothermal feedback in proximity-induced Josephson junctions. *Physical Review Letters*, 117(3):030802, 2016.

[39] M. I. Alomar and D. Sánchez. Thermoelectric effects in graphene with local spin-orbit interaction. *Phys. Rev. B*, 89:115422, 2014.

[40] Q.-f. Sun, J. Wang, and H. Guo. Quantum transport theory for nanostructures with Rashba spin-orbital interaction. *Phys. Rev. B*, 71:165310, 2005.

[41] P. Crespo, R. Litrán, T. C. Rojas, M. Multigner, J. M. de la Fuente, J. C. Sánchez-López, M. A. García, A. Hernando, S. Penadés, and A. Fernández. Permanent magnetism, magnetic anisotropy, and hysteresis of thiol-capped gold nanoparticles. *Phys. Rev. Lett.*, 93:087204, 2004.

[42] S. Banerjee, S.O. Raja, M. Sardar, N. Gayathri, B. Ghosh, and A. Dasgupta. How gold nanoparticle acquires magnetism?-Formation of large orbital moment at the interface. *arXiv preprint arXiv:0912.3319*, 2009.

[43] O. O. Brovko, P. Ruiz-Díaz, T. R. Dasa, and V. S. Stepanyuk. Controlling magnetism on metal surfaces with non-magnetic means: electric fields and surface charging. *Journal of Physics: Condensed Matter*, 26(9):093001, 2014.

[44] K. V. Raman and J. S. Moodera. A magnetic facelift for non-magnetic metals. *Nature*, 524(7563):42–43, 2015.

[45] D. C. Mattis. *The Many-Body Problem: An Encyclopedia of Exactly Solved Models in One Dimension*. World Scientific, 3rd edition, 1993.

[46] V. E. Korepin and F. H. L. Essler. *Exactly solvable models of strongly correlated electrons*, volume 18. World Scientific, 1st edition, 1994.

[47] U. Brandt and A. Giesekus. Hubbard and Anderson models on perovskitelike lattices: Exactly solvable cases. *Phys. Rev. Lett.*, 68:2648–2651, 1992.

[48] L. G. Sarasua. Superconducting ground states of the extended $t-j$ model. *Phys. Rev. B*, 75:054504, 2007.

[49] R. Strack and D. Vollhardt. Rigorous criteria for ferromagnetism in itinerant electron systems. *Phys. Rev. Lett.*, 72:3425–3428, 1994.

[50] H. Tasaki. Exact resonating-valence-bond ground state and possibility of superconductivity in repulsive Hubbard models. *Phys. Rev. Lett.*, 70:3303–3306, 1993.

[51] R. Strack. Exact ground-state energy of the periodic Anderson model in d=1 and extended Emery models in d=1,2 for special parameter values. *Phys. Rev. Lett.*, 70:833–836, 1993.

[52] L. G. Sarasua and Mucio A. Continentino. Exact results for the extended Anderson model with Falicov-Kimball interactions. *Phys. Rev. B*, 65:233107, 2002.

[53] I. Orlik and Zs. Gulácsi. Exact results for the one-dimensional periodic Anderson model at finite U. *Philosophical Magazine B*, 81(10):1587–1596, 2001.

[54] I. Orlik and Zs. Gulácsi. Exact results related to the periodic Anderson model in $D \gg 1$ dimensions. *Philosophical magazine letters*, 78(2):177–184, 1998.

[55] I. Orlik and Zs. Gulácsi. Exact results related to the periodic Anderson model in the strong-coupling $U=\infty$ limit. *Philosophical Magazine B*, 76(5):845–848, 1997.

[56] L. G. Sarasua and M. A. Continentino. Ground states of the Falicov-Kimball model with hybridization. *Phys. Rev. B*, 69:073103, 2004.

[57] R. Strack and D. Vollhardt. Hubbard model with nearest-neighbor and bond-charge interaction: Exact ground-state solution in a wide range of parameters. *Phys. Rev. Lett.*, 70:2637–2640, 1993.

[58] Zs. Gulácsi, A. Kampf, and D. Vollhardt. Exact many-electron ground states on the diamond Hubbard chain. *Phys. Rev. Lett.*, 99:026404, 2007.

[59] Zs. Gulácsi, A. Kampf, and D. Vollhardt. Route to ferromagnetism in organic polymers. *Phys. Rev. Lett.*, 105:266403, 2010.

[60] R. Trencsényi, E. Kovács, and Zs. Gulácsi. Correlation and confinement induced itinerant ferromagnetism in chain structures. *Philosophical Magazine*, 89(22-24):1953–1974, 2009.

[61] R. Trencsényi and Zs. Gulácsi. The emergence domain of an exact ground state in a non-integrable system: the case of the polyphenylene type of chains. *Philosophical Magazine*, 92(36):4657–4675, 2012.

[62] R. Trencsényi and Zs. Gulácsi. Ferromagnetism without flat bands in thin armchair nanoribbons. *The European Physical Journal B*, 75(4):511–525, 2010.

[63] Zs. Gulácsi and D. Vollhardt. Exact insulating and conducting ground states of a periodic Anderson model in three dimensions. *Phys. Rev. Lett.*, 91:186401, 2003.

[64] Zs. Gulácsi. Exact ground states of correlated electrons on pentagon chains. *International Journal of Modern Physics B*, 27(14):1330009, 2013.

[65] Zs. Gulácsi. Exact multielectronic electron-concentration-dependent ground states for disordered two-dimensional two-band systems in the presence of disordered hoppings and finite on-site random interactions. *Phys. Rev. B*, 69:054204, 2004.

[66] P. Gurin and Zs. Gulácsi. Exact solutions for the periodic Anderson model in two dimensions: A non-Fermi-liquid state in the normal phase. *Phys. Rev. B*, 64:045118, 2001.

[67] Zs. Gulácsi and D. Vollhardt. Exact ground states of the periodic Anderson model in $D = 3$ dimensions. *Phys. Rev. B*, 72:075130, 2005.

[68] Zs. Gulácsi and M. Gulácsi. Exact stripe, checkerboard, and droplet ground states in two dimensions. *Phys. Rev. B*, 73:014524, 2006.

[69] H. Li, M. Y. Zhou, S. Y. Wu, and X. R. Liang. Research of spin-orbit interaction in organic conjugated polymers. *IOP Conference Series: Materials Science and Engineering*, 213:012005, 2017.

[70] H. F. Rey and H. W. van der Hart. Probing spin-orbit-interaction-induced electron dynamics in the carbon atom by multiphoton ionization. *Phys. Rev. A*, 90:033402, 2014.

[71] E.J.G. Santos, A. Ayuela, and D. Sánchez-Portal. Universal magnetic properties of sp3-type defects in covalently functionalized graphene. *New Journal of Physics*, 14(4):043022, 2012.

[72] D. Sun, K. J. van Schooten, M. Kavand, H. Malissa, C. Zhang, M. Groesbeck, C. Boehme, and Z. Valy Vardeny. Inverse spin Hall effect from pulsed spin current in organic semiconductors with tunable spin–orbit coupling. *Nature materials*, 15(8):863–869, 2016.

[73] J. Nitta, T. Akazaki, H. Takayanagi, and T. Enoki. Gate control of spin-orbit interaction in an inverted $In_{0.53}Ga_{0.47}As/I_{0.52}Al_{0.48}$ As heterostructure. *Phys. Rev. Lett.*, 78:1335–1338, 1997.

[74] G. Engels, J. Lange, Th. Schäpers, and H. Lüth. Experimental and theoretical approach to spin splitting in modulation-doped In_x $Ga_{1-x}As$/InP quantum wells for $B \to 0$. *Phys. Rev. B*, 55:R1958–R1961, 1997.

[75] H. C. Lee and S.-R. Eric Yang. Collective excitation of quantum wires and effect of spin-orbit coupling in the presence of a magnetic field along the wire. *Phys. Rev. B*, 72:245338, 2005.

[76] R. Trencsényi, K. Gulácsi, E. Kovács, and Zs. Gulácsi. Exact ground states for polyphenylene type of hexagon chains. *Annalen der Physik*, 523(8-9):741–750, 2011.

[77] I. R. Nikolényi and J. Tóth. Magnetic field study of poly (p-phenylenevinylene) derivatives. *Journal of Magnetism and Magnetic Materials*, 517:167281, 2021.

[78] Y. Suwa, R. Arita, K. Kuroki, and H. Aoki. Flat-band ferromagnetism in organic polymers designed by a computer simulation. *Phys. Rev. B*, 68:174419, 2003.

[79] R. Arita, Y. Suwa, K. Kuroki, and H. Aoki. Gate-induced band ferromagnetism in

an organic polymer. *Phys. Rev. Lett.*, 88:127202, 2002.

[80] R. Arita, Y. Suwa, K. Kuroki, and H. Aoki. Flat-band ferromagnetism in undoped and doped polyaminotriazole crystal. *Phys. Rev. B*, 68:140403, 2003.

[81] A. Kormányos, V. Zólyomi, V. I. Fal'ko, and G. Burkard. Tunable Berry curvature and valley and spin Hall effect in bilayer mos_2. *Phys. Rev. B*, 98:035408, 2018.

[82] Z. Yu, Y. X. Huang, and S. C. Shen. Spin-orbit splitting of the valence bands in silicon determined by means of high-resolution photoconductive spectroscopy. *Phys. Rev. B*, 39:6287–6289, 1989.

[83] F. Musio and M. C. Ferrara. Low frequency ac response of polypyrrole gas sensors. *Sensors and Actuators B: Chemical*, 41(1-3):97–103, 1997.

[84] S. Bonardd, V. Moreno-Serna, G. Kortaberria, D. Díaz Díaz, A. Leiva, and C. Saldías. Dipolar glass polymers containing polarizable groups as dielectric materials for energy storage applications. A minireview. *Polymers*, 11(2), 2019.

[85] H. Mousavi, S. Jalilvand, J. Khodadadi, and M. Yousefvand. Tight-binding description of semiconductive conjugated polymers. *Computational and Theoretical Chemistry*, 1199:113190, 2021.

[86] N. Lazarides and G. P. Tsironis. Compact localized states in engineered flat-band PT metamaterials. *Scientific Reports*, 9(1):1–9, 2019.

[87] L.-L. Wan, X.-Y. Lü, J.-H. Gao, and Y. Wu. Hybrid interference induced flat band localization in bipartite optomechanical lattices. *Scientific Reports*, 7(1):1–11, 2017.

[88] H. Isobe and N. Nagaosa. Enhancement of spin-orbit interaction by competition between Hund's coupling and electron hopping. In *Journal of Physics: Conference Series*, volume 592, page 012058. IOP Publishing, 2015.

[89] M. Kollar, R. Strack, and D. Vollhardt. Ferromagnetism in correlated electron systems: Generalization of Nagaoka's theorem. *Physical Review B*, 53(14):9225, 1996.

[90] A. Farrell and T. Pereg-Barnea. Strong coupling expansion of the extended Hubbard model with spin-orbit coupling. *Phys. Rev. B*, 89:035112, 2014.

[91] Z. Yu. Short-range correlations in dilute atomic Fermi gases with spin-orbit coupling. *Phys. Rev. A*, 85:042711, 2012.

[92] A. Brinkman, M. Huijben, M. Van Zalk, J. Huijben, U. Zeitler, J.C. Maan, W. G. van der Wiel, G.J.H.M. Rijnders, D. H. A. Blank, and H. Hilgenkamp. Magnetic effects at the interface between non-magnetic oxides. *Nature materials*, 6(7):493–496, 2007.

[93] I. K. Kamilov, A. A. Stepurenko, and A. E. Gummetov. Spin–orbit interaction and carrier mobility in a longitudinal InSb autosoliton under a magnetic field. *Semiconductors (Woodbury, N.Y., Print)*, 53(8), 8 2019.

[94] L. Chen, Z. Ma, J. C. Cao, T. Y. Zhang, and C. Zhang. Phonon-limited mobility in two-dimensional semiconductors with spin-orbit coupling. *Applied Physics Letters*, 91(10):102115, 2007.

[95] H. Hori, Y. Yamamoto, T. Iwamoto, T. Miura, T. Teranishi, and M. Miyake. Diameter dependence of ferromagnetic spin moment in Au nanocrystals. *Phys. Rev. B*, 69:174411, 2004.

[96] H. Hori, T. Teranishi, Y. Nakae, Y. Seino, M. Miyake, and S. Yamada. Anomalous magnetic polarization effect of Pd and Au nano-particles. *Physics Letters A*, 263(4-6):406–410, 1999.

[97] Teruya Shinjo. Chapter 1 - overview. In Teruya Shinjo, editor, *Nanomagnetism and Spintronics*, pages 1–13. Elsevier, Amsterdam, 2009.

[98] A. Fernández-Pacheco, R. Streubel, O. Fruchart, R. Hertel, P. Fischer, and R. P. Cowburn. Three-dimensional nanomagnetism. *Nature communications*, 8(1):1–14, 2017.

[99] D. Winters, M. A. Abeed, S. Sahoo, A. Barman, and S. Bandyopadhyay. Reliability of magnetoelastic switching of nonideal nanomagnets with defects: A case study for the viability of straintronic logic and memory. *Phys. Rev. Applied*, 12:034010, 2019.

[100] Y. Yamamoto, T. Miura, M. Suzuki, N. Kawamura, H. Miyagawa, T. Nakamura, K. Kobayashi, T. Teranishi, and H. Hori. Direct observation of ferromagnetic spin polarization in gold nanoparticles. *Phys. Rev. Lett.*, 93:116801, 2004.

[101] G. L. Nealon, B. Donnio, R. Greget, J.-P. Kappler, E. Terazzi, and J.-L. Gallani. Magnetism in gold nanoparticles. *Nanoscale*, 4(17):5244–5258, 2012.

[102] C.-M. Wu, C.-Y. Li, Y.-T. Kuo, C.-W. Wang, S.-Y. Wu, and W.-H. Li. Quantum spins in Mackay icosahedral gold nanoparticles. *Journal of Nanoparticle Research*, 12(1):177–185, 2010.

[103] K. N. K. Kowlgi, G. J. M. Koper, S. J. Picken, U. Lafont, L. Zhang, and B. Norder. Synthesis of magnetic noble metal (nano) particles. *Langmuir*, 27(12):7783–7787, 2011.

[104] I. Carmeli, G. Leitus, R. Naaman, S. Reich, and Z. Vager. Magnetism induced by the organization of self-assembled monolayers. *The Journal of Chemical Physics*, 118(23):10372–10375, 2003.

[105] L. He. Comment on "Diameter dependence of ferromagnetic spin moment in Au nanocrystals". *Phys. Rev. B*, 81:096401, 2010.

[106] P. Dutta, S. Pal, M. S. Seehra, M. Anand, and C. B. Roberts. Magnetism in dodecanethiol-capped gold nanoparticles: Role of size and capping agent. *Applied Physics Letters*, 90(21):213102, 2007.

[107] U. Maitra, B. Das, N. Kumar, A. Sundaresan, and C. N. R. Rao. Ferromagnetism exhibited by nanoparticles of noble metals. *ChemPhysChem*, 12(12):2322–2327, 2011.

[108] E. Guerrero, M. A. Muñoz-Márquez, M. A. García, P. Crespo, E. Fernández-Pinel, A. Hernando, and A. Fernández. Surface plasmon resonance and magnetism of thiol-capped gold nanoparticles. *Nanotechnology*, 19(17):175701, 2008.

[109] P. de la Presa, M. Multigner, J. de la Venta, M. A. García, and M. L. Ruiz-González. Structural and magnetic characterization of oleic acid and oleylamine-capped gold nanoparticles. *Journal of Applied Physics*, 100(12):123915, 2006.

[110] S. Reich, G. Leitus, and Y. Feldman. Observation of magnetism in Au thin films. *Applied Physics Letters*, 88(22):222502, 2006.

[111] F. Michael, C. Gonzalez, V. Mujica, M. Marquez, and M. A. Ratner. Size dependence of ferromagnetism in gold nanoparticles: Mean field results. *Phys. Rev. B*, 76:224409, 2007.

[112] A. Hernando, P. Crespo, and M. A. García. Origin of orbital ferromagnetism and giant magnetic anisotropy at the nanoscale. *Phys. Rev. Lett.*, 96:057206, 2006.

[113] Y. Zhang and W. Yang. Comment on "generalized gradient approximation made simple". *Phys. Rev. Lett.*, 80:890–890, 1998.

[114] L. F. Pasteka, E. Eliav, A. Borschevsky, U. Kaldor, and P. Schwerdtfeger. Relativistic coupled cluster calculations with variational quantum electrodynamics resolve the discrepancy between experiment and theory concerning the electron affinity and ionization potential of gold. *Phys. Rev. Lett.*, 118:023002, 2017.

[115] A. Sekiyama, J. Yamaguchi, A. Higashiya, M. Obara, H. Sugiyama, M. Y. Kimura, S. Suga, S. Imada, I. A. Nekrasov, M. Yabashi, K. Tamasaku, and T. Ishikawa. The prominent 5d-orbital contribution to the conduction electrons in gold. *New Journal of Physics*, 12(4):043045, 2010.

[116] H. A. Alluhaybi, S. K. Ghoshal, B. O. Alsobhi, and W. N. Wan Shamsuri. Electronic and optical correlation effects in bulk gold: Role of spin–orbit coupling. *Computational Condensed Matter*, 18:e00360, 2019.

[117] E. Kovács, R. Trencsényi, and Zs. Gulácsi. Magnetic nano-grains from a non-magnetic material: A possible explanation. *IOP Conference Series: Materials Science and Engineering*, 47:012048, 2013.

[118] P. Crespo, M. A. García, E. Fernández Pinel, M. Multigner, D. Alcántara, J. M. de la Fuente, S. Penadés, and A. Hernando. Fe impurities weaken the ferromagnetic behavior in Au nanoparticles. *Phys. Rev. Lett.*, 97:177203, 2006.

[119] C. B. Sommers and H. Amar. Relativistic band structure of gold. *Phys. Rev.*, 188:1117–1120, 1969.

[120] N. E. Christensen and B. O. Seraphin. Relativistic band calculation and the optical properties of gold. *Phys. Rev. B*, 4:3321–3344, 1971.

[121] M. A. Flores and E. Menéndez-Proupin. Spin-orbit coupling effects in gold clusters: The case of Au_{13}. *Journal of Physics: Conference Series*, 720:012034, 2016.

[122] S. P. Chenakin and N. Kruse. Au 4f spin–orbit coupling effects in supported gold nanoparticles. *Physical Chemistry Chemical Physics*, 18:22778–22782, 2016.

[123] Hüger, E., Zelený, M., Kána, T., Osuch, K., and Sob, M. Spin–orbit coupling in low-dimensional gold. *Physica status solidi (RRL) – Rapid Research Letters*, 2(3):117–119, 2008.

[124] D. Jiang, M. Kühn, Q. Tang, and F. Weigend. Superatomic orbitals under spin–orbit coupling. *The Journal of Physical Chemistry Letters*, 5(19):3286–3289, 2014. PMID: 26278432.

[125] S. LaShell, B. A. McDougall, and E. Jensen. Spin splitting of an Au(111) surface state band observed with angle resolved photoelectron spectroscopy. *Phys. Rev. Lett.*, 77:3419–3422, 1996.

[126] S. Trudel. Cheminform abstract: Unexpected magnetism in gold nanostructures: Making gold even more attractive. *Gold Bulletin*, 44:3–13, 2012.

[127] L. Avakyan, V. Durimanov, D. Nemesh, V. Srabionyan, J. Ihlemann, and L. Bugaev. Theoretical approach for calculation of dielectric functions of plasmonic nanoparticles of noble metals, magnesium and their alloys. *Optical Materials*, 109:110264, 2020.

[128] L. He. Unexpected magnetic moments in ultrafine diamagnetic systems. *The Journal of Physical Chemistry C*, 114(29):12487–12489, 2010.

[129] D. Holec, L. Löfler, G. A. Zickler, D. Vollath, and F. D. Fischer. Surface stress of gold nanoparticles revisited. *International Journal of Solids and Structures*, 224:111044, 2021.

[130] D. C. Agrawal. *Introduction to Nanoscience and Nanomaterials*. World Scientific, 1st edition, 2013.

[131] B. Sampedro, P. Crespo, A. Hernando, R. Litrán, J. C. Sánchez López, C. López Cartes, A. Fernandez, J. Ramírez, J. González Calbet, and M. Vallet. Ferromagnetism in fcc twinned 2.4 nm size Pd nanoparticles. *Phys. Rev. Lett.*, 91:237203, 2003.

[132] D. Maynau, H. Bolvin, W. Van den Heuvel, M. Bénard, M.-M. Rohmer, and N. Ben Amor. Ferromagnetic coupling induced by spin-orbit coupling in dipyridylamide linear trinuclear Cu-Pd-Cu and Cu-Pt-Cu complexes. *Comptes Rendus Chimie*, 15(2):170–175, 2012.

[133] S. Hadjoudj, S. Senoussi, M.F. Mosbah, and Y. Öner. Influence of palladium on the unidirectional anisotropy field in NiMn disordered systems. *Journal of Magnetism and Magnetic Materials*, 175(3):328–332, 1997.

[134] H. Ohlsén and J. L. Calais. Effect of spin-orbit coupling on the conduction-electron Zeeman splitting in platinum-group metals. *Phys. Rev. B*, 35:7914–7921, 1987.

[135] T. Matsushita, T. Asada, and S. Koseki. Relativistic study on emission mechanism in palladium and platinum complexes. *The journal of physical chemistry. A*, 110:13295–302, 2007.

[136] K. C. Kwon, E. Jo, Y.-W. Kwon, B. Lee, J. H. Ryu, E. J. Lee, K. Kim, and J. Lee. Superparamagnetic gold nanoparticles synthesized on protein particle scaffolds for cancer theragnosis. *Advanced Materials*, 29(38):1701146, 2017.

[137] T. Hotta. Existence of a metallic ferromagnetic phase in models for undoped manganites. *Phys. Rev. B*, 67:104428, 2003.

[138] J. Goraus and A. Ślebarski. Onsite hybridization between Ce 4f and 5d states as the indicator of the transition from Kondo insulator to metallic state in CeRhSb. *Physics Letters A*, 375(39):3469–3473, 2011.